haematologica
Journal of the Ferrata Storti Foundation

Altered immune and treatment response gene expression signatures among poverty-exposed children with B-cell acute lymphoblastic leukemia

by Amy Guillaumet-Adkins, Elnaz Mirzaei Mehrabad, Noori Sotudeh, Sayalee Potdar, Tushara Vijaykumar, Monica Nair, Valeriya Dimitrova, Julia Frede, Yana Pikman, Marian Harris, Andrew E. Place, Lewis B. Silverman, Jens G. Lohr, Kira Bona and Birgit Knoechel

Received: October 7, 2025.
Accepted: April 28, 2026.

Citation: Amy Guillaumet-Adkins, Elnaz Mirzaei Mehrabad, Noori Sotudeh, Sayalee Potdar, Tushara Vijaykumar, Monica Nair, Valeriya Dimitrova, Julia Frede, Yana Pikman, Marian Harris, Andrew E. Place, Lewis B. Silverman, Jens G. Lohr, Kira Bona, and Birgit Knoechel Altered immune andtreatment response gene expression signatures among poverty-exposed children with B-cell acute lymphoblastic leukemia.
Haematologica. 2026 May 7. doi: 10.3324/haematol.2025.289187 [Epub ahead of print]

Altered immune and treatment response gene expression signatures among poverty-exposed children with B-cell acute lymphoblastic leukemia

Amy Guillaumet-Adkins[1,2,#], Elnaz Mirzaei Mehrabad[3#], Noori Sotudeh[1o], Sayalee Potdar[1], Tushara Vijaykumar[4], Monica Nair[4], Valeriya Dimitrova[1], Julia Frede[4], Yana Pikman[1,5,6], Marian Harris[6,7], Andrew E. Place[1,5,6], Lewis B. Silverman[1,6,8], Jens G. Lohr[3,4,6], Kira Bona[1,5,6$,*], Birgit Knoechel[1,3,5,6$,*]

Affiliations
[1] Pediatric Oncology, Dana-Farber Cancer Institute, Boston, MA, USA
[2] Broad Institute of Harvard and MIT, Cambridge, MA, USA
[3] Huntsman Cancer Institute, Salt Lake City, UT, USA
[4] Medical Oncology, Dana-Farber Cancer Institute, Boston, MA, USA
[5] Department of Pediatrics, Boston Children's Hospital, Boston, MA, USA
[6] Harvard Medical School, Boston, MA, USA
[7] Department of Pathology, Boston Children's Hospital, Boston, MA, USA
[8] Department of Pediatric Oncology, Columbia University, New York City, NY, USA
[o] Current Affiliation: AtlasXomics Inc., New Haven, CT, USA
[#] Contributed equally to this work
[$] Co-senior Author
* Co-corresponding Author

Author Contributions: K.B. and B.K. conceptualized and supervised this study. A.G.A., E.M.M., N.S., K.B. and B.K. co-wrote the manuscript. A.G. performed experiments and analyzed the data. E.M.M., N.S. performed data analysis. A.G.A., S.P., T.V., M.N., V.D. and J.F. performed experiments. Y.P., M.H., A.E.P., and L.B.S. provided clinical samples; J.G.L provided scientific input for study design and/or data analysis. All authors reviewed and edited the manuscript.

Running title: Poverty-associated treatment signatures in pediatric B-ALL

Corresponding authors: Birgit Knoechel, Huntsman Cancer Institute, 2000 Circle of Hope Drive, Salt Lake City, UT 84112, USA; Phone: (801) 213-8428; E-mail: birgit.knoechel@hci.utah.edu, or Kira Bona, Dana-Farber Cancer Institute, 450 Brookline Avenue, MA-656, Boston, MA 02215, USA; Phone: (617) 632-4866; Fax: (617) 632-6845; E-mail: kira.bona@childrens.harvard.edu

Data Sharing: Sequencing data have been deposited in GEO (reference number GSE237888). Codes used for all analyses are available upon request from the corresponding author.

Acknowledgments: We thank the Flow Cytometry Core at Dana-Farber Cancer Institute for their assistance, the Pediatric Oncology Outcomes research team and the Clinical Research Coordinators ALL study team at Dana-Farber Cancer Institute for their help with primary patient samples, and Dr. Judy Ou at Huntsman Cancer Institute for critical comments.

Financial Support: This work was supported by a Helen Trailblazers Award by Dana-Farber Cancer Institute/Pussycat Foundation (to K.B, B.K.), National Cancer Institute – DF/HCC Nodal Award (2P30CA006516-52) (to K.B., B.K) and R01CA249185 (to B.K.), and a Children's Cancer Research Fund award (to B.K.).

Conflict of Interest Disclosure Statement: J.G.L. received research funding from Bristol Myers Squibb for an unrelated project. The other authors declared no relevant conflicts of interest.

ABSTRACT

Children diagnosed with cancer typically receive standardized treatment regimens. Despite highly protocolized care, children living in poverty experience a greater risk of cancer relapse and higher mortality compared to their more affluent peers[1,2]. Acute lymphoblastic leukemia (ALL) is the most prevalent childhood cancer, and children with ALL exposed to poverty are more likely to experience early relapse[3]. Using single-cell RNA sequencing to analyze leukemic blasts and their microenvironment at diagnosis we found that poverty-exposed patients with standard-risk B-ALL exhibit transcriptional signatures of steroid resistance at time of diagnosis. Additionally, we observe increased expression of inflammatory signatures in myeloid cells and reduced effector signatures in CD8+ T-cells in children with B-ALL living in poverty. Further investigation of the mechanisms underlying these associations may identify opportunities for risk-adapted therapeutic strategies to improve disease outcomes in pediatric ALL.

INTRODUCTION

Acute lymphoblastic leukemia (ALL) is the most common cancer of childhood, and 20% of children will suffer relapsed disease[4–6]. Despite improvements in therapy, only 50% of children who experience relapse will be long-term survivors[6]. Elucidating mechanisms of treatment resistance among populations at risk of relapse is essential to identify opportunities to improve pediatric ALL outcomes.

Early ALL relapse has been defined as relapse <36 months in complete remission[6] and is associated with particularly poor survival. Recent data have identified children exposed to poverty as a cohort at significantly higher risk of early relapse compared to unexposed children, despite uniform treatment on multi-center clinical trials. Among children who experienced leukemia relapse on a Dana-Farber ALL Consortium trial, 92% of relapses were early among poverty-exposed children compared to 48% relapses among unexposed children[3,7]. Additionally, recent publications have identified an association more broadly between proxied exposure to poverty and relapse and survival among children with ALL[8,9].

Poverty is associated with profound health disparities in the US in diseases ranging from asthma to cancer[10–12].While structural and sociobehavioral mechanisms underlying these associations—including access to care and adherence—have been delineated, they only partly explain observed disparities[13].Emerging evidence suggests that gene-environment interactions may contribute to health outcome disparities in asthma, obesity and cardiovascular disease—and help to explain the influence of stress on disease outcomes[14,15].Early childhood exposure to poverty is associated with "toxic stress," defined by excessive activation of stress regulatory systems that impacts neuroendocrine stress response axes including upregulation of the hypothalamic-pituitary-axis, elevated cortisol and cytokine responses to stress, and altered metabolism[16–18],yet no studies have been performed to assess whether similar responses might be at play among children with cancer. Understanding the mechanistic pathways underlying these associations has the potential to inform both therapeutic targets and risk-adapted therapy.

Single-cell analyses have emerged as a powerful way to gain information about heterogeneity within cancer cell populations and have illustrated the importance of co-existing diverse genetic, epigenetic or transcriptional subpopulations for treatment response[19,20].We hypothesized that single-cell transcriptomics would allow to capture leukemia-intrinsic and immune microenvironmental differences in pathways associated with drug resistance between leukemia and normal immune cells from poverty-exposed and unexposed children with ALL. To address these hypotheses, we employed full-length single-cell RNA-sequencing of leukemic blasts and microenvironmental cells from poverty-exposed and unexposed children with B-cell ALL (B-ALL). Notably, we identified several differentially enriched pathways in leukemia cells from poverty-exposed and unexposed patients including steroid responsiveness and signatures consistent with altered immune responses in the leukemia microenvironment that may be associated with treatment resistance.

METHODS

Patient samples

Banked diagnostic bone marrow samples from children with *de novo* B-cell ALL diagnosed between 2005 and 2018, who had consented to biobanking for future research (Dana-Farber Cancer Institute (DFCI) protocols 06-078, 05-001 [NCT00400946], 11-001 [NCT01574274]) were utilized in this analysis. Parent-reported socioeconomic data from concurrent poverty-focused research protocols (DFCI 11-198 and 16-544) were utilized to annotate biospecimens. Patient demographics and tumor characteristics (immunophenotype, cytogenetics, targeted

DNA sequencing) were abstracted from study data and the electronic medical record. This study was approved by the DFCI Institutional Review Board.

Poverty-exposure
Poverty was the primary exposure of interest and was defined a priori at the household-level utilizing both income-poverty and unmet resource needs. Specifically, patients were considered poverty-exposed if they had concurrent parents reported low-income (annual household income <200% of the Federal Poverty Level (FPL) and household material hardship (HMH; food, housing, or transportation insecurity) at time of diagnosis. Those with reported income >200% FPL were considered unexposed, regardless of whether HMH data were available.

Cohort assembly
We excluded biospecimens from patients with high-risk immunophenotypic or genetic abnormalities at diagnosis including T-cell immunophenotype, KMT2A or BCR-ABL1 gene rearrangements, or high-risk cytogenetic abnormalities (low hypodiploidy; t[17;19], iAMP21). Analytic specimens were restricted to lymphoblasts with B-cell immunophenotype, *ETV6::RUNX1* translocations or a hyperdiploid karyotype, two genetic features frequently associated with standard risk prognosis, or normal FISH and cytogenetic testing. Biospecimens were analyzed in a deidentified fashion.

Flow cytometry
Mononuclear cells (PBMCs) were isolated using Ficoll-Paque PLUS from GE Healthcare according to the manufacturer's protocol. Samples were stained for CD45-FITC, CD3-PerCP-Cy5.5, CD14-APC-Cy7, CD19-PE, and DAPI (1 µg/mL, Sigma Aldrich) to exclude dead cells. Single cells were sorted into 96-well plates containing TCL buffer (Qiagen) using a Sony SH800 sorter. Minipools of 100 leukemic cells from each patient were sorted in the same way and used for bulk RNA-seq. The number of sorted and sequenced cells per sample are listed in Supplemental Table 4.

scRNA-seq library preparation and sequencing
Full-length single-cell RNA-seq libraries were prepared using the SMART-seq2 protocol[21]. Libraries were pooled and quantified using Qubit dsDNA High Sensitivity reagents. Paired-end sequencing was performed on a NextSeq 500 (Illumina) targeting a sequencing depth of 1 million reads per single cell. Sequencing reads were trimmed using trimmomatic and aligned to the hg19 version reference genome using STAR aligner[22]. Raw counts and normalized TPM values using HTSeq and RSEM, respectively. Detailed library preparation protocols are provided in Supplementary Methods.

Statistical analysis
All statistical analyses were conducted using R (version 4.0.4) and R packages available at BioConductor. P-values were adjusted for false discovery rate (FDR) across all comparisons using Holm-Bonferroni. An adjusted P-value equal or lower than 0.05 and a log2-fold change of more or equal to 0.58 was considered significant. A parametric student's t-tests or one-way ANOVA was used to compare means of 2 groups or multiple groups, respectively. All data represent mean ± standard deviation (SD). * $p < 0.05$; ** $p < 0.01$; *** $p < 0.001$, **** $p < 0.0001$, were considered statistically significant.

RESULTS
Single-cell transcriptomic profiling delineates malignant from normal cells in low-risk pediatric B-ALL

We assembled a cohort of poverty-exposed (N=7) (defined as both parent-reported low-income [annual household income <200% FPL] and at least one unmet basic resource need [HMH; food, utility or housing insecurity) and unexposed (N=7) children with *de novo* B-cell ALL who had consented to biobanking of diagnostic bone marrow specimens to assess transcriptional profiles of lymphoblasts and microenvironmental cell populations at diagnosis. To minimize heterogeneity, we excluded patients with high-risk immunophenotype, *KMT2A* or *BCR-ABL1* gene rearrangements, or high-risk cytogenetic abnormalities (low hypodiploidy; t(17;19); iAMP21). The remaining biospecimens included B-cell immunophenotype, *ETV6::RUNX1* translocations or hyperdiploid karyotypes—two genetic features frequently associated with standard risk prognosis. Clinical, immunophenotype and molecular characteristics are listed in Table 1.

We enriched for leukemia cells from bone marrow by sorting on CD45low expressing blasts and also collected normal T-cells, B-cells, myeloid and NK cells by sorting on appropriate surface markers (CD45high CD3+ T-cells, CD45high. CD19+ B-cells, CD45high CD14+ myeloid cells; Figure 1A; see methods). Percentage of each sorted cell type is listed in Table 2.

After single-cell sorting, we performed full-length single-cell transcriptome analysis of 3,166 malignant (852 "poverty-exposed" and 936 "unexposed") and 1,378 normal immune cells (T-cells, B-cells and myeloid cells) using the Smartseq2 protocol for full-length RNAseq[21] (Supplemental Figure S1). For comparison, we also included normal donor cells from 6 normal donors from published datasets in our analyses (GSE16191, GSE162337)[20,23]. As these normal donors were all from adult individuals, we verified that main cell types and proportions were similar for pediatric individuals by comparing with public pediatric datasets downloaded from GSE132509 (Supplemental Figure S2)[24].

After several single-cell RNA-seq quality control filtering steps (see Methods and Supplemental Figure S1), we performed t-Stochastic Neighbor Embedding (t-SNE)[25]and graph-based clustering from Seurat package to explore cellular compositions, which revealed 17 distinct cell clusters (Supplemental Figure S3A). Seven clusters (clusters 4, 7, 8, 10, 11, 15 and 16) were shared between patients and normal donors, thus presumably representing normal immune cells, whereas the remaining clusters (1, 2, 5, 9, 13, 14, and 17) were specific to B-ALL patients. Lineage annotation of the single-cell profiles with singleR[26]based on BLUEPRINT[27]and Human Cell Atlas datasets[28,29]of immune cell populations revealed that shared clusters indeed represented CD4+ T-cells, CD8+ T-cells, NK-cells, B-cells, and myeloid cells, respectively; whereas leukemic cells fell into clusters annotated as Pro-B cells, consistent with their developmental state (Figure 1C, Supplemental Figure S3B). Additionally, differential expression analysis of well-established canonical lineage marker genes distinguished normal from leukemic clusters (Figure 1D, E). For example, leukemic clusters 1, 2, 5, 9, 13, 14 and 17 expressed *TCF4, ERG, MEF2C* and *SOX4,* all of which are transcription factors with known function in B-ALL[30–32]. Cluster 4 contained B-cells as demonstrated by expression of *IRF8, CIITA, BIRC3, CD19* and *CD22*. T-cells localized into clusters 3, 7, and 10 with strong expression of *IL7R, CD3G, CD3D*, and *TCF7*. Cluster 8 contained myeloid cells that express *LYZ* and *FOS*. NK cells with expression of the NK markers *NKG7, PRF1* and *GZMB* were found in cluster 11 (Figure 1 D, E, Supplemental Figure S3A).

To ensure that clusters 1, 2, 5, 9, 13, 14, and 17 were indeed malignant, we called arm level copy number variations (CNV) in normal and presumed malignant clusters using InferCNV (see methods) CNVs were limited to leukemic clusters, with copy number events being most prominent in hyperdiploid B-ALL samples (Supplemental Figure S4).

Leukemia cells fall into distinct clusters based on underlying genetic characteristics and poverty exposure

Interestingly, while some leukemic clusters were patient-specific, other clusters contained cells of several patients (Figure 1B, C). To understand leukemic cluster formation, we first tested

whether underlying genetic events might be causal for cluster formation. Leukemic cells that were hyperdiploid or carried *ETV6::RUNX1* translocations clustered separately in t-SNE (Table 1; Figure 2A). Aberrant developmental hierarchies have been described in many cancers including in acute leukemia and have been associated with treatment failure[19].To address whether leukemic cells from poverty-exposed or unexposed patients may demonstrate aberrant differentiation states, we performed Louvain clustering[33] focusing on genes involved in hematopoietic progenitor and B-lymphoid differentiation using validated signatures from the Human Cell Atlas (Table S1, see methods). This analysis revealed 7 clusters (Figure 2B). Leukemia cells from poverty-exposed patients were enriched in clusters 3, 4, 5, 7 while leukemic cells from unexposed patients dominated in clusters 1, 2 and 6 (Figure 2C, D). Of note, all 7 clusters contained cells from both genetic subtypes, even though some were enriched in cells from either hyperdiploid or *ETV6::RUNX1* translocated leukemias (i.e., clusters 2 and 4 enriched in hyperdiploid, clusters 3 and 5 enriched in *ETV6::RUNX1* translocated specimens (Supplemental Figure S5A, B, C, D), suggesting that genetic events alone were not solely responsible for cluster formation (Supplemental Figure S5C, D).

To further characterize these clusters, we performed marker gene and geneset enrichment analysis, comparing clusters enriched in poverty-exposed to those enriched in unexposed specimens. Notably, clusters enriched in poverty-exposed leukemic cells (clusters 3, 4, 5 and 7) demonstrated expression of genes with known relation to treatment response in B-ALL, including genes associated with hematopoietic progenitors (*FOXO1, SMARCA4, JUN, ARID5B, STAG3* and *NPY*), resistance to vincristine (*SOX11, DSC2, KCNN1 ABHD3,* and *MTF2*), and glucocorticoid therapy (*SSPB2, PCNA, IGLL1, ADGRAA3, STMN1* and *PCCA*). In contrast, clusters enriched in unexposed leukemic cells (clusters 1, 2, and 6) were characterized by expression of signatures related to metabolism (*PSAP, COTL2, LOW, CYBB, GLIPR1, ALDH3B1*, *MTHFD1*) and immune activation (*CD74, ISG20, GBP4*, and *PSME2*) (Figure 2E, Table S2). These analyses reveal distinct heterogenous signatures related to inflammation, metabolism and treatment resistance differentially expressed in leukemic cells from poverty-exposed versus unexposed patients.

In further analyses, we collapsed expressed genes of all signatures enriched in poverty-exposed single-cell clusters or unexposed single-cell clusters, respectively, and computed an average expression score (see Methods; supplemental Table S3). We then assessed the expression of the poverty-exposed and unexposed signatures among patients who had either ETV6::RUNX1 translocated or hyperdiploid B-ALL, respectively. Notably, expression of the poverty-exposed signature was higher in poverty-exposed patients within both groups (Supplemental Figure S6A, B).

We next evaluated whether these signatures might also be differentially expressed in bulk RNA-seq of leukemic cells from poverty-exposed and unexposed patients. To this end, we generated bulk RNA-seq data of the same 7 poverty-exposed and 7 unexposed patients on whom we had performed single-cell transcriptome analysis. Indeed, poverty-exposed signatures were enriched in the poverty-exposed cohort compared to the unexposed cohort, whereas the unexposed signatures were enriched in the unexposed compared to the poverty-exposed cohort (Figure 2F). We observed a similar trend when analyzing *ETV6::RUNX1* translocated and hyperdiploid samples separately (Supplemental Figure S6C, D). We confirmed this trend using CIBERSORTx[34] for deconvolution. Although poverty-exposed signatures were detected in all patients, they were enriched in the poverty-exposed cohort, whereas unexposed signatures were enriched in the unexposed cohort (Supplemental Figure S7).

We next investigated how these signatures performed in an independent dataset from our institution. To this end, we analyzed public bulk RNA-seq data downloaded from GSE181157[35] for which we had poverty-exposure annotation (Table S5). The poverty-exposed

signature was anti-correlated with the unexposed signature and higher expressed in poverty-exposed patients compared to unexposed patients (Supplemental Figure S8, see methods).

Taken together, these analyses suggest that leukemia-intrinsic transcriptional circuits differ in diagnostic B-lymphoblasts from poverty-exposed children compared to non-poverty-exposed children with enrichment of signatures associated with drug resistance in poverty-exposed children.

Modulation of myeloid microenvironment in poverty-exposed children with B-ALL

Chronic inflammation has been implicated in adverse outcomes associated with low-socioeconomic status in several childhood diseases, including asthma and obesity[36,37].To investigate whether the observed differences in inflammatory signatures in leukemic blasts from poverty-exposed versus unexposed B-ALL patients might be associated with changes in the immune microenvironment, we identified the composition and transcriptional landscape of the leukemia microenvironment in the same cohort of patients, focusing on B-cells, T-cells, and myeloid cells as well-defined immune cells. There was no difference in immune cell population frequency between poverty-exposed or unexposed patients (Table S4).

Non-classical monocytes expressing *CD16* (*FCGR3A*) have recently been shown to be enriched in B-ALL at time of diagnosis and at relapse[38].Indeed, transcriptional analysis revealed that while normal donor myeloid cells strongly express *CD14*, myeloid cells from B-ALL patients, expressed lower levels of *CD14* with concurrently higher expression of *CD16* (*FCGR3A*) (Figure 3A, left). Notably, myeloid cells from unexposed patients showed stronger expression of *CD16* (*FCGR3A*) than those from poverty-exposed patients (Figure 3A, right). This trend was also present when analyzing samples from *ETV6::RUNX1* translocated patients separately from hyperdiploid samples (Supplemental Figure S9A).

To further investigate possible transcriptional differences in myeloid cells from poverty-exposed and unexposed leukemia patients, we employed SC3 clustering[39](see Methods) and identified 5 myeloid clusters (Supplemental Figure S9B), with cluster 1 being dominated by normal donor myeloid cells (Supplemental Figure S9B, C). Interestingly, while the remaining 4 clusters contained mostly myeloid cells from leukemic patients, clusters 2 and 4 were dominated by unexposed patients, whereas cluster 3 was enriched in myeloid cells from poverty-exposed patients (Supplemental Figure S9B, C). To further characterize these clusters, we first looked at validated myeloid expression signatures, including expression signatures for classical monocytes (Mono1), and non-classical monocytes (Mono2)[40]. As expected, cluster 1, which contained the largest fraction of normal donor myeloid cells showed strong expression for the classical monocyte signature Mono1 (Supplemental Figure S9D). Cluster 2 (enriched in unexposed patients) was dominated by expression of the non-classical monocyte signature Mono2 and likely represents non-classical monocytes that had been previously shown to be enriched in B-ALL[38]. In contrast, clusters 3 (enriched in poverty-exposed patients) and 4 (enriched in unexposed patients) demonstrated expression of classical monocyte signatures, but in addition expressed the Mono3 signature (associated with differentiation and trafficking in cycling monocytes)[41], and Mono4 signature (associated with cytotoxicity)[40], respectively (Supplemental Figure S9D). Cluster 5, which consists of poverty-exposed and unexposed myeloid cells, did not show strong enrichment for any of the 4 monocyte signatures.

To further characterize differences between these clusters, we performed marker gene and geneset enrichment analysis (Figure 3B, C; Table S3). This analysis confirmed that genes associated with classical monocytes such as *TREM1, CD163, ALDH1A1, NLRP3, LYZ,* and *PLD3* were strongly expressed in cluster 1. Cluster 2 expressed the non-classical monocyte signature genes *CX3CR1, SIGLEC10* and *CYTIP*, and in addition expressed genes involved in inflammatory response (*FCGR3A, SAT1, GCH1, LYN*, and *LST1*), immune regulation (*LILRB2*, *IFITM1*, *PILRA*, *ITGAL* and *ICAM2),* and cytotoxicity (*FCGR3B, TNF, FCER1G,* and *PTPN6)*.

Interestingly, myeloid cells in cluster 3—which were enriched in poverty-exposed patients—expressed signatures associated with cytokine signaling (*IL1B, SOCS3, TNFRSF1A, IL4R, SELL*, *IL4R* and *IL6R*), complement (*CD55, CLU, GCA* and *S100A12)*, and reactive oxygen species (ROS) pathway (*PRDX1, TXN* and *FES*). In contrast, cluster 4, enriched in myeloid cells from unexposed patients was enriched for genes associated with interferon alpha and beta signaling (*OAS3, OAS1, STAT2, MX2, RSAD2* and *PARP9*). Lastly, cluster 5, shared by both poverty-exposed and unexposed patients, demonstrated enrichment in interferon gamma response, but to lesser extent than cluster 4 (*LCP2, STAT1, IFI44,* and *ISG15)*.

Signaling alterations in myeloid cells have been associated with response to social adversity[42,43].To evaluate whether similar mechanisms may be at play in pediatric leukemia patients we assessed expression of the conserved transcriptional response to adversity (CTRA)[44].Indeed, we observed higher expression of the inflammatory CTRA signature in myeloid cells from patients exposed to poverty compared to unexposed which showed higher expression of the interferon CTRA signature (Figure 3D, see methods).

These findings indicate that myeloid cells from children exposed to poverty exhibit altered immune responses including expression of the inflammatory CTRA signature previously described in health adversity.

Alterations in T- and B-cell profiles among poverty-exposed children with B-ALL

We next explored differences in mature lymphoid cell composition between poverty-exposed and unexposed B-ALL patients. Overall percentages of B-cells, CD4+ and CD8+ T-cells from leukemia patients were comparable to normal donor and did not differ between poverty-exposed and unexposed patients (Table S4).

To explore if B-cell subtypes might differ between poverty-exposed and unexposed patients, we clustered B-cells using Louvain in t-SNE space and identified 5 clusters (Figure 4A, B). SingleR annotation using validated human cell atlas annotations showed that these clusters included mostly naïve, immature and memory B-cells, respectively, with clusters 2 and 4 being enriched in naïve B-cells, and clusters 1 and 5 in memory B-cells (Figure 4C). Notably, while cluster 2 representing naïve B-cells was enriched in normal donor B-cells, the remaining clusters contained B-cells from both poverty-exposed and unexposed patients (Figure 4D). We were also unable to detect differences when analyzing samples from *ETV6::RUNX1* translocated patients separately from hyperdiploid patients, albeit these analyses are limited by the small sample size (Supplemental Figure S10A - D). Thus, representation of B-cell subsets was overall similar between poverty-exposed and unexposed patients with B-ALL.

Next, we focused on T-cells and first separated CD4+ from CD8+ T-cells using validated human cell atlas annotations (Figure 5A). We then performed Louvain clustering of CD4+ annotated T-cells and identified 4 clusters (Figure 5B, Supplemental S11A). Further annotation using singleR, marker gene and geneset enrichment analysis demonstrated that cluster 1 was dominated by CD4+ central memory cells, clusters 2 and 3 consisted of naïve CD4+ T-cells, and cluster 4 contained effector memory CD4+ T-cells (Figure 5C, D). While normal donor T-cells were enriched in cluster 1, all CD4+ T-cell clusters contained cells from poverty-exposed and unexposed B-ALL patients. Poverty-exposed patients demonstrated slightly higher frequencies of CD4+ T-cells in clusters 2 and 3, while unexposed patients contained slightly more cells in cluster 4 (Figure 5E). While overall percentages of CD4+ T-cells were comparable, poverty-exposed patients demonstrated relatively more naïve and central memory CD4+ T-cells and fewer effector memory CD4 T-cells (Supplemental Figure S11B). We detected similar differences when analyzing samples from *ETV6::RUNX1* translocated patients separately from hyperdiploid patients, with the caveat that these analyses are limited by the small sample size (Supplemental Figure S11C - F).

CD8+ T-cells separated into 2 clusters by Louvain (Figure 6A), with cluster 1 containing higher frequencies of CD8+ T-cells from unexposed patients, and cluster 2 being enriched in CD8+ T-cells from poverty-exposed patients (Figure 6B). By marker gene analysis, cells in cluster 1 expressed genes associated with T-cell activation and dysfunction including *GZMA*, *GMZB*, *PRF1, TIGIT* and *IL10RA,* whereas cluster 2 cells expressed genes associated with naïve or central memory T-cells, such as *CCR7, TCF7, LEF1* and *SELL* (Figure 6C). We next computed the average expression of genes that have been previously validated as expressed in naïve, cytotoxic, and dysfunctional T-cells (see Methods). The cytotoxic signature was expressed at a higher level in cluster 1 compared to cluster 2, whereas the naïve and exhausted signature was higher expressed in cluster 2 (Figure 6D). Thus, these analyses point towards an imbalance of naïve, activated, and dysfunctional T-cells in poverty-exposed patients that are enriched in cluster 2 compared to T-cells from unexposed patients which were preferentially enriched in cluster 1.

DISCUSSION

Using single-cell RNA-seq of leukemic blasts and their immune microenvironment in a cohort of children with B-ALL, we identified several differentially enriched pathways in leukemia cells from poverty-exposed and unexposed patients including steroid responsiveness and signatures consistent with altered immune responses in the leukemia microenvironment that may be associated with treatment resistance.

These data point toward several potential mechanisms of adverse treatment response that may explain observed disparities in relapse and survival among children with B-ALL living in poverty. First, our data suggest that poverty-exposed patients with B-ALL have fewer leukemia cells susceptible to steroids at diagnosis. Steroids are a core component of ALL chemotherapy and poor response to steroids is a well-accepted mechanism of treatment failure in ALL[45].Poverty exposure is associated with “toxic stress,” defined by the National Research Council as the excessive activation of stress regulatory systems in the absence of adequate buffering[14].Toxic stress physiology includes dysregulation of the hypothalamic-pituitary-adrenocortical axis and the sympathetic-adrenomedullary system that result in perturbations in stress hormones, elevated inflammatory cytokine responses, and altered cellular metabolism[14,16,46].It is intriguing to speculate that elevated levels of endogenous cortisol may potentially contribute to inherent steroid resistance of leukemic blasts. Notably, prior studies in adult acute myeloid leukemia patients with low SES undergoing hematopoietic stem cell transplantation have demonstrated higher expression of glucocorticoid receptor signaling signatures in PBMCs pre-transplant compared to non-exposed patients.

Prior studies have demonstrated the coexistence of toxic stress and chronic inflammation in asthma, cardiovascular disease, and depression, among other chronic diseases[10,13,14],and it is unknown how this might affect the development of cancer or its immune surveillance. Related, prior work in solid tumor mouse-models suggest that interventions targeting adrenergic receptor responses of the microenvironment—such as beta-blockade—may impact chemotherapy responsiveness.

Inflammatory signatures in tumor cells, including leukemias, have been linked to inferior treatment response—hypothesized to be due in part to immune dysfunction in the tumor microenvironment that prevents a host-immune response against the tumor[47,48].Mechanisms of immune dysfunction are well established in many solid tumors and emerging data suggest an important role for aberrant immune activation in ALL[20,47].There is sparse knowledge with regards to the composition and functional characteristics of the tumor immune microenvironment among patients who experience poverty and other adverse social determinants of health. Our results point towards unique immune derangements that occur in

children with B-ALL in the context of poverty exposures, notably an increased expression of inflammatory signatures in myeloid cells and an imbalance of CD8 naïve and effector cells. Importantly, myeloid cells from poverty-exposed B-ALL patients also express inflammatory signatures that have previously been associated with adversity in other disease contexts[42,43], arguing that these alterations might represent universal changes that occur in the setting of hardship and may offer unique therapeutic possibilities. For example, interventions targeting adrenergic receptor responses through beta-blockade have been shown to reduce chemotherapy resistance in select solid tumors[49], yet possible effects on the immune microenvironment have not been explored.

It is notable that 1 in 3 children with ALL is exposed to poverty at the time of diagnosis[50], and these children are more likely to experience early relapse of their disease. Consequently, our data highlighting potential mechanisms of treatment resistance in the context of poverty-exposure hold immediate relevance for a third of children with the most common pediatric cancer diagnosis—a number far higher than any high-risk ALL genomic alteration. Specifically, further work to clarify associations between poverty-exposure, steroid resistance and immune microenvironment have the potential to be translated to future risk-adapted therapeutic approaches—for example, chemotherapy regimens that are relatively steroid-sparing, or those that directly target the tumor microenvironment to induce or maintain remission. If successful, such risk-adapted approaches to treatment could reduce excess relapse—an outcome to both improve ALL survival and concurrently to reduce the toxicity associated with the treatment of relapsed ALL and concurrently improve survival outcomes.

Our data are limited by a small sample size, including 7 children in each cohort, and thus exploratory in nature. Future replication of these findings in a larger cohort is necessary and will allow investigation of poverty-associated signatures stratified by genetic sub-type that is not possible in our sample. More detailed studies are needed to better understand the relative contributions of myeloid cells and CD8-T-cells and their interactions with leukemic cells in the context of poverty-exposure employing additional single-cell sequencing approaches that allow profiling of a larger number of cells such as the multimodal approaches available on the 10X platform. Further studies may also shed light on the relative contributions of underlying leukemic genetic events in shaping the leukemia immune microenvironment. Additionally, future studies are needed to determine if the observed leukemia-intrinsic and microenvironmental alterations are limited to children with B-ALL or if they also occur in the setting of genomic high-risk ALL and their relevance for other pediatric cancers.

One in three children with ALL lives in poverty at the time of diagnosis, and these children disproportionately experience treatment failure in the form of early relapse of their disease[3]. Future work to unravel tumor microenvironmental and epigenetic state changes associated with poverty-exposure may identify opportunities for therapeutic targeting and resistance-adapted chemotherapy relevant to a strikingly high proportion of children with ALL.

REFERENCES

1. Bona K, London WB, Guo D, Frank DA, Wolfe J. Trajectory of Material Hardship and Income Poverty in Families of Children Undergoing Chemotherapy: A Prospective Cohort Study. Pediatr Blood Cancer. 2016;63(1):105-111.
2. Gupta S, Dai Y, Chen Z, et al. Racial and ethnic disparities in childhood and young adult acute lymphocytic leukaemia: secondary analyses of eight Children's Oncology Group cohort trials. Lancet Haematol. 2023;10(2):e129-e141.
3. Bona K, Blonquist TM, Neuberg DS, Silverman LB, Wolfe J. Impact of Socioeconomic Status on Timing of Relapse and Overall Survival for Children Treated on Dana-Farber Cancer Institute ALL Consortium Protocols (2000-2010). Pediatr Blood Cancer. 2016;63(6):1012-1018.
4. Inaba H, Pui C-H. Advances in the Diagnosis and Treatment of Pediatric Acute Lymphoblastic Leukemia. J Clin Med. 2021;10(9):1926.
5. Ward E, DeSantis C, Robbins A, Kohler B, Jemal A. Childhood and adolescent cancer statistics, 2014. CA Cancer J Clin. 2014;64(2):83-103.
6. Hunger SP, Raetz EA. How I treat relapsed acute lymphoblastic leukemia in the pediatric population. Blood. 2020;136(16):1803-1812.
7. Vrooman LM, Blonquist TM, Stevenson KE, et al. Efficacy and Toxicity of Pegaspargase and Calaspargase Pegol in Childhood Acute Lymphoblastic Leukemia: Results of DFCI 11-001. J Clin Oncol. 2021;39(31):3496-3505.
8. Wadhwa A, Chen Y, Hageman L, et al. Poverty and relapse risk in children with acute lymphoblastic leukemia: a Children's Oncology Group study AALL03N1 report. Blood. 2023;142(3):221-229.
9. Hoppmann AL, Hurley DM, Cramer S, et al. Neighborhood socioeconomic status and overall survival among children with acute lymphoblastic leukemia. Blood Adv. 2025;9(22):5861-5869.
10. Singh GK, Jemal A. Socioeconomic and Racial/Ethnic Disparities in Cancer Mortality, Incidence, and Survival in the United States, 1950-2014: Over Six Decades of Changing Patterns and Widening Inequalities. J Environ Public Health. 2017;2017:2819372.
11. Chen E, Miller GE. Socioeconomic status and health: mediating and moderating factors. Annu Rev Clin Psychol. 2013;9:723-749.
12. Adler NE, Newman K. Socioeconomic disparities in health: pathways and policies. Health Aff (Millwood). 2002;21(2):60-76.
13. Braveman P, Gottlieb L. The social determinants of health: it's time to consider the causes of the causes. Public Health Rep. 2014;129 Suppl 2(Suppl 2):19-31.
14. Seeman M, Stein Merkin S, Karlamangla A, Koretz B, Seeman T. Social status and biological dysregulation: the "status syndrome" and allostatic load. Soc Sci Med. 2014;118:143-151.
15. Shonkoff JP. Leveraging the biology of adversity to address the roots of disparities in health and development. Proc Natl Acad Sci U S A. 2012;109 Suppl 2(Suppl 2):17302-17307.
16. Blair C, Raver CC. Poverty, Stress, and Brain Development: New Directions for Prevention and Intervention. Acad Pediatr. 2016;16(3 Suppl):S30-36.
17. Schiavone S, Colaianna M, Curtis L. Impact of early life stress on the pathogenesis of mental disorders: relation to brain oxidative stress. Curr Pharm Des. 2015;21(11):1404-1412.
18. Lupien SJ, McEwen BS, Gunnar MR, Heim C. Effects of stress throughout the lifespan on the brain, behaviour and cognition. Nat Rev Neurosci. 2009;10(6):434-445.
19. van Galen P, Hovestadt V, Wadsworth Ii MH, et al. Single-Cell RNA-Seq Reveals AML Hierarchies Relevant to Disease Progression and Immunity. Cell. 2019;176(6):1265-1281.e24.

20. Anand P, Guillaumet-Adkins A, Dimitrova V, et al. Single-cell RNA-seq reveals developmental plasticity with coexisting oncogenic states and immune evasion programs in ETP-ALL. Blood. 2021;137(18):2463-2480.
21. Picelli S, Faridani OR, Björklund AK, Winberg G, Sagasser S, Sandberg R. Full-length RNA-seq from single cells using Smart-seq2. Nat Protoc. 2014;9(1):171-181.
22. Dobin A, Davis CA, Schlesinger F, et al. STAR: ultrafast universal RNA-seq aligner. Bioinformatics. 2013;29(1):15-21.
23. Frede J, Anand P, Sotudeh N, et al. Dynamic transcriptional reprogramming leads to immunotherapeutic vulnerabilities in myeloma. Nat Cell Biol. 2021;23(11):1199-1211.
24. Caron M, St-Onge P, Sontag T, et al. Single-cell analysis of childhood leukemia reveals a link between developmental states and ribosomal protein expression as a source of intra-individual heterogeneity. Sci Rep. 2020;10(1):8079.
25. Kobak D, Berens P. The art of using t-SNE for single-cell transcriptomics. Nat Commun. 2019;10(1):5416.
26. Aran D, Looney AP, Liu L, et al. Reference-based analysis of lung single-cell sequencing reveals a transitional profibrotic macrophage. Nat Immunol. 2019;20(2):163-172.
27. Fernández JM, de la Torre V, Richardson D, et al. The BLUEPRINT Data Analysis Portal. Cell Syst. 2016;3(5):491-495.e5.
28. Hay SB, Ferchen K, Chetal K, Grimes HL, Salomonis N. The Human Cell Atlas bone marrow single-cell interactive web portal. Exp Hematol. 2018;68:51-61.
29. Regev A, Teichmann SA, Lander ES, et al. The Human Cell Atlas. Elife. 2017;6:e27041.
30. Ramezani-Rad P, Geng H, Hurtz C, et al. SOX4 enables oncogenic survival signals in acute lymphoblastic leukemia. Blood. 2013;121(1):148-155.
31. Wu Z, Zhang F, Liu C, et al. Whole transcriptome sequencing reveals a TCF4-ZNF384 fusion in acute lymphoblastic leukemia. Front Oncol. 2022;12:900054.
32. Zhang J, McCastlain K, Yoshihara H, et al. Deregulation of DUX4 and ERG in acute lymphoblastic leukemia. Nat Genet. 2016;48(12):1481-1489.
33. Blondel VD, Guillaume J-L, Lambiotte R, Lefebvre E. Fast unfolding of communities in large networks. J Stat Mech 2008;2008(10):P10008.
34. Newman AM, Steen CB, Liu CL, et al. Determining cell type abundance and expression from bulk tissues with digital cytometry. Nat Biotechnol. 2019;37(7):773-782.
35. Tran TH, Langlois S, Meloche C, et al. Whole-transcriptome analysis in acute lymphoblastic leukemia: a report from the DFCI ALL Consortium Protocol 16-001. Blood Adv. 2022;6(4):1329-1341.
36. Trivedi M, Denton E. Asthma in Children and Adults-What Are the Differences and What Can They Tell us About Asthma? Front Pediatr. 2019;7:256.
37. Furman D, Campisi J, Verdin E, et al. Chronic inflammation in the etiology of disease across the life span. Nat Med. 2019;25(12):1822-1832.
38. Witkowski MT, Dolgalev I, Evensen NA, et al. Extensive Remodeling of the Immune Microenvironment in B Cell Acute Lymphoblastic Leukemia. Cancer Cell. 2020;37(6):867-882.e12.
39. Kiselev VY, Kirschner K, Schaub MT, et al. SC3: consensus clustering of single-cell RNA-seq data. Nat Methods. 2017;14(5):483-486.
40. Villani A-C, Satija R, Reynolds G, et al. Single-cell RNA-seq reveals new types of human blood dendritic cells, monocytes, and progenitors. Science. 2017;356(6335):eaah4573.
41. Olingy CE, Dinh HQ, Hedrick CC. Monocyte heterogeneity and functions in cancer. J Leukoc Biol. 2019;106(2):309-322.
42. Taylor MR, Cole SW, Strom J, et al. Unfavorable transcriptome profiles and social disadvantage in hematopoietic cell transplantation: a CIBMTR analysis. Blood Adv. 2023;7(22):6830-6838.

43. Cole SW. The Conserved Transcriptional Response to Adversity. Curr Opin Behav Sci. 2019;28:31-37.
44. Knight JM, Rizzo JD, Hari P, et al. Propranolol inhibits molecular risk markers in HCT recipients: a phase 2 randomized controlled biomarker trial. Blood Adv. 2020;4(3):467-476.
45. Pui C-H, Yang JJ, Hunger SP, et al. Childhood Acute Lymphoblastic Leukemia: Progress Through Collaboration. J Clin Oncol. 2015;33(27):2938-2948.
46. Johnson SB, Riley AW, Granger DA, Riis J. The science of early life toxic stress for pediatric practice and advocacy. Pediatrics. 2013;131(2):319-327.
47. Witkowski MT, Kousteni S, Aifantis I. Mapping and targeting of the leukemic microenvironment. J Exp Med. 2020;217(2):e20190589.
48. Chu Y, Dai E, Li Y, et al. Pan-cancer T cell atlas links a cellular stress response state to immunotherapy resistance. Nat Med. 2023;29(6):1550-1562.
49. Manoleras AV, Sloan EK, Chang A. The sympathetic nervous system shapes the tumor microenvironment to impair chemotherapy response. Front Oncol. 2024;14:1460493.
50. Newman H, Paul M, Kairalla J, et al. Feasibility of collecting social determinants of health data in the frontline pediatric acute lymphoblastic leukemia (ALL) trial AALL1731: A report from the Children's oncology group. Blood. 2025;146(Supplement 1):2742.

TABLES

Table 1. Sociodemographic, clinical, and molecular characteristics at time of diagnosis for N=14 children with standard-risk *de novo* B-cell ALL. Poverty was defined *a priori* as both parent-reported low-income (annual household income <200% Federal Poverty Level [FPL]) and the presence of household material hardship ([HMH]; food, housing, or utility insecurity).

Sample Number	Sex	Age at diagnosis	Source	*ETV6::RUNX1*	Cytogenetics	HMH	Income, $	% FPL
Unexposed 1	F	4y	Bone Marrow	neg	High hyperdiploid	No	350K	>200%
Unexposed 2	M	3y	Bone Marrow	neg	High hyperdiploid	No	100K	>200%
Unexposed 3	M	15y	Bone Marrow	neg	Unremarkable	Unknown	125K	>200%
Unexposed 4	F	3y	Bone Marrow	neg	High hyperdiploid	Unknown	200K	>200%
Unexposed 5	F	2y	Bone Marrow	pos	Unremarkable	Unknown	113K	>200%
Unexposed 6	M	4y	Bone Marrow	pos	Unremarkable	Unknown	150K	>200%
Unexposed 7	F	2y	Bone Marrow	neg	High hyperdiploid	Unknown	200K	>200%
Poverty-exposed 1	M	2y	Bone Marrow	pos	Unremarkable	Yes	6K	<200%
Poverty-exposed 2	M	2y	Bone Marrow	neg	High hyperdiploid	Yes	7K	<200%
Poverty-exposed 3	M	15y	Bone Marrow	neg	Failed	Yes	14K	<200%
Poverty-exposed 4	M	3y	Bone Marrow	pos	Unremarkable	Yes	0K	<200%
Poverty-exposed 5	M	2y	Bone Marrow	pos	Unremarkable	Yes	10K	<200%
Poverty-exposed 6	F	5y	Bone Marrow	neg	High hyperdiploid	Yes	21K	<200%
Poverty-exposed 7	M	3y	Bone Marrow	pos	Unremarkable	Yes	10K	<200%

FIGURE LEGENDS

Figure 1. Single-cell transcriptome analysis of pediatric B-ALL in poverty-exposed versus unexposed children. (A) Schematic representation depicting the cohort, sample collection, processing, and sorting of cells for single-cell transcriptional profiling using SMART-seq2 protocol. (B) t-stochastic network embedding (t-SNE) clustering of single-cell gene expression (ND = normal donor; pov.-exp. = poverty-exposed, un-exp. = unexposed). (C) t-stochastic network embedding (t-SNE) clustering of single-cell gene expression colored by cell type (human cell atlas). (D) Expression of marker genes for each cell type is depicted as a heatmap. (E) Violin plots of canonical marker genes for white blood cells (CD45+), T-cells, B-cells, monocytes, NK-cells, and B-ALL blasts.

Figure 2. Leukemia blasts from poverty-exposed pediatric B-ALL patients carry distinct transcriptome features. (A) t-SNE annotated by known cytogenetic abnormalities (ND – normal donor). (B) t-SNE plot of malignant cells clustered based on expression of known progenitor and lymphoid differentiation signatures (see methods). (C) t-SNE annotated by poverty-exposure (pov.-exp. = poverty-exposed, un-exp. = unexposed). (D) Stacked bar plot depicts relative percentage of single leukemic cells from poverty-exposed and unexposed patients. (E) GSEA analysis comparing clusters enriched in single cells from poverty-exposed or unexposed patients (poverty-exposed = clusters 3, 4, 5 and 7, unexposed = clusters 1, 2, and 6). (F) Expression of poverty-exposed and unexposed signatures (see methods) in bulk RNA-seq (n = 14; *p<0.05, **p<0.01*).* using Wilcoxon rank test).

Figure 3. Distinct monocyte population in poverty-exposed versus unexposed patients. (A) Violin plots demonstrating expression of *CD14* and *CD16* (*FCGFR3A*) in normal donor (normal), monocytes from leukemia patients or poverty-exposed and unexposed patients, respectively (*p<0.05, **p<0.01, ****p<0.0001 by two-sided Wilcoxon test). (B) Heatmap depicting the expression of marker genes per cluster. (C) Functional enrichment of different clusters using FSGEA (see methods). (D) Box plots showing expression of inflammatory and interferon CTRA signatures (***p<0.001 by two-sided Wilcoxon test).

Figure 4. B-cell populations in poverty-exposed and unexposed children with B-ALL compared to normal donors. (A) t-SNE plot depicting 5 B-cell clusters by Louvain clustering. (B) t-SNE plot depicting distribution of B-cells from normal donors (ND), poverty-exposed (pov.-exp.) and unexposed (un-exp.) children with B-ALL. (C) Bar plot depicting relative proportions of B-cell subtypes as annotated by human cell atlas per cluster. (D) Bar plot depicting relative proportions of B-cells from normal donors (ND), poverty-exposed (pov.-exp.) and unexposed (un-exp.) children with B-ALL across 5 clusters.

Figure 5. CD4+ T-cell populations in poverty-exposed and unexposed children with B-ALL compared to normal donors. (A) t-SNE plot depicting T-cells annotated as CD4+ or CD8+ T-cells (human cell atlas), respectively. (B) t-SNE of CD4+ T-cells separating into 4 clusters by Louvain clustering. (C) Bar plot depicting relative proportions of CD4+ T-cell subtypes as annotated by human cell atlas. (D) Heatmap depicting expression of marker genes of CD4+ T-cells per cluster. (E) Bar plot depicting relative proportions of CD4+ T-cells from normal donors (ND), poverty-exposed (pov.-exp.) and unexposed (un-exp.) children with B-ALL across 4 clusters.

Figure 6. Distinct CD8+ T-cell subpopulations in poverty-exposed compared to unexposed children with B-ALL. (A) t-SNE plot of CD8+ T-cells separating into 2 clusters by Louvain clustering. (B) Bar plot depicting relative proportions of CD8+ T-cells from normal

donors (ND), poverty-exposed (pov.-exp.) and unexposed (un-exp.) children with B-ALL across 2 clusters. (C) Heatmap depicting marker gene expression of CD8+ T-cells per cluster. (D) Gene expression signature scores for naïve, cytotoxic and exhaustion CD8+ T-cells in cluster 1 versus cluster 2 (see methods).

Figure 1

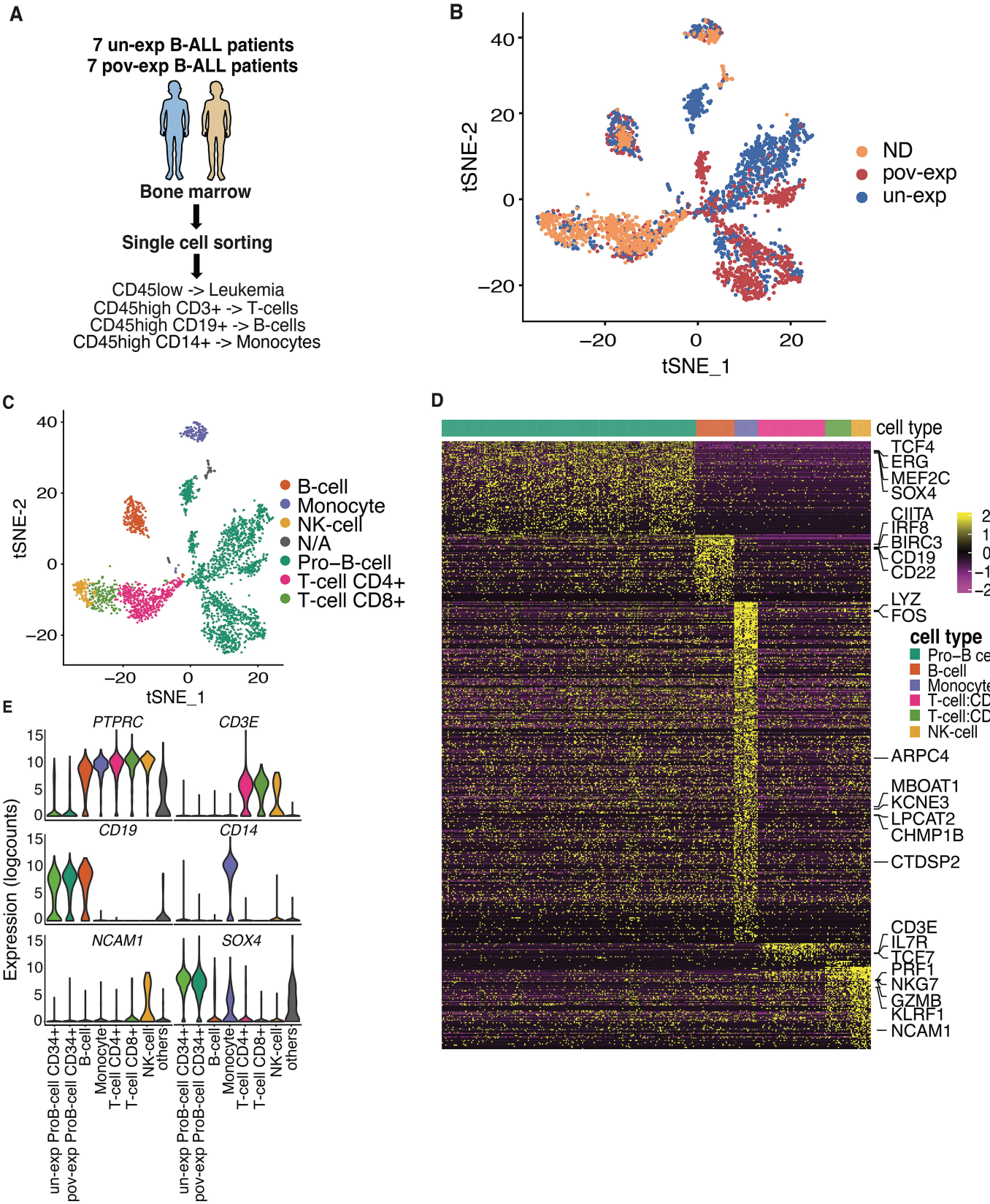
A
7 un-exp B-ALL patients
7 pov-exp B-ALL patients
Bone marrow
Single cell sorting
CD45low -> Leukemia
CD45high CD3+ -> T-cells
CD45high CD19+ -> B-cells
CD45high CD14+ -> Monocytes
B
tSNE-2
tSNE_1
ND
pov-exp
un-exp
C
tSNE-2
tSNE_1
B-cell
Monocyte
NK-cell
N/A
Pro−B-cell
T-cell CD4+
T-cell CD8+
D
cell type
TCF4
ERG
MEF2C
SOX4
CIITA
IRF8
BIRC3
CD19
CD22
LYZ
FOS
cell type
Pro−B cell
B-cell
Monocyte
T-cell:CD4+
T-cell:CD8+
NK-cell
ARPC4
MBOAT1
KCNE3
LPCAT2
CHMP1B
CTDSP2
CD3E
IL7R
TCF7
PRF1
NKG7
GZMB
KLRF1
NCAM1
E
PTPRC
CD3E
CD19
CD14
NCAM1
SOX4
Expression (logcounts)
un-exp ProB-cell CD34+
pov-exp ProB-cell CD34+
B-cell
Monocyte
T-cell CD4+
T-cell CD8+
NK-cell
others

Figure 2

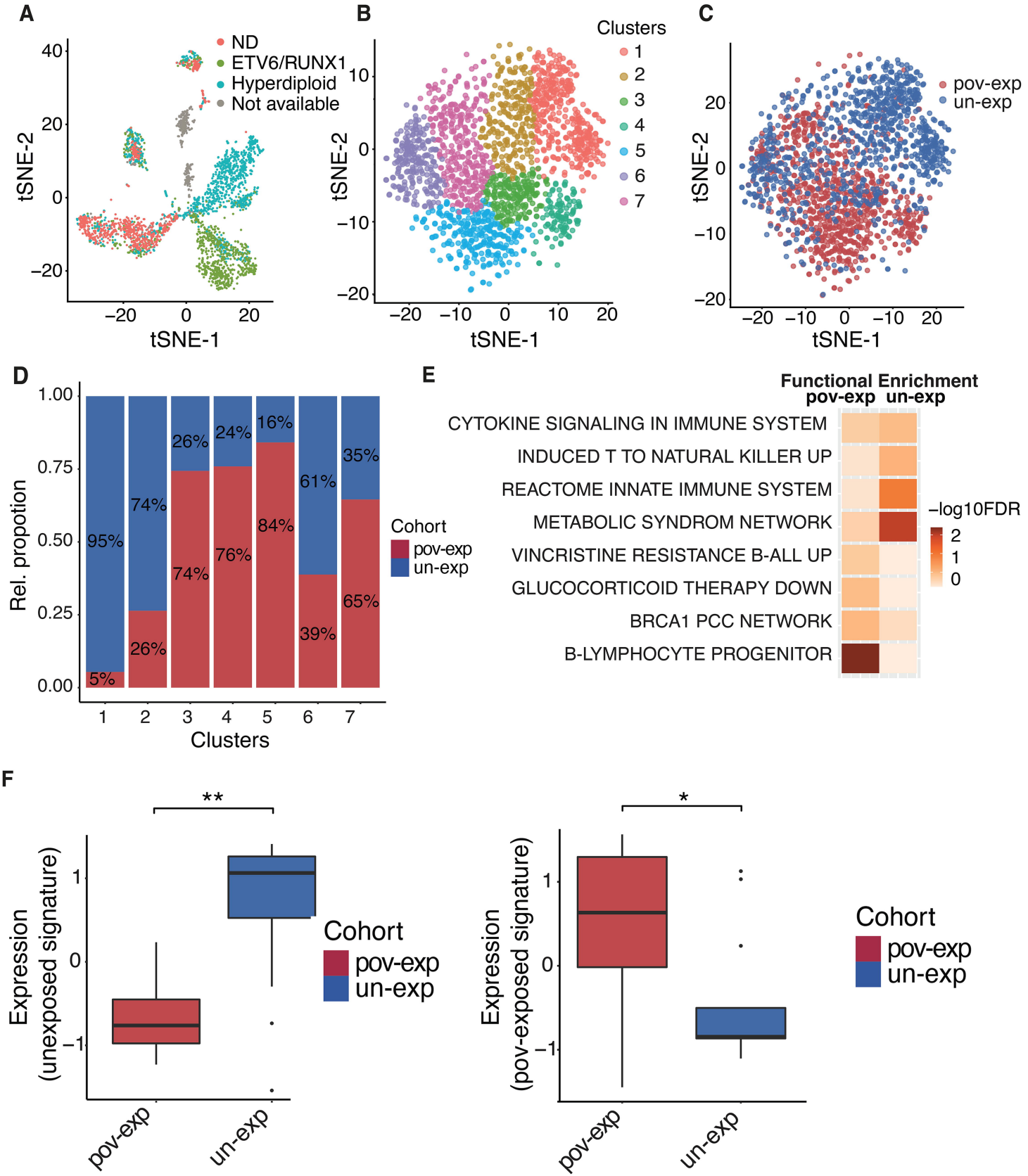
A
ND
ETV6/RUNX1
Hyperdiploid
Not available
tSNE-2
tSNE-1
B
Clusters
1
2
3
4
5
6
7
tSNE-2
tSNE-1
C
pov-exp
un-exp
tSNE-2
tSNE-1
D
Rel. propotion
Clusters
Cohort
pov-exp
un-exp
95%
5%
74%
26%
26%
74%
24%
76%
16%
84%
61%
39%
35%
65%
E
Functional Enrichment
pov-exp un-exp
CYTOKINE SIGNALING IN IMMUNE SYSTEM
INDUCED T TO NATURAL KILLER UP
REACTOME INNATE IMMUNE SYSTEM
METABOLIC SYNDROM NETWORK
VINCRISTINE RESISTANCE B-ALL UP
GLUCOCORTICOID THERAPY DOWN
BRCA1 PCC NETWORK
B-LYMPHOCYTE PROGENITOR
−log10FDR
F
Expression (unexposed signature)
Cohort
pov-exp
un-exp
Expression (pov-exposed signature)
Cohort
pov-exp
un-exp

Figure 3

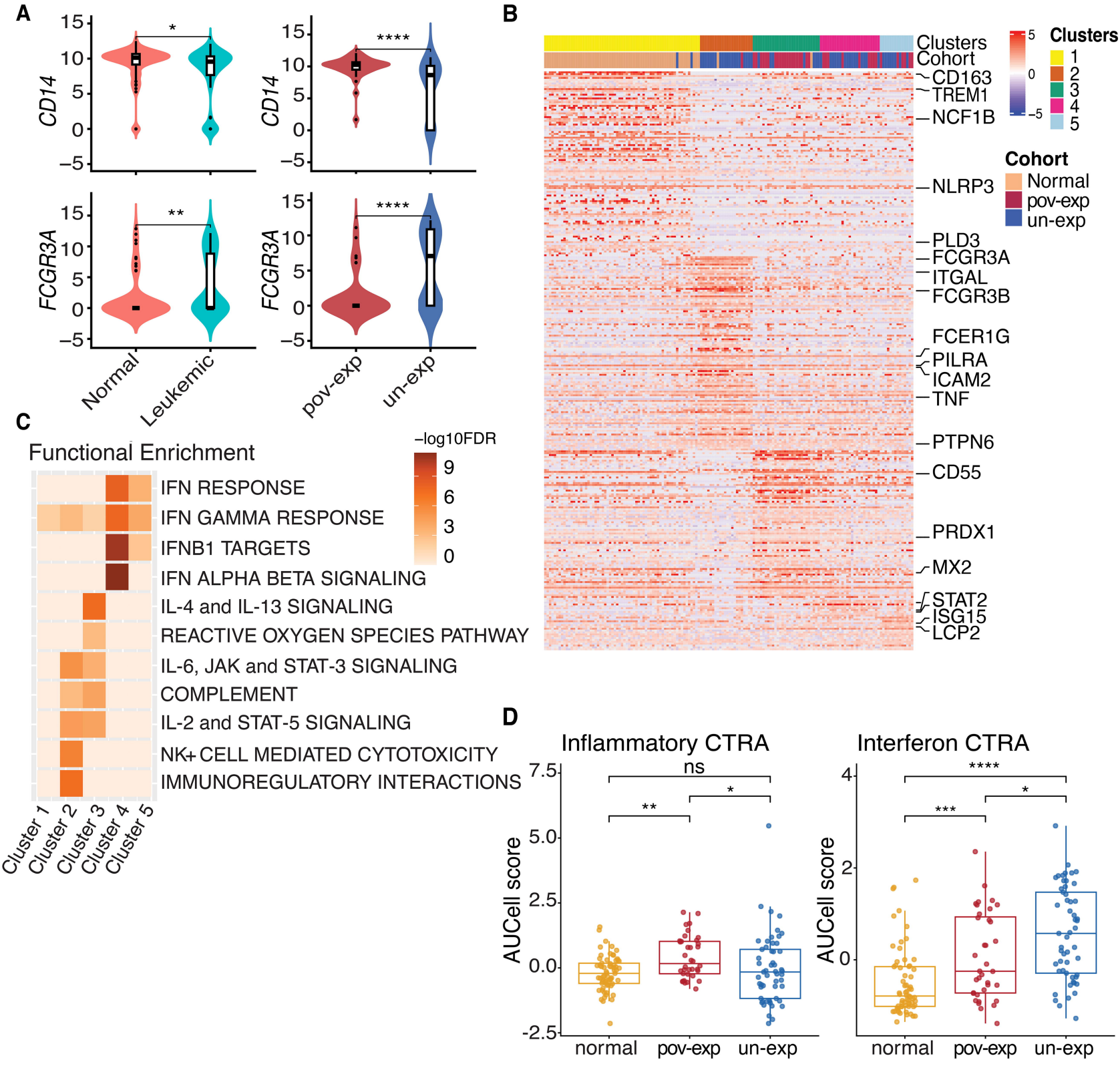
A
CD14
FCGR3A
*
**
****
Normal
Leukemic
pov-exp
un-exp
B
Clusters
Cohort
CD163
TREM1
NCF1B
NLRP3
PLD3
FCGR3A
ITGAL
FCGR3B
FCER1G
PILRA
ICAM2
TNF
PTPN6
CD55
PRDX1
MX2
STAT2
ISG15
LCP2
Normal
pov-exp
un-exp
C
Functional Enrichment
−log10FDR
IFN RESPONSE
IFN GAMMA RESPONSE
IFNB1 TARGETS
IFN ALPHA BETA SIGNALING
IL-4 and IL-13 SIGNALING
REACTIVE OXYGEN SPECIES PATHWAY
IL-6, JAK and STAT-3 SIGNALING
COMPLEMENT
IL-2 and STAT-5 SIGNALING
NK+ CELL MEDIATED CYTOTOXICITY
IMMUNOREGULATORY INTERACTIONS
Cluster 1
Cluster 2
Cluster 3
Cluster 4
Cluster 5
D
Inflammatory CTRA
Interferon CTRA
AUCell score
ns
normal
pov-exp
un-exp

Figure 4

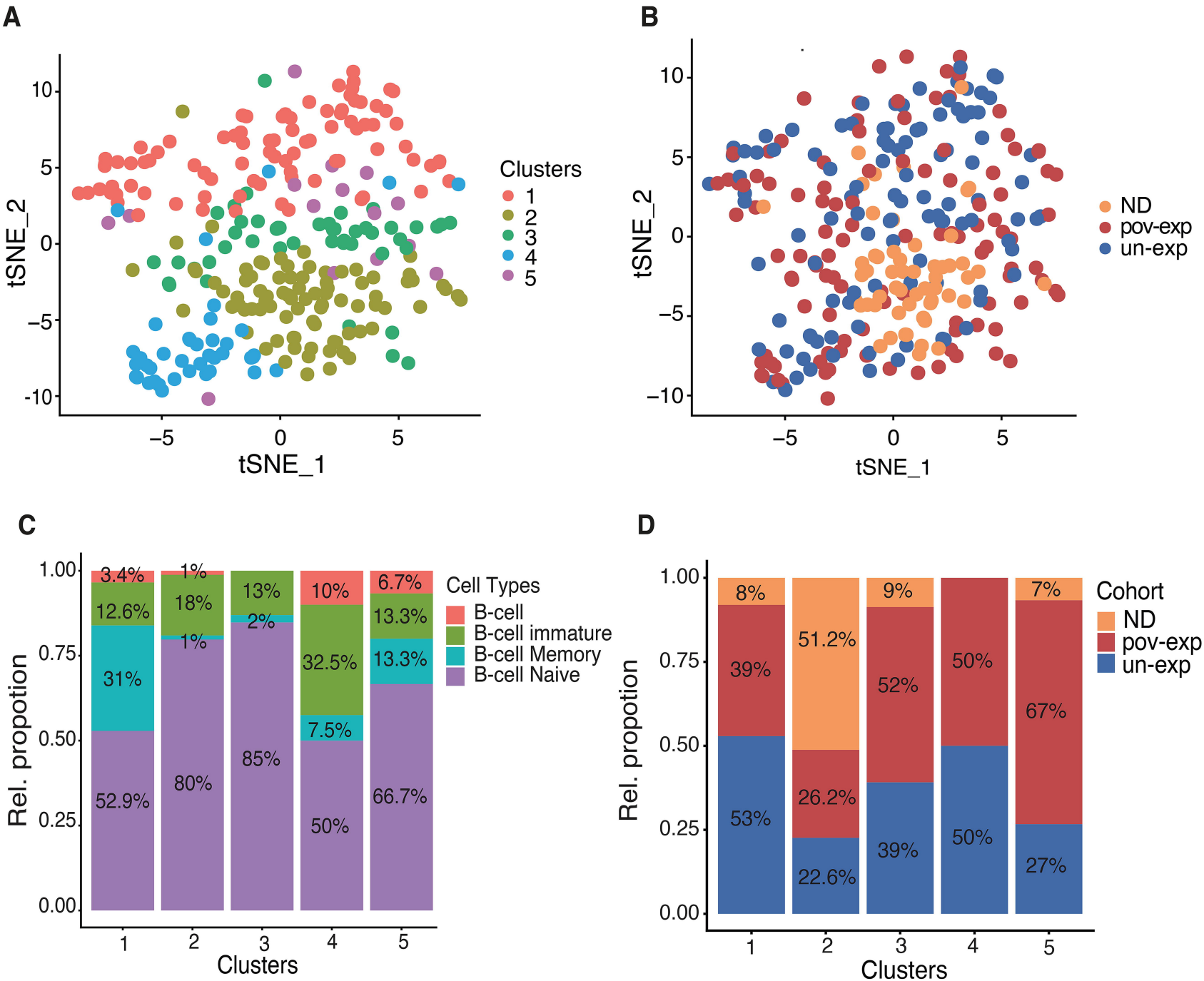
A
tSNE_2
tSNE_1
Clusters
1
2
3
4
5
B
tSNE_2
tSNE_1
ND
pov-exp
un-exp
C
Rel. propotion
Clusters
Cell Types
B-cell
B-cell immature
B-cell Memory
B-cell Naive
3.4%
12.6%
31%
52.9%
1%
18%
1%
80%
13%
2%
85%
10%
32.5%
7.5%
50%
6.7%
13.3%
13.3%
66.7%
D
Rel. propotion
Clusters
Cohort
ND
pov-exp
un-exp
8%
39%
53%
51.2%
26.2%
22.6%
9%
52%
39%
50%
50%
7%
67%
27%

Figure 5

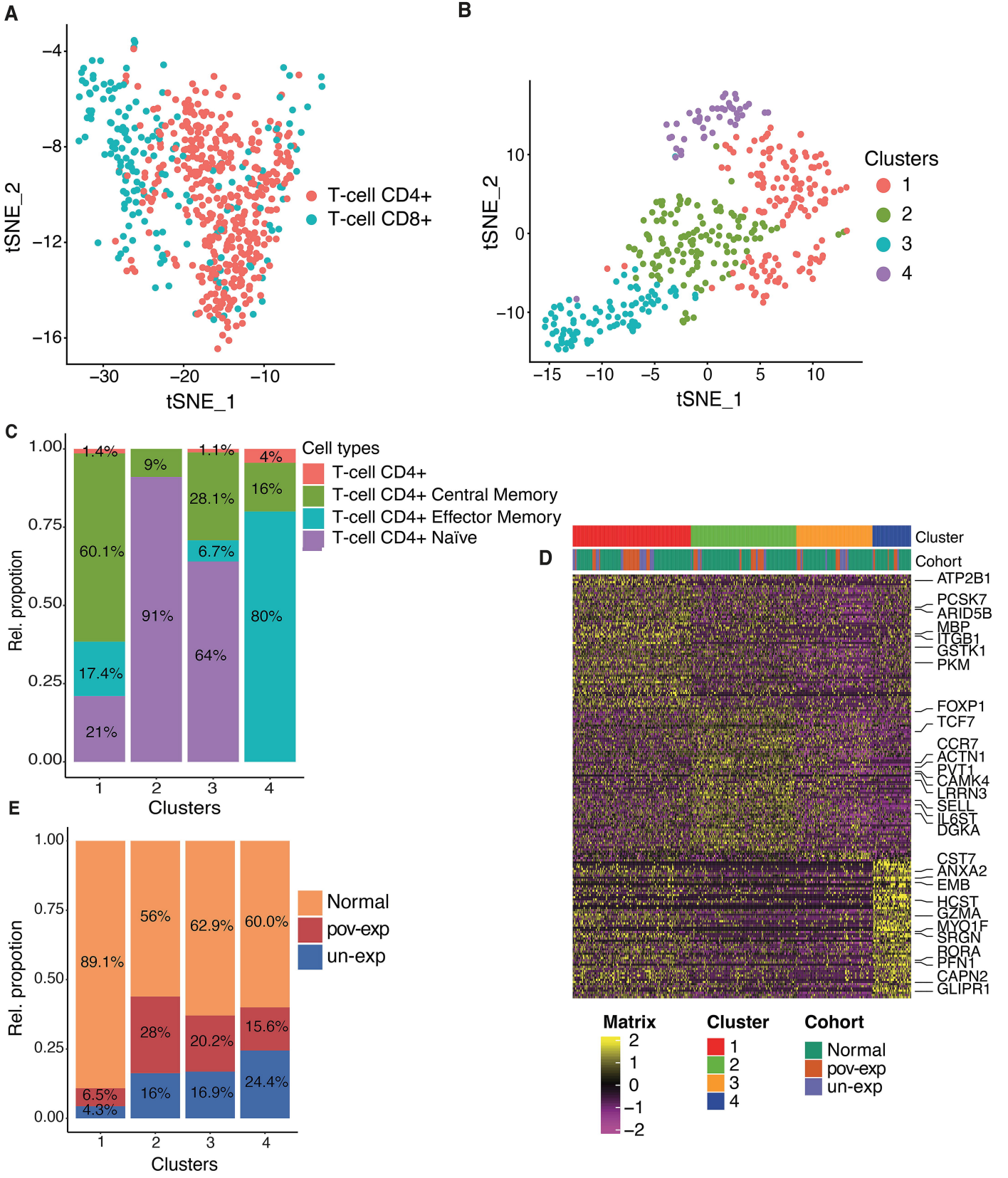
A
tSNE_2
tSNE_1
T-cell CD4+
T-cell CD8+
B
tSNE_2
tSNE_1
Clusters
1
2
3
4
C
Rel. propotion
Clusters
Cell types
T-cell CD4+
T-cell CD4+ Central Memory
T-cell CD4+ Effector Memory
T-cell CD4+ Naïve
1.4%
60.1%
17.4%
21%
9%
91%
1.1%
28.1%
6.7%
64%
4%
16%
80%
D
Cluster
Cohort
ATP2B1
PCSK7
ARID5B
MBP
ITGB1
GSTK1
PKM
FOXP1
TCF7
CCR7
ACTN1
PVT1
CAMK4
LRRN3
SELL
IL6ST
DGKA
CST7
ANXA2
EMB
HCST
GZMA
MYO1F
SRGN
RORA
PFN1
CAPN2
GLIPR1
Matrix
Cluster
Cohort
Normal
pov-exp
un-exp
E
Rel. propotion
Clusters
Normal
pov-exp
un-exp
89.1%
6.5%
4.3%
56%
28%
16%
62.9%
20.2%
16.9%
60.0%
15.6%
24.4%

Figure 6

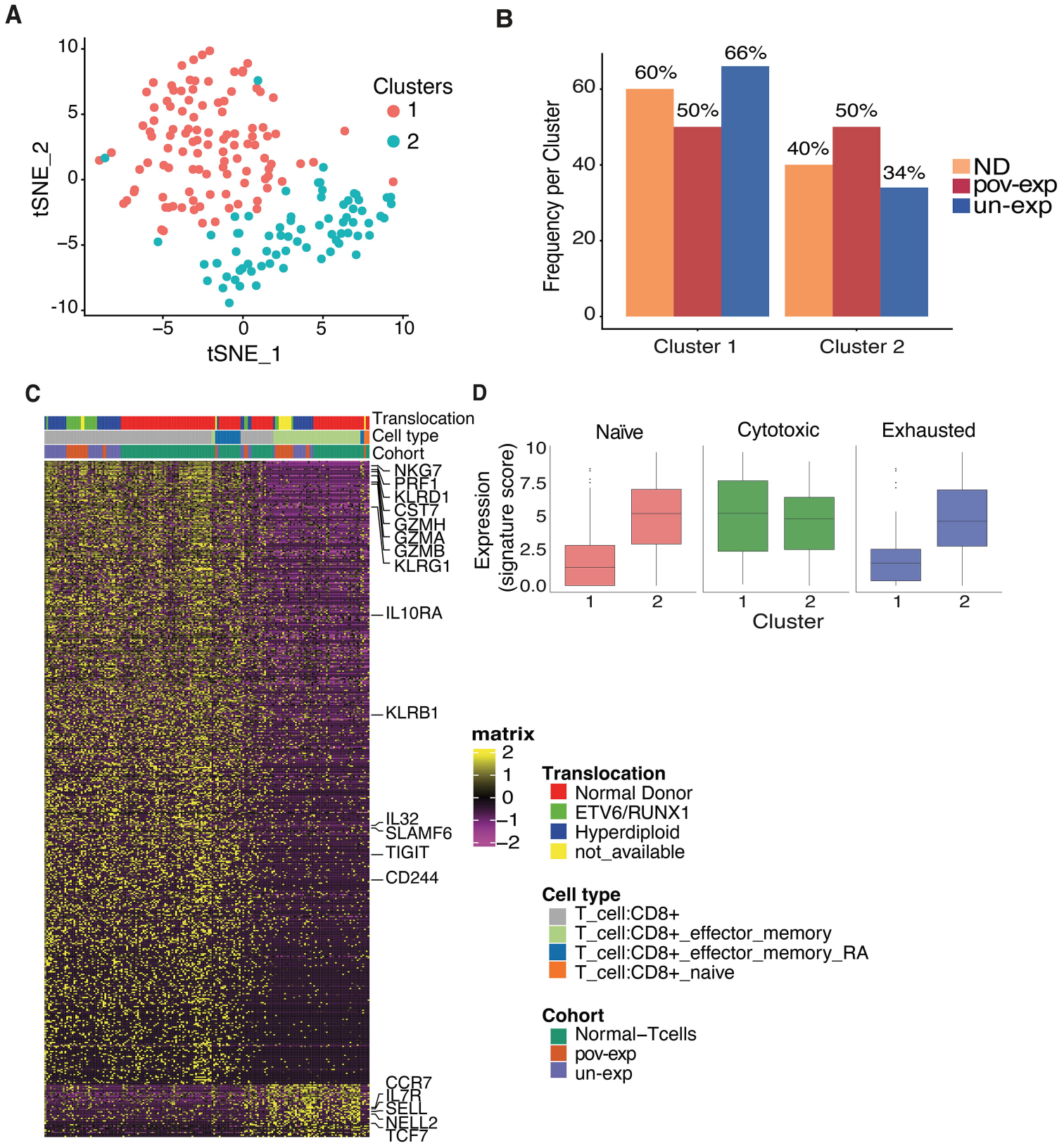
A
Clusters
1
2
tSNE_2
tSNE_1
B
Frequency per Cluster
60%
50%
66%
40%
50%
34%
ND
pov-exp
un-exp
Cluster 1
Cluster 2
C
Translocation
Cell type
Cohort
NKG7
PRF1
KLRD1
CST7
GZMH
GZMA
GZMB
KLRG1
IL10RA
KLRB1
IL32
SLAMF6
TIGIT
CD244
CCR7
IL7R
SELL
NELL2
TCF7
matrix
Translocation
Normal Donor
ETV6/RUNX1
Hyperdiploid
not_available
Cell type
T_cell:CD8+
T_cell:CD8+_effector_memory
T_cell:CD8+_effector_memory_RA
T_cell:CD8+_naive
Cohort
Normal–Tcells
pov-exp
un-exp
D
Naïve
Cytotoxic
Exhausted
Expression (signature score)
Cluster

SUPPLEMENTAL METHODS AND MATERIALS

SUPPLEMENTARY METHODS

Detailed flow cytometry antibodies

B-ALL samples were stained for CD45 FITC (Thermo Fisher Scientific Cat# 11-0459-41, RRID: AB_10854279), T-cells for CD3 PerCP-Cy5.5 (Thermo Fisher Scientific Cat# 45-0037-41, RRID:AB_10548354), monocytes for CD14 APC-Cy7 (BD Biosciences Cat# 557831, RRID:AB_396889), B-cells for CD19 PE (BioLegend Cat# 302208, RRID:AB_314238).

Detailed scRNA-seq library preparation

Full-length single-cell RNA-seq libraries were prepared using the SMART-seq2 protocol[1]. RNA was purified by RNAClean XP beads (Beckman Coulter) and reverse transcribed using Maxima RNAse H-minus (Thermo Fisher Scientific) in the presence of oligo-dT30VN, template-switching oligonucleotides, and betaine. cDNA was then amplified using the KAPA Hifi Hotstart ReadyMix (Kappa Biosystems) and ISPCR primers with the following protocol: 98°C - 3 min, 24 x [98°C - 15s, 67°C - 20s, 72°C – 6min], 72°C - 5 min. After purification with Agencourt Ampure XP beads (Beckmann Coulter), product size distribution was assessed on a Bioanalyzer using a High Sensitivity DNA Kit (Agilent Technologies). The quantity of amplified cDNA was determined by Qubit (Thermo Fisher Scientific). 0.15 ng of the product was fragmented and indexed using Nextera XT and Nextera PCR primers (Illumina). Following another purification step, quality control was assessed by Bioanalyzer High Sensitivity DNA Kit.

Processing of scRNA-seq reads

Following sequencing reads were trimmed using trimmomatic[2] and aligned to the hg19 version of the genome using STAR aligner[3] with following parameters '– twopassMode Basic –alignIntronMax 100000 –alignMatesGapMax 100000 –alignSJDBoverhangMin 10 –alignSJstitchMismatchNmax 5 -1 5 5'. Raw counts and normalized TPM values were obtained from the aligned bam file using HTSeq and RSEM, respectively[3,4].

Quality filtering of scRNA-seq data

To filter out low quality cells from our dataset, we used four different parameters – i) library size, ii) number of genes detected, iii) percentage of reads mapping to house-keeping genes, and iv) percentage of reads mapping to mitochondrial genes (Supplemental Figure S1A). QC parameters were calculated for each cell using addPerCellQC function from *scater*[5]. Then, outlier cells were identified for all defined metrics, based on the median absolute deviation (MAD) by calculation of the median of each metric across all samples. 1,347 single cells (from 4,513 samples) with median absolute deviations (M.A.D's) of more than 3 were identified as low quality cells (Supplemental Figure S1B). Cells that were detected as outliers were removed from the dataset (Supplemental Figure S1 B-C). This resulted in retention of 3,166 high-quality cells for further downstream analyses (Supplemental Figure S1C). On average, around 3,618 genes were detected in 25% of cells (Supplemental Figure S1C). The variance in the dataset was used to systematically investigate the contribution of various technical factors and batch effects. The proportion of variance due to cohort, total number of genes detected, percentage of housekeeping and mitochondrial genes and library size were found to be low (Supplemental Figure S1D).

Clustering of scRNA-seq profiles and identification of cell types

For comparison, analyses included data from 719 normal donor cells (after quality control) derived from published datasets[6,7]. Clustering of high-quality cells was performed using the Louvain algorithm for t-SNE representation[8]. To rule out the possibility of clusters being purely driven by cell-cycle, each individual cell was analyzed for expression of G1, G2M and S phase markers to

predict the cell-cycle phase using Seurat, and cell cycle phases (S.Score, G2M.Score) were regressed out from the dataset using the Seurat ScaleData function[9]. Cell types were initially inferred using the Human primary cell atlas (HPCA) panel in the Bioconductor package SingleR (https://github.com/dviraran/SingleR)[10], cell identity was confirmed using the findMarker function in the scran package, and clusters were annotated as CD4+ T-cells, CD8+ T-cells, NK cells, myeloid, B- or Pro-B-cells (Figure 1). Cluster 15 included marker genes from several other cell types and was therefore labelled as "not annotated" (N/A). Cells were clustered based on expression of signatures for hematopoietic stem cells (HSC, 25 genes), common lymphoid progenitors (CLP, 31 genes), pro-B (169 genes), immature B (19 genes) and naïve-B cells (33 genes) that were derived from the literature (Figure 2, Table S1)[7], using AUCell (Version 1.12.0 R-package)[11]. Single-cell consensus clustering SC3[12] was used with ks set to 5 (Figure 3). For comparison of pediatric versus adult bone marrow composition, we downloaded single cell RNA-seq data from pediatric bone marrow from GSE132509[6,7]. We used Read10x() function[9] to read and create a raw count matrix and then integrated the count matrix of the pediatric dataset with our adult raw count matrix. To annotate the cell types in the created dataset we used the Azimuth R package. Subsequently, visualization was carried out using the ggboxplot function from the ggpubr and ggplot2 packages in R.

Detection of copy number variations from scRNA-seq and cytogenetics

The copy number variants of individual cells were inferred from the scRNA-seq data using InferCNV (https://github.com/broadinstitute/inferCNV) using normal donor B-cells (see above) as reference.

Gene set enrichment analysis (GSEA)

We performed GSEA using fgsea (version 1.18.0 R-package)[13]. We first annotated genes (produced by findMarker function) with Entrez ID using EnsDb.Hsapiens.v86 (version 2.99.0 R-package). Then, gene lists were ranked by $\log_2$fold (0.58) change or FDR values before subjecting to fgseaMultilevel function. FDR-adjusted $P < 0.05$ was considered significant. Genes for which there was no Entrez IDs were excluded.

Scoring of expression signatures in bulk and single cells

To generate poverty-exposed versus unexposed signatures, we compiled signatures by intersecting marker genes with expressed genes of enriched GSEA signatures (Figure 2E) and scored their expression in bulk using AUCell (Version 1.28.0)[11], using aucMaxRank set to default value of 0.05.

Monocyte subsets were scored employing AUCell[11] for published myeloid expression signatures and published conserved signatures of adversity[14–16]. Upregulated genes: *IL1A, IL1B, IL6, IL8/CXCL8, TNF, PTGS1, PTGS2, FOS, FOSB, FOSL1, FOSL2, JUN, JUNB, JUND, NFKB1, NFKB2, REL, RELA*, and *RELB*. Downregulated genes: *GBP1, IFI27, IFI27L1-2, IFI30, IFI35, IFI44, IFI44L, IFI6, IFIH1, IFIT1-3, IFIT5, IFIT1B, IFITM1-3, IFITM4P, IFITM5, IFNB1, IRF2, IRF7-8, MX1-2, OAS1-3, OASL, JCHAIN,* and *IGLL1*[17].

T-cell exhaustion, naïve and cytotoxic scores were calculated using an average relative expression of key marker genes from the literature[18]. The exhaustion score was defined as the difference between average relative expression of exhaustion markers – *PDCD1, TIGIT, LAG3, HAVCR2, CTLA4* and naïve markers; *CCR7, TCF7, LEF1* and *SELL*. The cytotoxic score was defined as the difference between average relative expression of cytotoxic markers; *NKG7, CCL4, CST7, PRF1, GZMA, GZMB, IFNG, CCL3* and naïve markers.

Scoring relative proportions of poverty-exposed and unexposed signatures in bulk RNA-seq

Output for bulk RNA-seq was generated in FASTQ format (http://www.bioinformatics.babraham.ac.uk/projects/fastqc) and mapped to the human genome GRCh37 (hg19). Gene expression at transcript-level resolution was calculated using RSEM (v1.2.31) after alignment with STAR[3] (and duplicates marked with Picard (https://broadinstitute.github.io/picard/). Processed bulk RNA-seq read counts from patient samples undergoing treatment on 16-001 were obtained from GSE181157, and used to calculate correlation of the collapsed poverty-exposed and unexposed signatures[19]. We calculated correlations for gene set variation scores using the GSVA R package[20] to compute the statistical significance differences for the two gene set signatures of poverty-exposed and unexposed by transforming DESeq2-normalized (size factor–adjusted and log-transformed) gene expression data into enrichment scores. Given the imbalance of the two groups, we randomly sampled n=6 per group, repeating random sampling 10x (Supplemental Figure S8).

To analyze relative enrichment of poverty-exposed/unexposed signatures we used the CIBERSORTx web portal (https://cibersort.stanford.edu)[21], using a custom reference matrix file.

REFERENCES

1. Picelli S, Faridani OR, Björklund AK, Winberg G, Sagasser S, Sandberg R. Full-length RNA-seq from single cells using Smart-seq2. Nat Protoc 2014;9(1):171–181.
2. Bolger AM, Lohse M, Usadel B. Trimmomatic: a flexible trimmer for Illumina sequence data. Bioinformatics 2014;30(15):2114–2120.
3. Dobin A, Davis CA, Schlesinger F, et al. STAR: ultrafast universal RNA-seq aligner. Bioinformatics 2013;29(1):15–21.
4. Li B, Dewey CN. RSEM: accurate transcript quantification from RNA-Seq data with or without a reference genome. BMC Bioinformatics 2011;12323.
5. McCarthy DJ, Campbell KR, Lun ATL, Wills QF. Scater: pre-processing, quality control, normalization and visualization of single-cell RNA-seq data in R. Bioinformatics 2017;33(8):1179–1186.
6. Anand P, Guillaumet-Adkins A, Dimitrova V, et al. Single-cell RNA-seq reveals developmental plasticity with coexisting oncogenic states and immune evasion programs in ETP-ALL. Blood 2021;137(18):2463–2480.
7. Frede J, Anand P, Sotudeh N, et al. Dynamic transcriptional reprogramming leads to immunotherapeutic vulnerabilities in myeloma. Nat Cell Biol 2021;23(11):1199–1211.
8. Kobak D, Berens P. The art of using t-SNE for single-cell transcriptomics. Nat Commun 2019;10(1):5416.
9. Stuart T, Butler A, Hoffman P, et al. Comprehensive Integration of Single-Cell Data. Cell 2019;177(7):1888-1902.e21.
10. Aran D, Looney AP, Liu L, et al. Reference-based analysis of lung single-cell sequencing reveals a transitional profibrotic macrophage. Nat Immunol 2019;20(2):163–172.
11. Aibar S, González-Blas CB, Moerman T, et al. SCENIC: single-cell regulatory network inference and clustering. Nat Methods 2017;14(11):1083–1086.
12. Kiselev VY, Kirschner K, Schaub MT, et al. SC3: consensus clustering of single-cell RNA-seq data. Nat Methods 2017;14(5):483–486.
13. Korotkevich G, Sukhov V, Budin N, Shpak B, Artyomov MN, Sergushichev A. Fast gene set enrichment analysis. 2021;060012.
14. Villani A-C, Satija R, Reynolds G, et al. Single-cell RNA-seq reveals new types of human blood dendritic cells, monocytes, and progenitors. Science 2017;356(6335):eaah4573.

15. Taylor MR, Cole SW, Strom J, et al. Unfavorable transcriptome profiles and social disadvantage in hematopoietic cell transplantation: a CIBMTR analysis. Blood Adv 2023;7(22):6830–6838.
16. Cole SW. The Conserved Transcriptional Response to Adversity. Curr Opin Behav Sci 2019;2831–37.
17. Knight JM, Rizzo JD, Hari P, et al. Propranolol inhibits molecular risk markers in HCT recipients: a phase 2 randomized controlled biomarker trial. Blood Adv 2020;4(3):467–476.
18. Heng TSP, Painter MW, Immunological Genome Project Consortium. The Immunological Genome Project: networks of gene expression in immune cells. Nat Immunol 2008;9(10):1091–1094.
19. Tran TH, Langlois S, Meloche C, et al. Whole-transcriptome analysis in acute lymphoblastic leukemia: a report from the DFCI ALL Consortium Protocol 16-001. Blood Adv 2022;6(4):1329–1341.
20. Hänzelmann S, Castelo R, Guinney J. GSVA: gene set variation analysis for microarray and RNA-seq data. BMC Bioinformatics 2013;147.
21. Newman AM, Steen CB, Liu CL, et al. Determining cell type abundance and expression from bulk tissues with digital cytometry. Nat Biotechnol 2019;37(7):773–782.

SUPPLEMENTAL FIGURE AND TABLE LEGENDS

SUPPLEMENTAL FIGURE LEGENDS

Supplemental Figure S1. Quality filtering of scRNA-seq dataset. (A) Distribution of features in the unfiltered dataset – (i) library size per cell, (ii) number of genes detected in each cell, (iii) percentage of counts mapping to house-keeping genes and (iv) percentage of counts mapping to mitochondrial genes in each cell in all cells sequenced. (B) The distribution of the features after filtering out the cells detected to be outlier. (C) Scatter plot depicting the quality of data from the remaining 3,166 cells through expression frequency and mean read counts per gene. (D) the density plot depicting the contribution of various technical factors contributing to the total variation observed in entire dataset.

Supplemental Figure S2. Cell Type Proportion Adult vs Pediatric. (A) B-cell proportions. (B) T-cell proportions. (C) Monocyte proportions.

Supplemental Figure S3. Clustering and inferred human cell atlas annotations. (A) 17 clusters identified by Seurat package (v5.4.0) in R and cell embedding using t-Stochastic Neighbor Embedding (t-SNE) is used for dimension reduction and visualization. (B) Lineage annotation of the single-cell profiles according to Human Cell Atlas (HCA) dataset.

Supplemental Figure S4. Copy Number Variations (CNV) called in single leukemia or normal cells. The copy number variants were inferred from the scRNA-seq data using InferCNV. The detected CNVs were compared to the cytogenetics report obtain as clinical routine (Table 1).

Supplemental Figure S5. Genetic features in leukemic single cell clusters. (A) t-SNE plot color-coded based on presence of genetic feature (hyperdiploid or *ETV6::RUNX1* translocated). (B) Bar plot representing relative proportions of genetic features across the 7 leukemic clusters. (C, D) Stacked bar plots depicting relative percentages of single leukemic cells from poverty-exposed and unexposed patients with either *ETV6::RUNX1* translocations (C) or hyperdiploidy (D).

Supplemental Figure S6. *ETV6::RUNX1* and hyperdiploid vs. poverty exposed and un-exposed signatures. (A, B) Violin plots depicting gene expression signature scores within (A) *ETV6::RUNX1* unexposed (left) and poverty exposed (right), and (B) hyperdiploid unexposed (left), poverty exposed (right). (C, D) Box plots showing AUCell scores of poverty exposed or unexposed signatures in *ETV6::RUNX1* (C) or hyperdiploid samples (D).

Supplemental Figure S7. Expression of poverty-exposed and unexposed signatures in bulk leukemia RNA-seq. Signature scores of poverty-exposed and unexposed pathways using CIBERSORTx (see methods).

Supplemental Figure S8. Expression of poverty-exposed vs unexposed gene expression signatures in 16-001 bulk RNA-seq. Top ranked correlations of poverty exposed and unexposed signatures (left), and bar plots with collapsed poverty exposed and unexposed signatures in randomly sampled patients per group (see methods).

Supplemental Figure S9. Expression signatures in myeloid cells from poverty-exposed vs unexposed B-ALL samples. (A) Violin plots demonstrating expression of *CD14* and *CD16* (*FCGFR3A*) in normal donor (normal), monocytes from leukemia patients or poverty-exposed and unexposed patients, respectively, separated by *ETV6::RUNX1* or hyperdiploidy (*p<0.05,

**p<0.01, ****p<0.0001 by two-sided Wilcoxon test). (B) Consensus clustering of myeloid cells using SC3. (C) Bar plot depicting the relative proportion of each cluster in normal donors, poverty-exposed or unexposed patients (*p<0.05, **p<0.01, ***p<0.001 by two-sided Wilcoxon test). (D) Canonical monocyte expression signatures derived from per cluster (*p<0.05, ****p<0.0001 by two-sided Wilcoxon test).

Supplemental Figure S10. B-cell populations in poverty-exposed vs unexposed *ETV6::RUNX1* or hyperdiploid samples. (A, B) Relative proportions of B-cell populations as annotated by human cell atlas in *ETV6::RUNX1* (A), hyperdiploid (B). (C, D) Stacked bar plots depicting relative proportions of B-cells from normal donors (ND), poverty-exposed (pov.-exp.) and unexposed (un-exp.) children with B-ALL across 5 clusters separated by *ETV6::RUNX1* (C) and hyperdiploid (D).

Supplemental Figure S11. CD4+ T-cell populations in B-ALL patients compared to normal donors. (A) t-SNE plot depicting distribution of CD4+ T-cells from normal donors (ND), poverty-exposed (pov.-exp.) and unexposed (un-exp.) children with B-ALL. (B, C, D) Bar plots showing relative proportions of CD4+ T-cell subtypes (human cell atlas) in poverty-exposed or unexposed B-ALL patients and normal donors B), within *ETV6::RUNX1* (C) or hyperdiploid samples (D). (E, F) Stacked bar plots depicting relative proportion of CD4+ T-cells from normal donor (ND), poverty-exposed (pov.-exp.) and unexposed (in-exp.) separated by *ETV6::RUNX1* (E) and hyperdiploid (F).

SUPPLEMENTAL TABLE LEGENDS

Supplemental Table S1. Progenitor signatures from Human Cell Atlas (HCA). Genes included in signatures for HSC, CLP, pro-B, immature B-cell, and naïve B-cells.

Supplemental Table S2. Marker genes of clusters upregulated in poverty-exposed or unexposed leukemia cells. Log2FC poverty-exposed to unexposed clusters.

Supplemental Table S3. Poverty-exposed and unexposed signatures. List of genes included in poverty-exposed and unexposed signature.

Supplemental Table S4. Percentages and sorted number of leukemia and immune cells in poverty-exposed and unexposed B-ALL patients. Flow percentages of $CD45^{low}$ leukemia cells, $CD45^{high}CD3^{+}$ T-cells, $CD45^{high}CD19^{+}$ B-cells and $CD34^{high}CD14^{+}$ myeloid cells in bone marrow from poverty-exposed and unexposed children with B-ALL at time of diagnosis.

Supplemental Table S5. List of poverty-exposed vs. unexposed B-ALL samples in dataset GSE181157.[19]

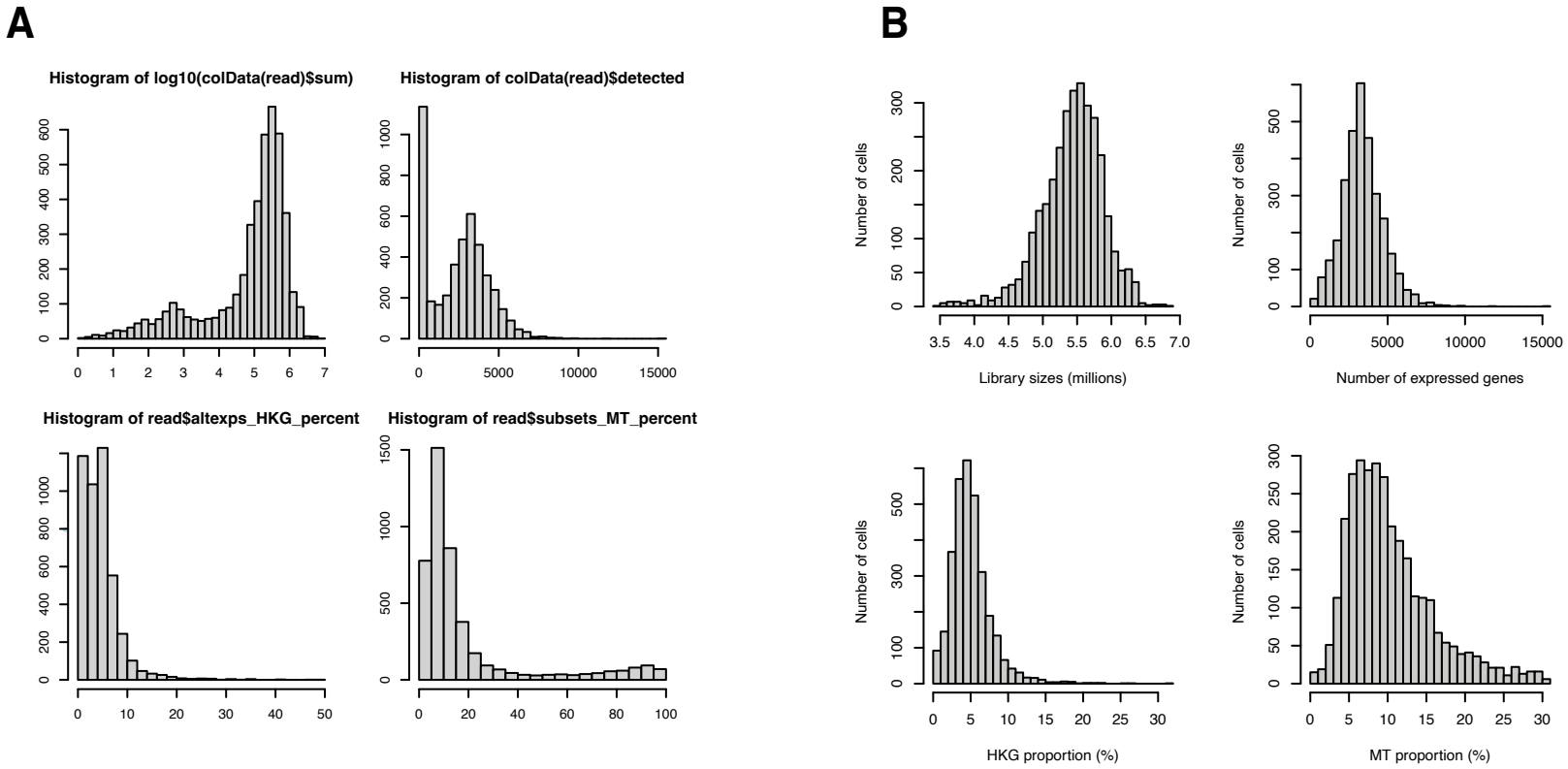
A
Histogram of log10(colData(read)$sum)
Histogram of colData(read)$detected
Histogram of read$altexps_HKG_percent
Histogram of read$subsets_MT_percent
B
Number of cells
Library sizes (millions)
Number of expressed genes
HKG proportion (%)
MT proportion (%)
C
Frequency of expression (% of 3166 cells)
Mean expression level (all features)
799 genes are expressed
in at least 50% of cells
3618 genes are expressed
in at least 25% of cells
D
Density
% variance explained
cohort
detected
altexps_HKG_percent
subsets_MT_percent
sum

Figure S1

A

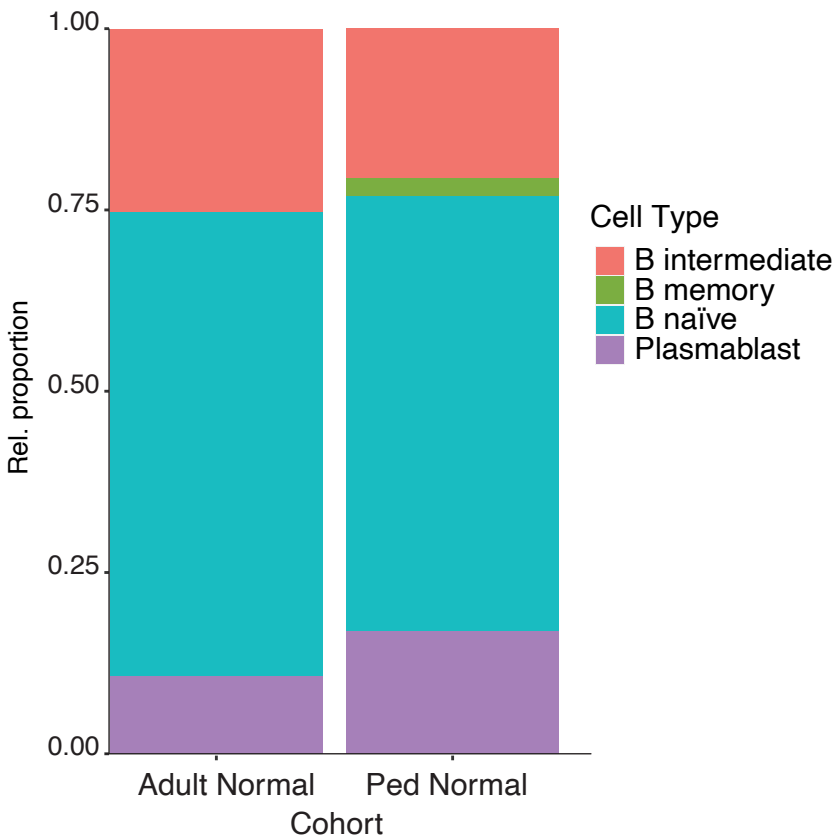

B

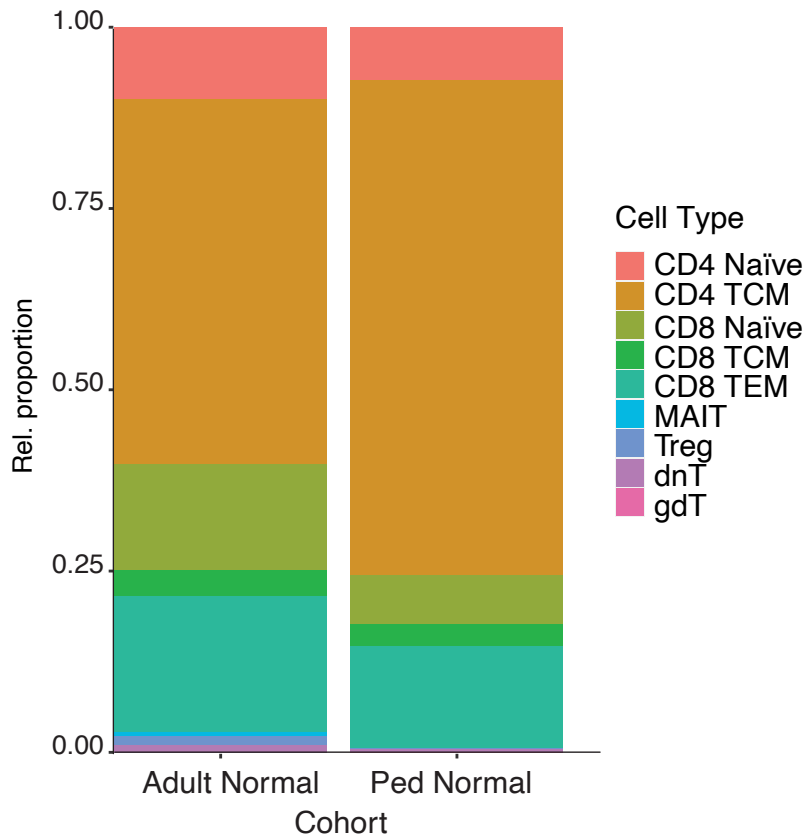

C

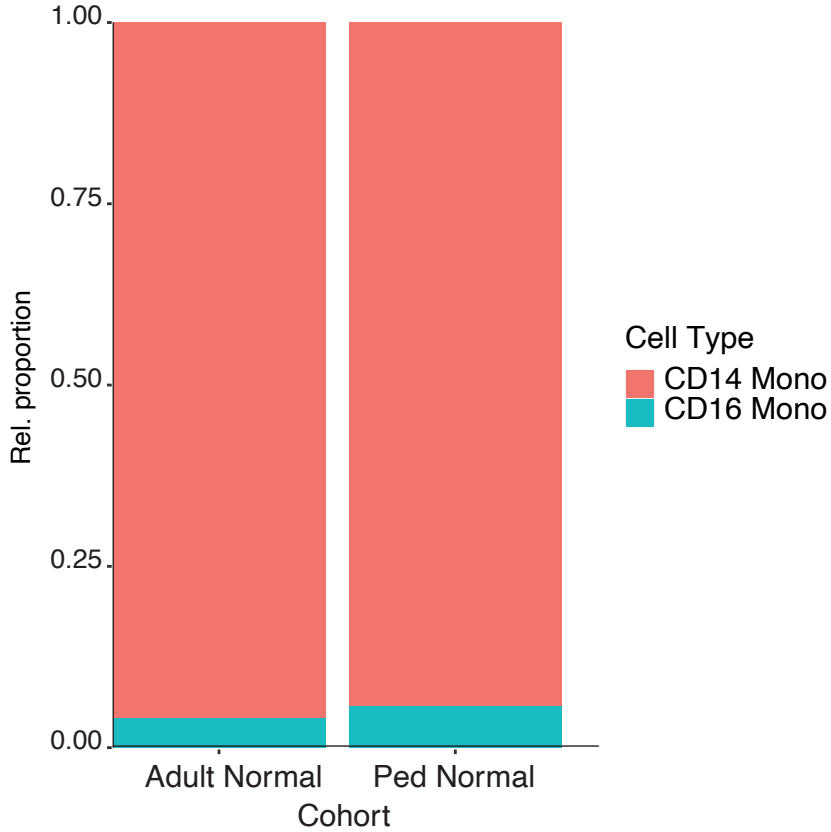

Figure S2

A

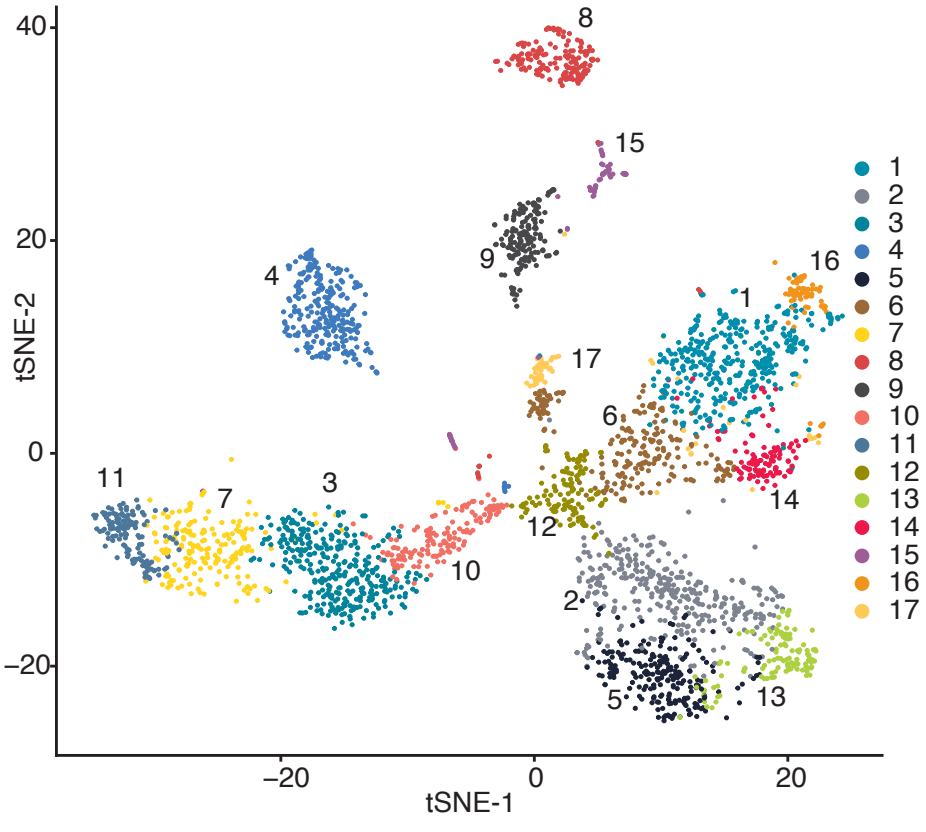
40
20
0
−20
tSNE-2
−20
0
20
tSNE-1
8
15
9
4
16
1
17
6
11
7
3
12
10
14
2
5
13
1
2
3
4
5
6
7
8
9
10
11
12
13
14
15
16
17

B

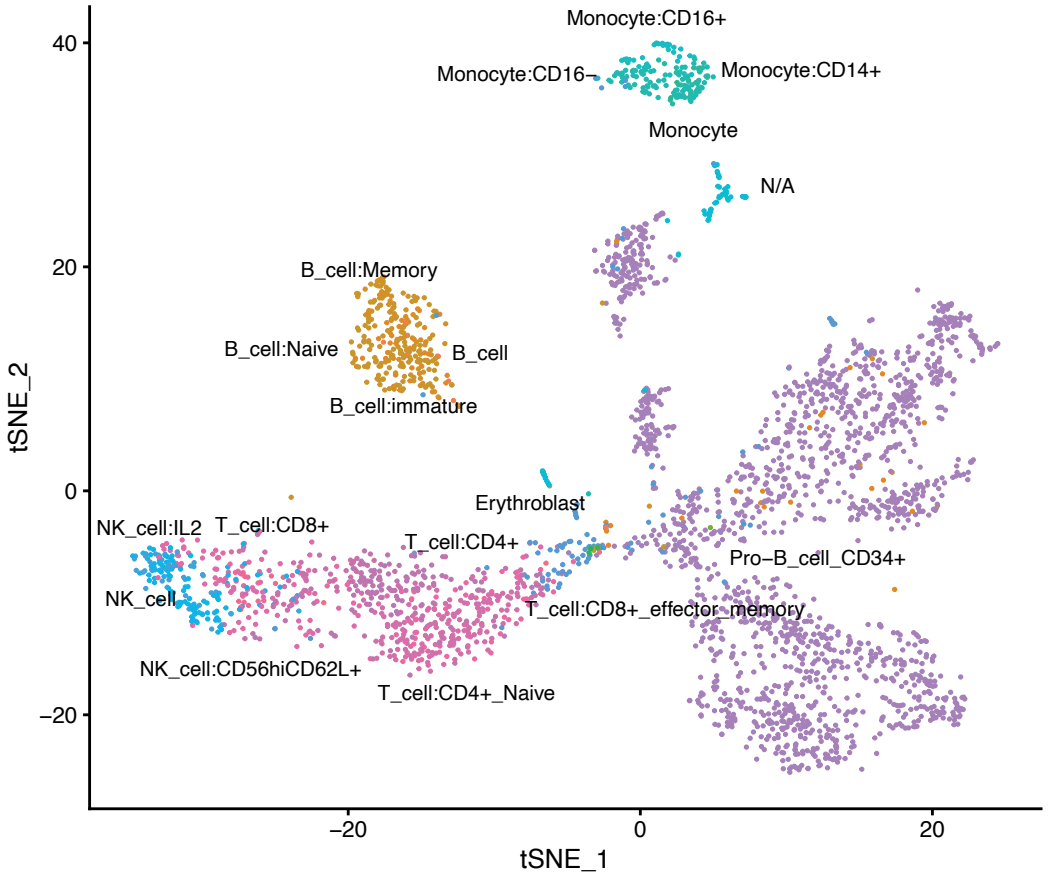
Monocyte:CD16+
Monocyte:CD16−
Monocyte:CD14+
Monocyte
N/A
B_cell:Memory
B_cell:Naive
B_cell
B_cell:immature
Erythroblast
NK_cell:IL2
T_cell:CD8+
T_cell:CD4+
Pro−B_cell_CD34+
NK_cell
T_cell:CD8+_effector_memory
NK_cell:CD56hiCD62L+
T_cell:CD4+_Naive
40
20
0
−20
tSNE_2
−20
0
20
tSNE_1

Figure S3

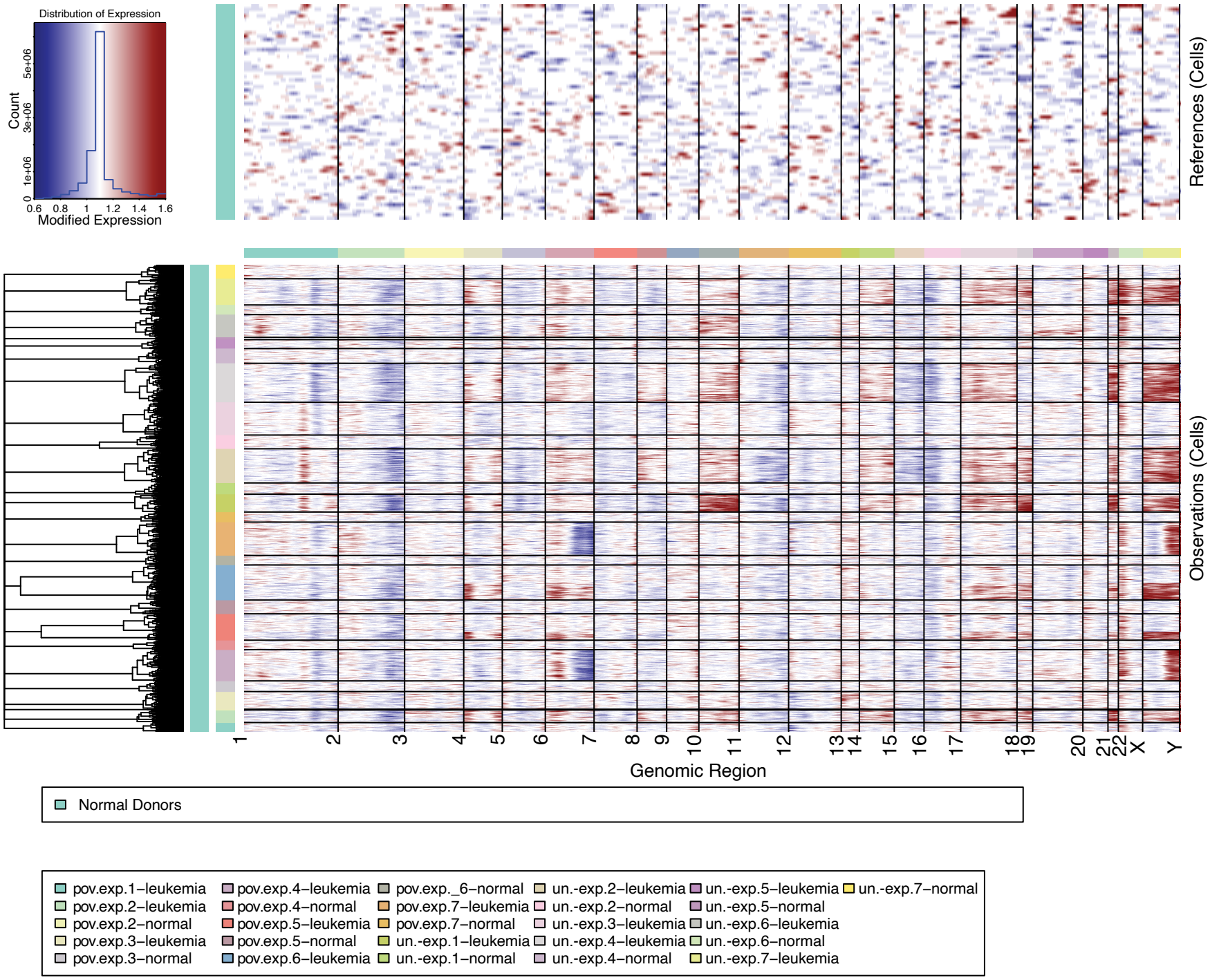
Distribution of Expression
Count
0
1e+06
3e+06
5e+06
0.6
0.8
1
1.2
1.4
1.6
Modified Expression
References (Cells)
Observations (Cells)
1
2
3
4
5
6
7
8
9
10
11
12
13
14
15
16
17
18
19
20
21
22
X
Y
Genomic Region
Normal Donors
pov.exp.1–leukemia
pov.exp.2–leukemia
pov.exp.2–normal
pov.exp.3–leukemia
pov.exp.3–normal
pov.exp.4–leukemia
pov.exp.4–normal
pov.exp.5–leukemia
pov.exp.5–normal
pov.exp.6–leukemia
pov.exp._6–normal
pov.exp.7–leukemia
pov.exp.7–normal
un.-exp.1–leukemia
un.-exp.1–normal
un.-exp.2–leukemia
un.-exp.2–normal
un.-exp.3–leukemia
un.-exp.4–leukemia
un.-exp.4–normal
un.-exp.5–leukemia
un.-exp.5–normal
un.-exp.6–leukemia
un.-exp.6–normal
un.-exp.7–normal
un.-exp.7–leukemia

Figure S4

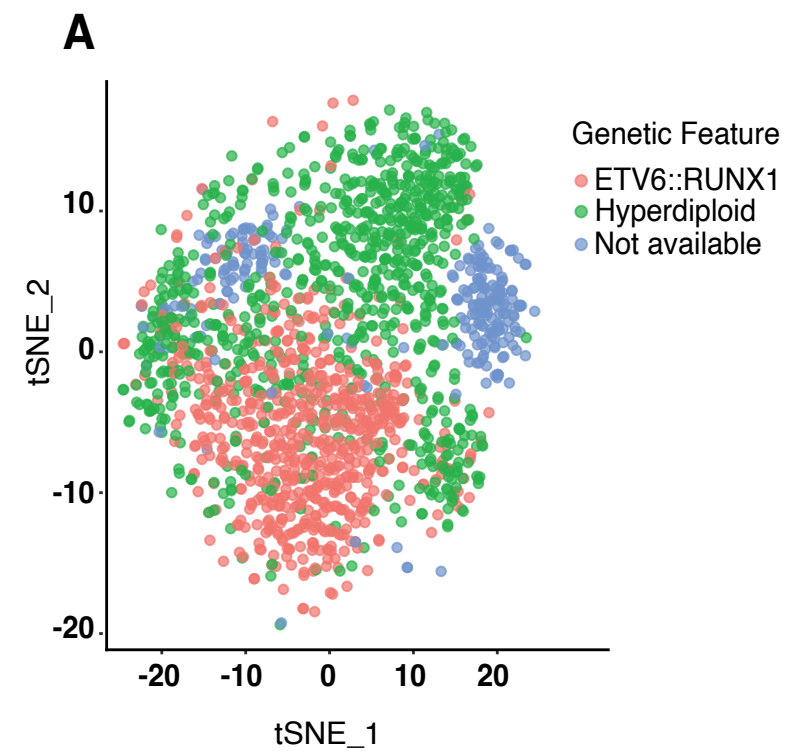
A
tSNE_2
tSNE_1
10
0
-10
-20
-20
-10
0
10
20
Genetic Feature
ETV6::RUNX1
Hyperdiploid
Not available

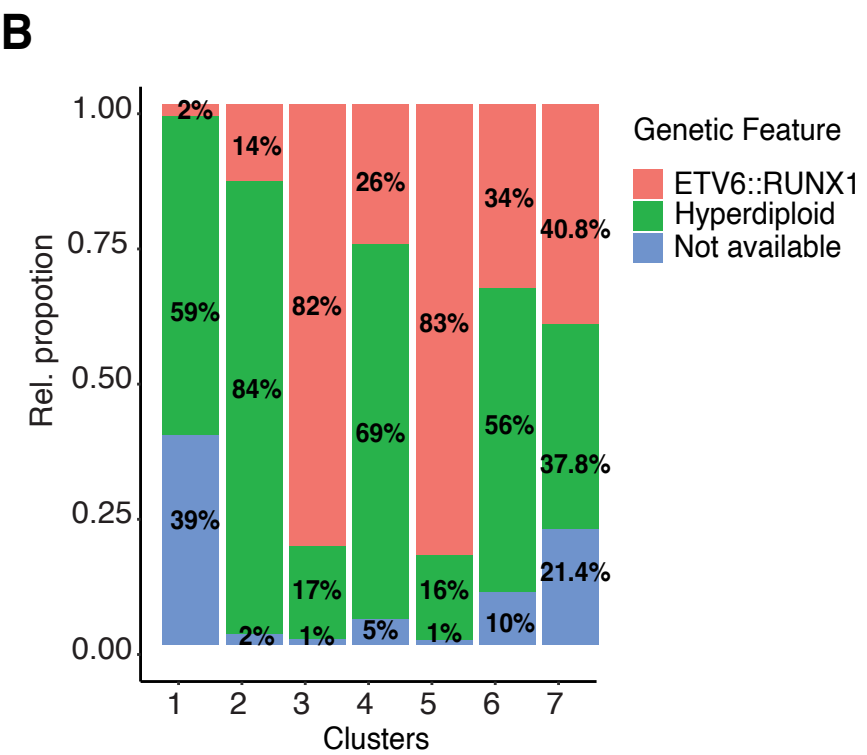
B
Rel. propotion
1.00
0.75
0.50
0.25
0.00
1
2
3
4
5
6
7
Clusters
2%
59%
39%
14%
84%
2%
82%
17%
1%
26%
69%
5%
83%
16%
1%
34%
56%
10%
40.8%
37.8%
21.4%
Genetic Feature
ETV6::RUNX1
Hyperdiploid
Not available

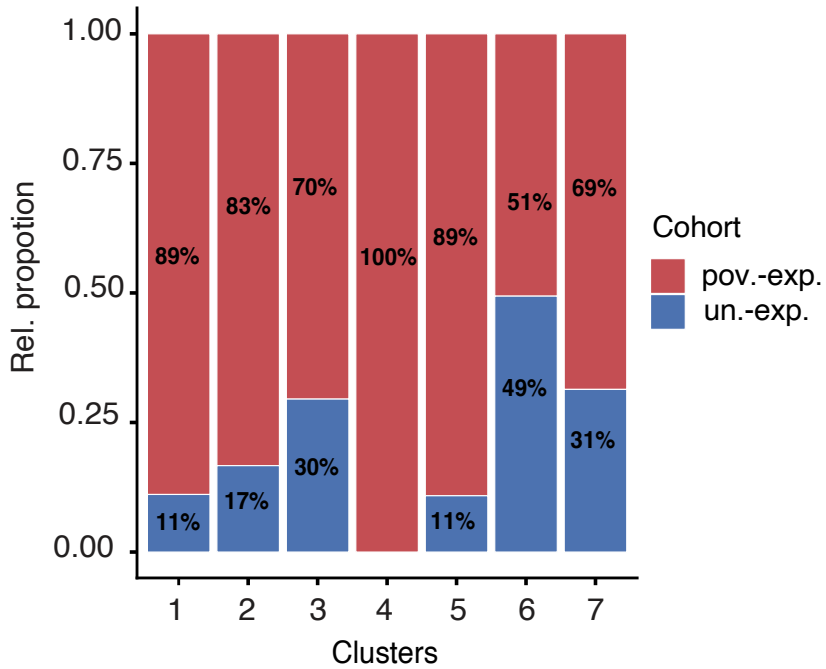
C
ETV6::RUNX1
Rel. propotion
1.00
0.75
0.50
0.25
0.00
1
2
3
4
5
6
7
Clusters
89%
11%
83%
17%
70%
30%
100%
89%
11%
51%
49%
69%
31%
Cohort
pov.-exp.
un.-exp.

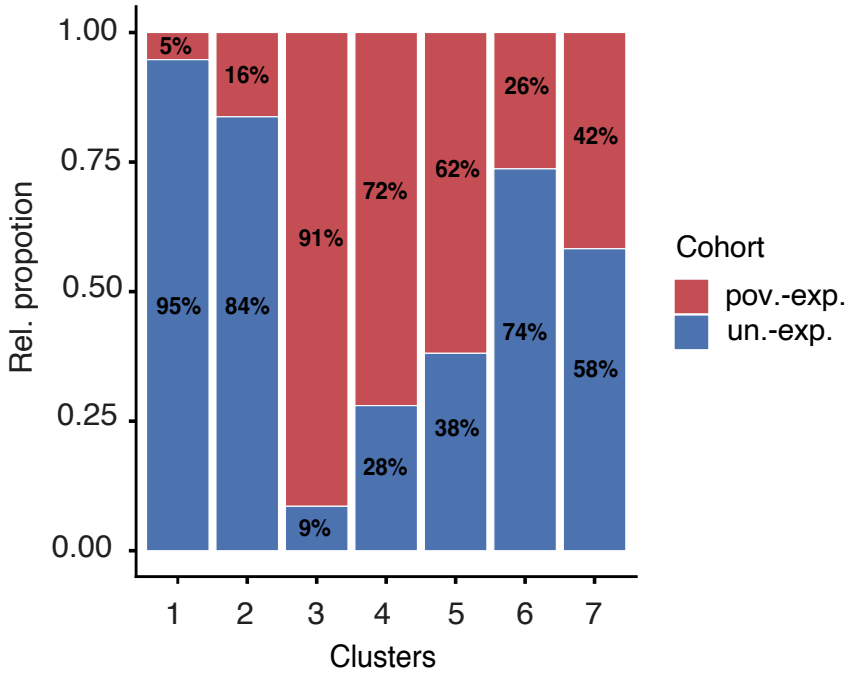
D
Hyperdiploid
Rel. propotion
1.00
0.75
0.50
0.25
0.00
1
2
3
4
5
6
7
Clusters
5%
95%
16%
84%
91%
9%
72%
28%
62%
38%
26%
74%
42%
58%
Cohort
pov.-exp.
un.-exp.

Figure S5

ETV6::RUNX1

A

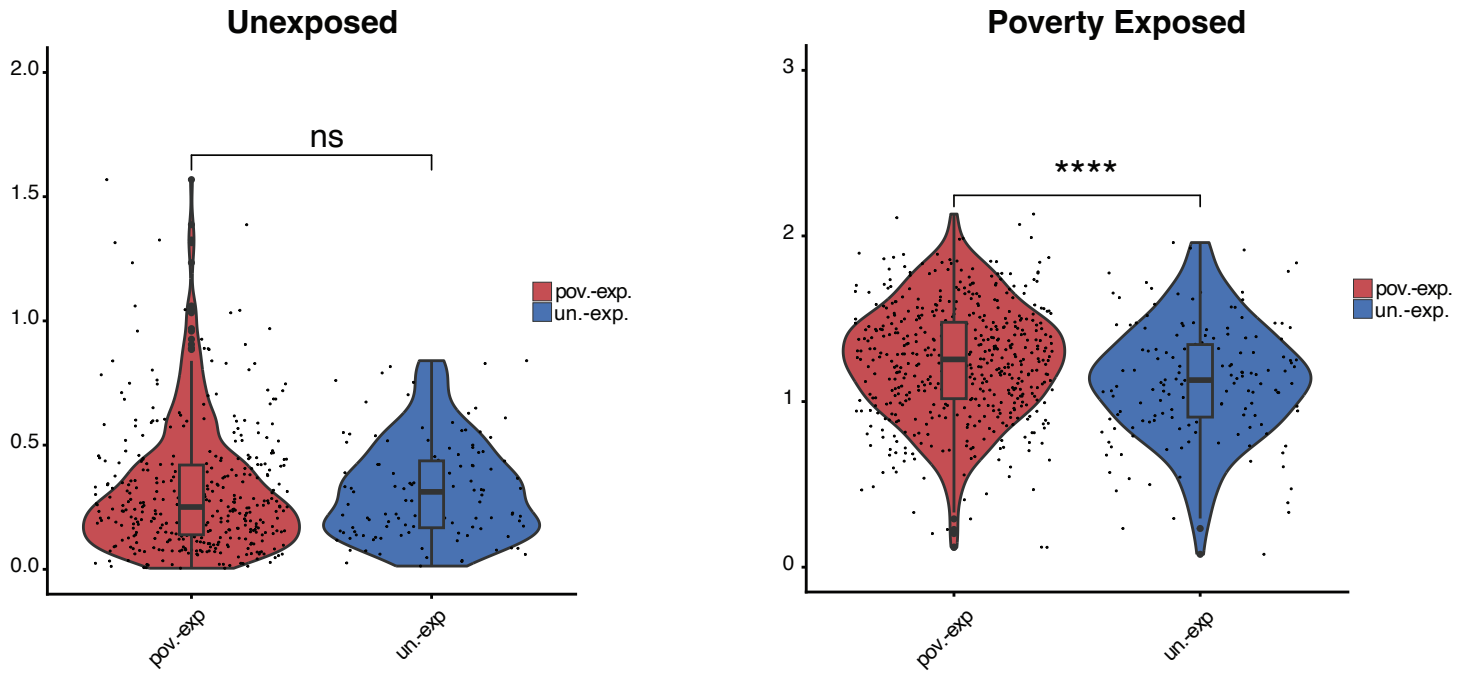

Hyperdiploid

B

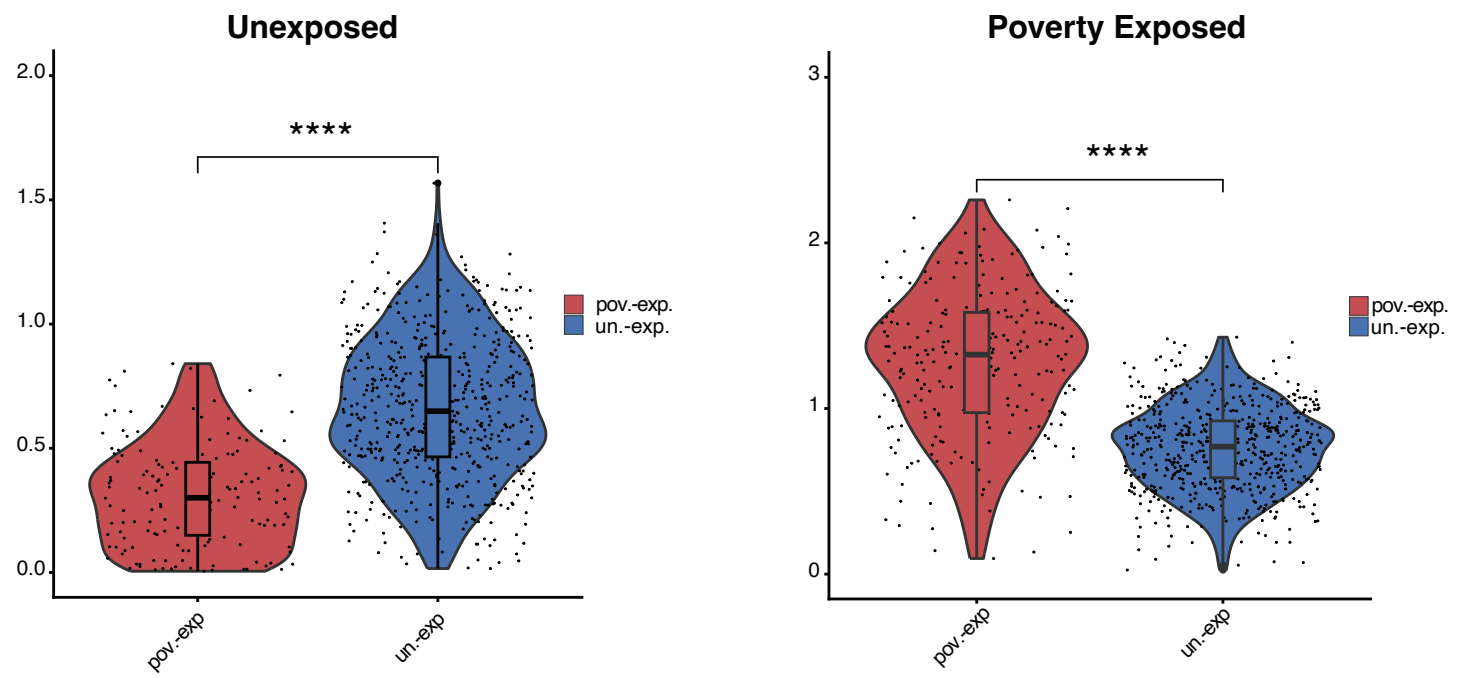

C

ETV6::RUNX1

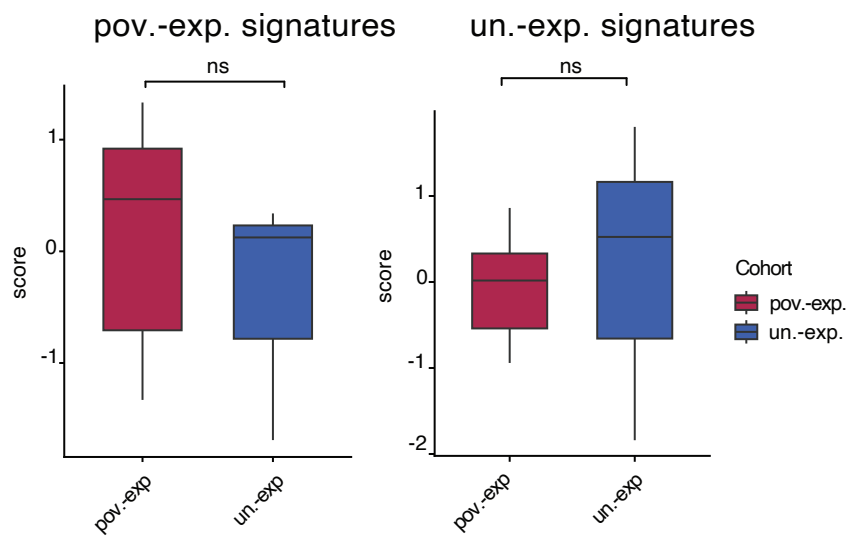

D

Hyperdiploid

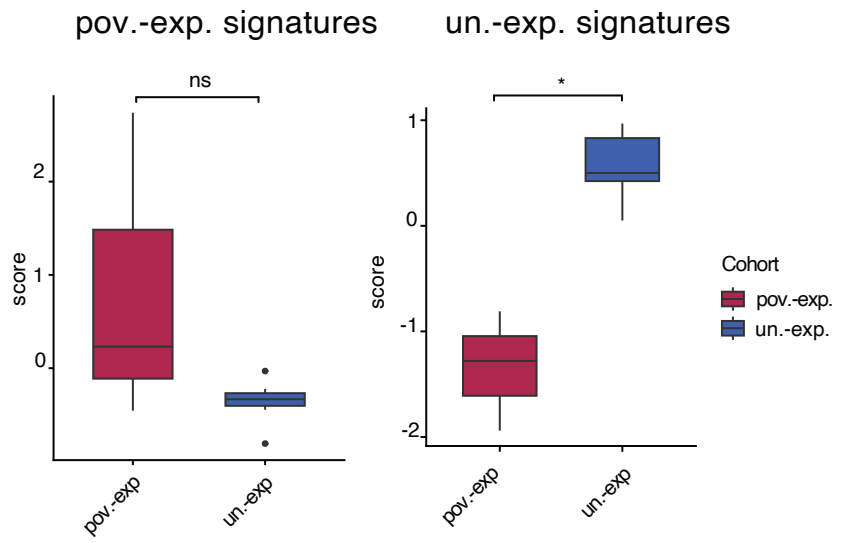

Figure S6

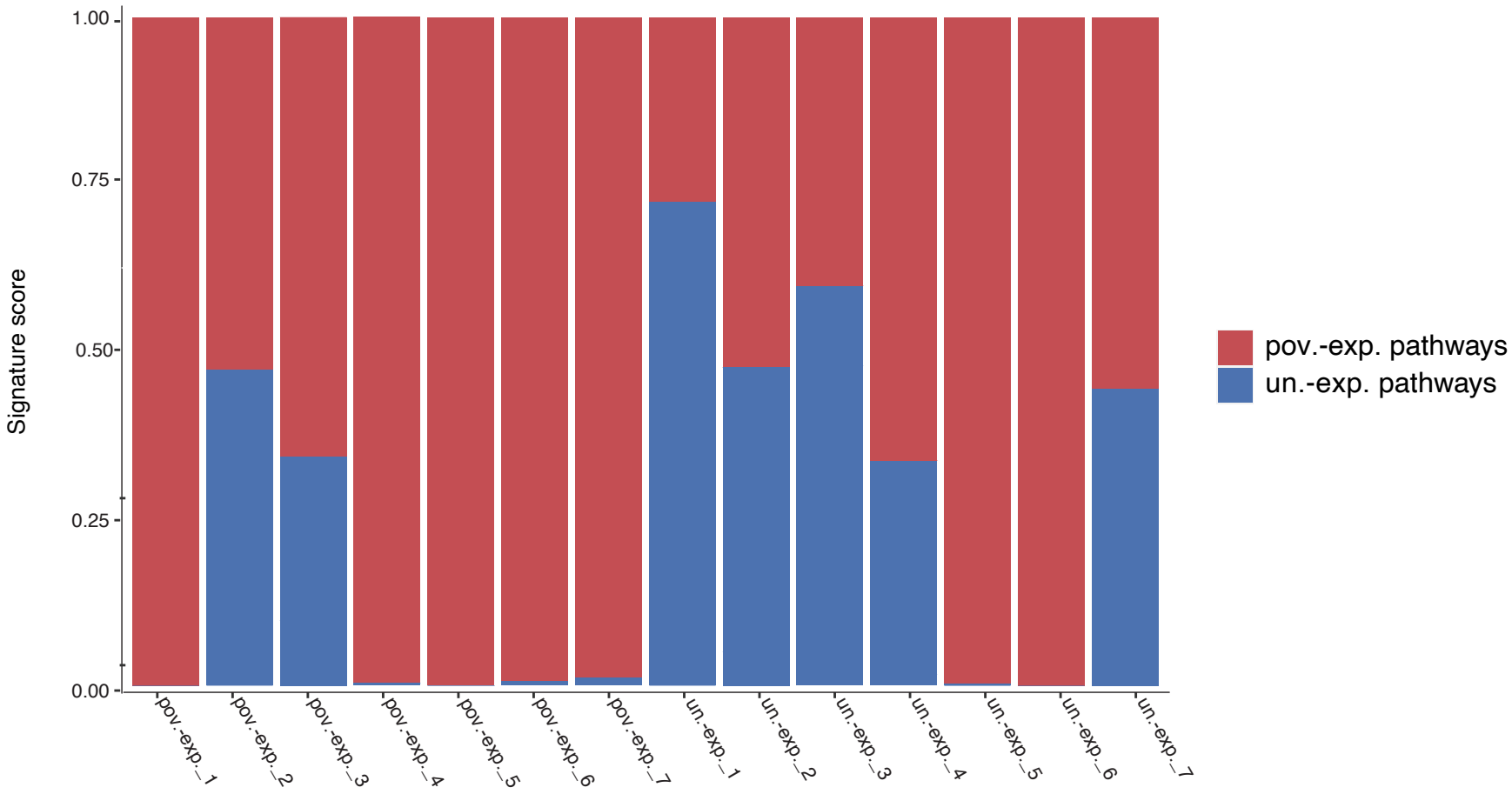
Signature score
1.00
0.75
0.50
0.25
0.00
pov.-exp._1
pov.-exp._2
pov.-exp._3
pov.-exp._4
pov.-exp._5
pov.-exp._6
pov.-exp._7
un.-exp._1
un.-exp._2
un.-exp._3
un.-exp._4
un.-exp._5
un.-exp._6
un.-exp._7
pov.-exp. pathways
un.-exp. pathways

Figure S7

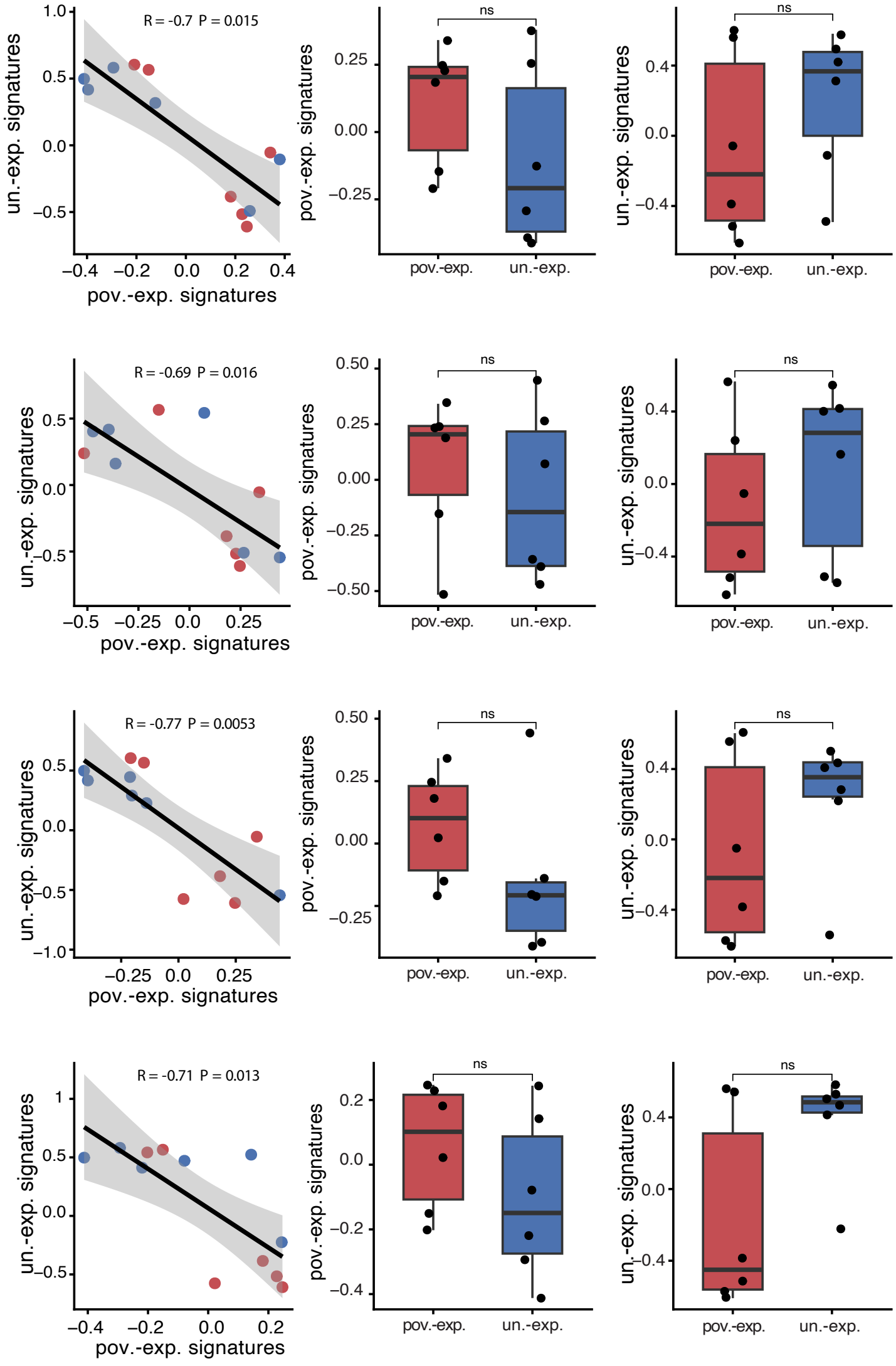
R = -0.7 P = 0.015
un.-exp. signatures
pov.-exp. signatures
ns
pov.-exp.
un.-exp.
R = -0.69 P = 0.016
R = -0.77 P = 0.0053
R = -0.71 P = 0.013

Figure S8

A

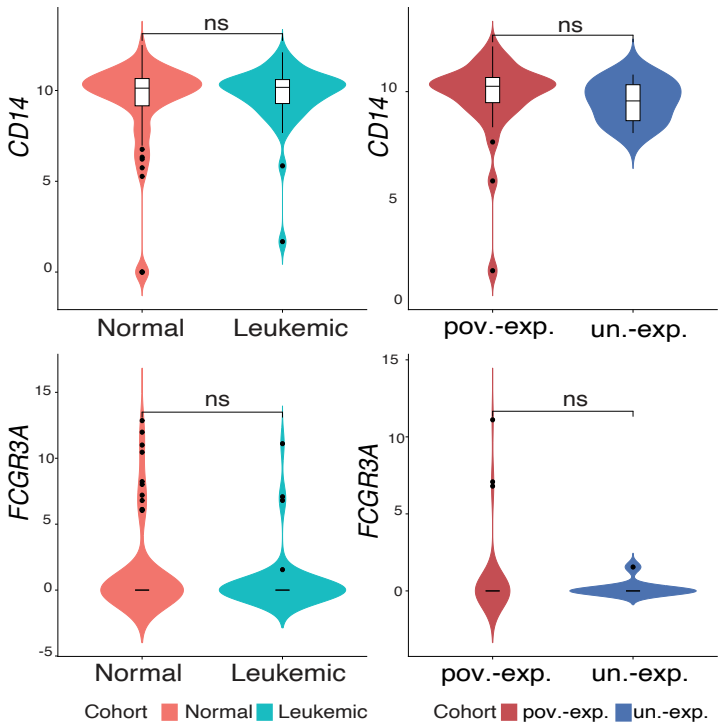

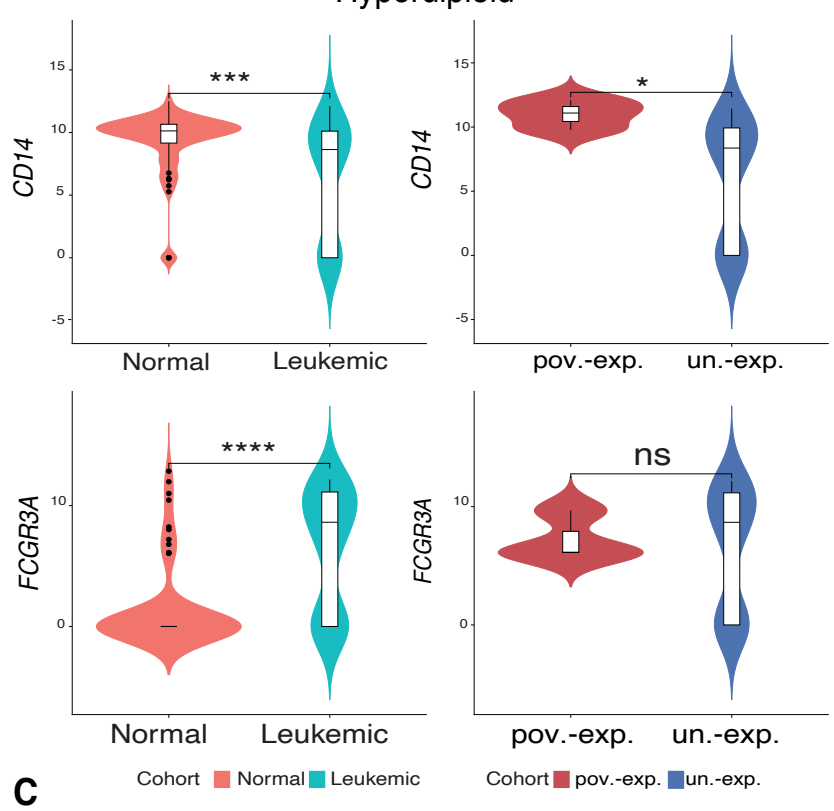

B

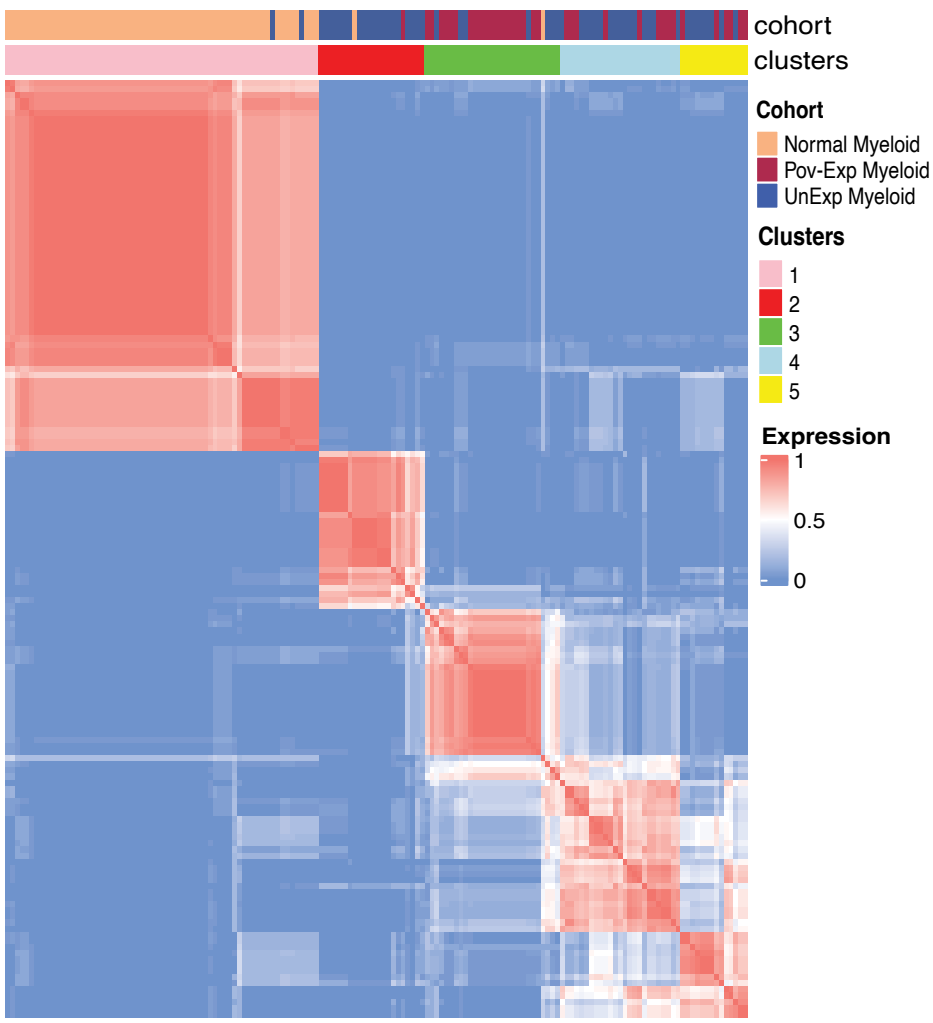

C

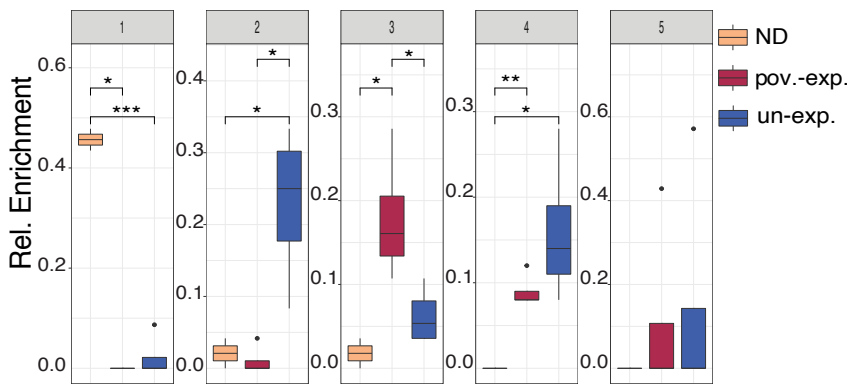

D

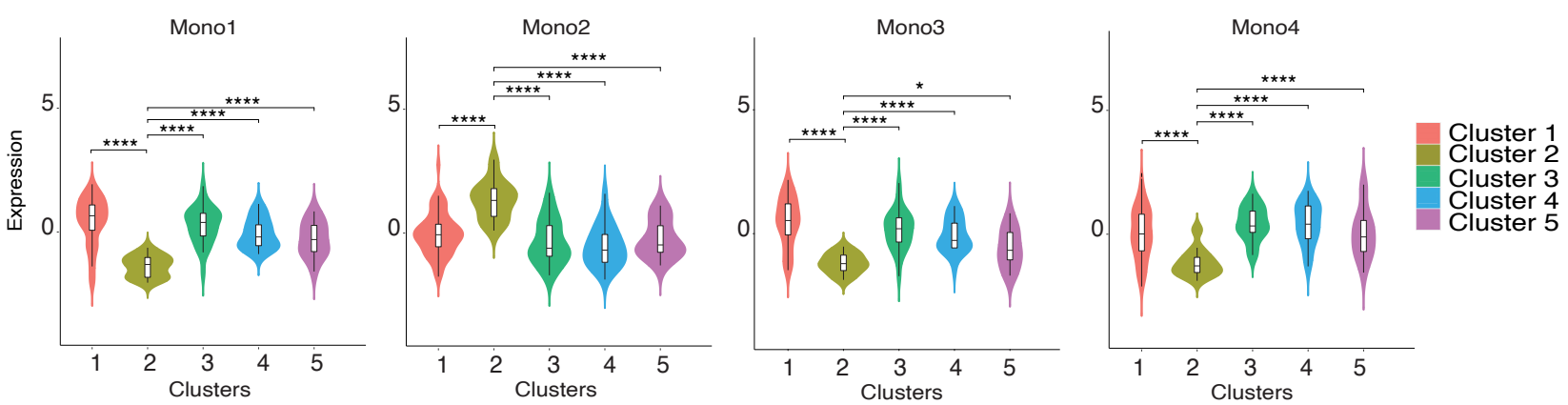

Figure S9

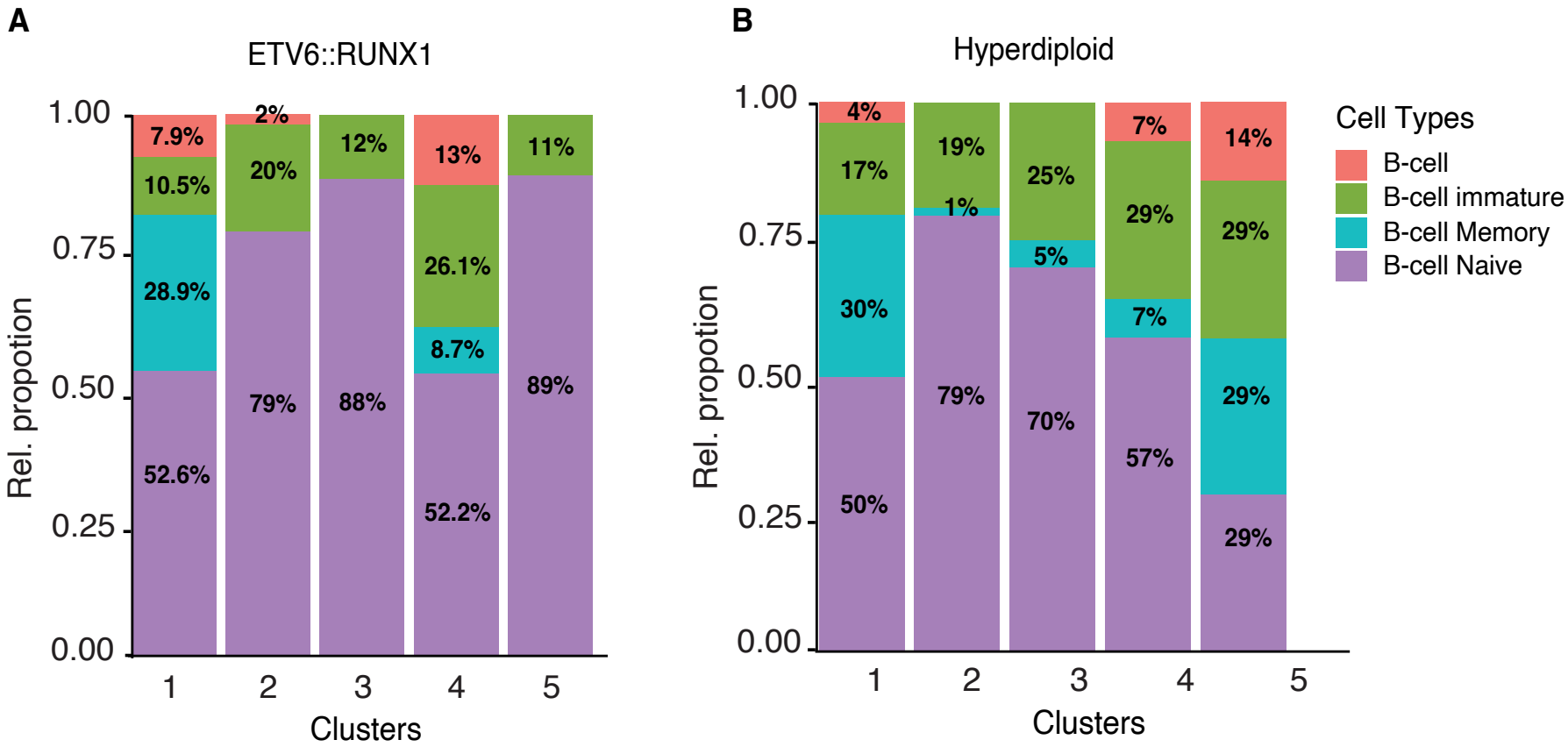
A
ETV6::RUNX1
Rel. propotion
1.00
0.75
0.50
0.25
0.00
7.9%
10.5%
28.9%
52.6%
2%
20%
79%
12%
88%
13%
26.1%
8.7%
52.2%
11%
89%
1
2
3
4
5
Clusters
B
Hyperdiploid
4%
17%
30%
50%
19%
1%
79%
25%
5%
70%
7%
29%
7%
57%
14%
29%
29%
29%
Cell Types
B-cell
B-cell immature
B-cell Memory
B-cell Naive

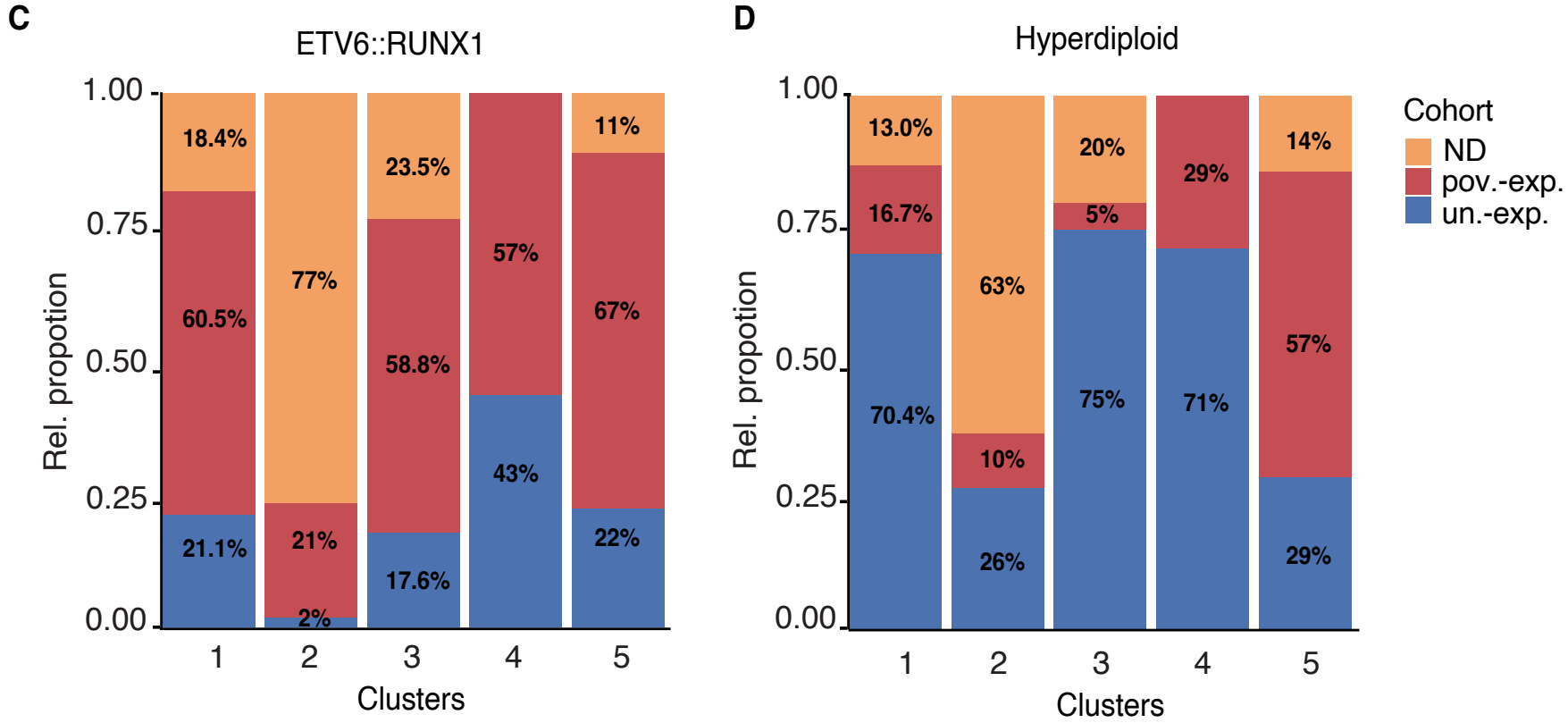
C
ETV6::RUNX1
Rel. propotion
1.00
0.75
0.50
0.25
0.00
18.4%
60.5%
21.1%
77%
21%
2%
23.5%
58.8%
17.6%
57%
43%
11%
67%
22%
1
2
3
4
5
Clusters
D
Hyperdiploid
13.0%
16.7%
70.4%
63%
10%
26%
20%
5%
75%
29%
71%
14%
57%
29%
Cohort
ND
pov.-exp.
un.-exp.

Figure S10

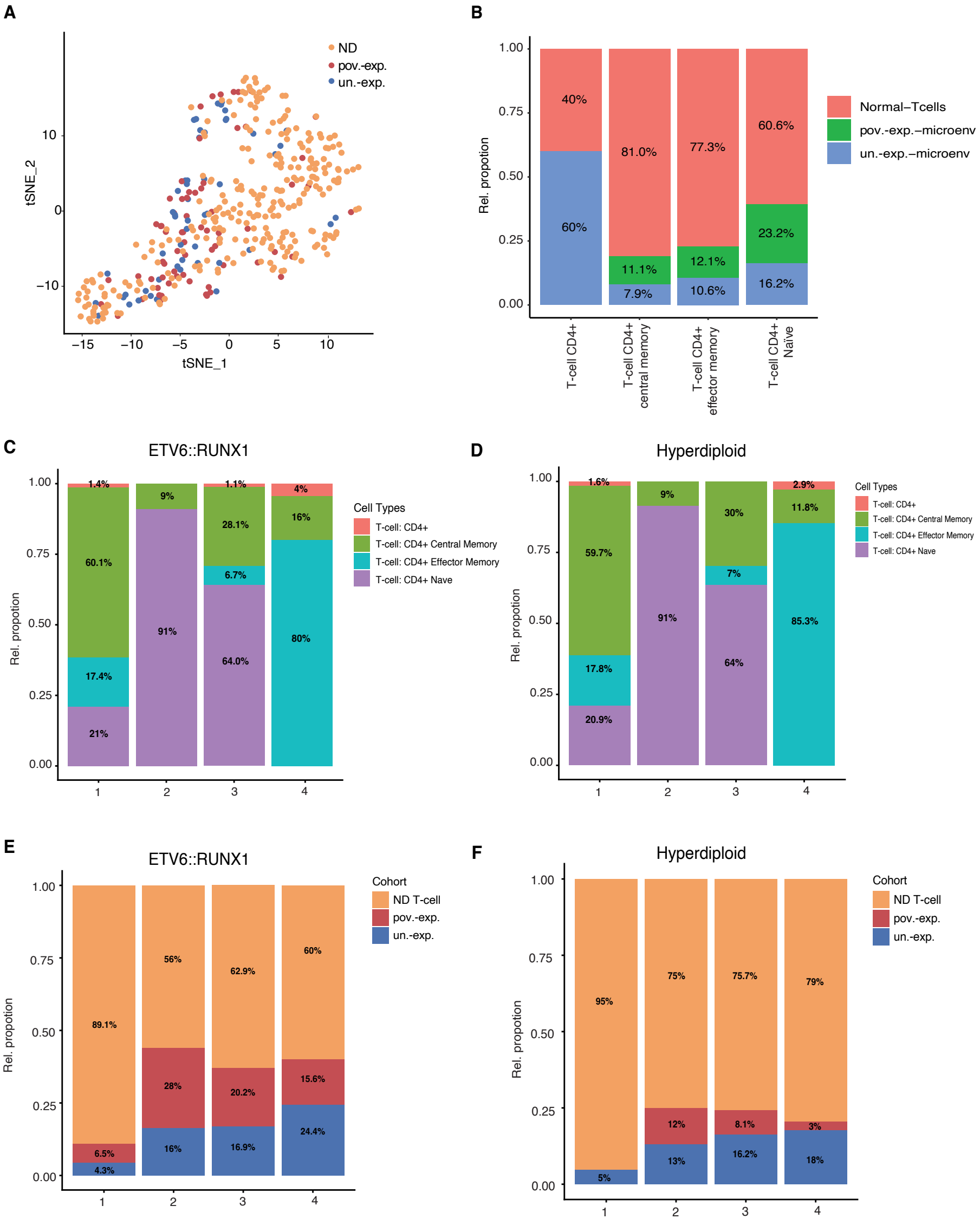
A
ND
pov.-exp.
un.-exp.
tSNE_2
tSNE_1
B
Rel. propotion
Normal–Tcells
pov.-exp.–microenv
un.-exp.–microenv
40%
60%
81.0%
11.1%
7.9%
77.3%
12.1%
10.6%
60.6%
23.2%
16.2%
T-cell CD4+
T-cell CD4+ central memory
T-cell CD4+ effector memory
T-cell CD4+ Naïve
C
ETV6::RUNX1
Rel. propotion
Cell Types
T-cell: CD4+
T-cell: CD4+ Central Memory
T-cell: CD4+ Effector Memory
T-cell: CD4+ Nave
1.4%
60.1%
17.4%
21%
9%
91%
1.1%
28.1%
6.7%
64.0%
4%
16%
80%
D
Hyperdiploid
Rel. propotion
Cell Types
T-cell: CD4+
T-cell: CD4+ Central Memory
T-cell: CD4+ Effector Memory
T-cell: CD4+ Nave
1.6%
59.7%
17.8%
20.9%
9%
91%
30%
7%
64%
2.9%
11.8%
85.3%
E
ETV6::RUNX1
Rel. propotion
Cohort
ND T-cell
pov.-exp.
un.-exp.
89.1%
6.5%
4.3%
56%
28%
16%
62.9%
20.2%
16.9%
60%
15.6%
24.4%
F
Hyperdiploid
Rel. propotion
Cohort
ND T-cell
pov.-exp.
un.-exp.
95%
5%
75%
12%
13%
75.7%
8.1%
16.2%
79%
3%
18%

Figure S11

Table_S1_HCA signatures

	hsc	clp	prob	immature	naiveb
1	AHSP	ADNP	AFM	CD22	BLK
2	ALAS2	AIMP1	ALPL	CYBB	CXCR5
3	ATP8B4	ASCC1	CCR8	FAM129C	CD19
4	CA1	ATP6V1G1	CRX	FCRL1	MS4A1
5	CCDC121	C11orf57	DCC	FCRL3	CD72
6	CD34	C19orf53	DNTT	FCRL5	SPIB
7	CRHBP	CALM1	GABRA6	FCRLA	TCL1A
8	ERG	COX6C	GCK	HDAC9	FCRL2
9	EXD2	DNTT	GPR3	HLA-DQA1	BLK
10	FAM124B	DSTN	GPR4	HVCN1	CXCR5
11	FLT3	FAM76A	GRIK3	KIAA0226	CD19
12	GSTM5	GAPDH	GYS2	NCF1	MS4A1
13	GYPA	GPN3	TLX2	NCF1B	CD22
14	GYPE	H3F3B	KNG1	P2RY10	CD72
15	KLHL9	HIVEP3	MEN1	SP100	CD79B
16	LAPTM4B	IDH3A	MUSK	TXNIP	CCR6
17	LSM2	IGBP1	OMD	STAP1	GPR18
18	MMRN1	IGLL1	PARK2	TAGAP	CD180
19	MYCT1	METAP2	POU3F1	ZCCHC2	MGAT5
20	PLS3	MYL12B	RAG2	NA	SPIB
21	SCARF1	NGLY1	RPE65	NA	TCL1A
22	SLC4A1	OXA1L	SLC2A2	NA	MBD4
23	TCEAL4	PLP2	SLC12A1	NA	TSPAN13
24	XPO7	PSMA6	SRY	NA	UTP6
25	ZMYM3	PSMB3	VPREB1	NA	FCRL2
26	NA	RFC4	CSRP3	NA	TREML2
27	NA	RPL8	HIST1H2BM	NA	BLK
28	NA	SNRPD1	SOX14	NA	CXCR5
29	NA	TOMM20	CACNA1G	NA	CD19
30	NA	VPREB1	GREB1	NA	MS4A1
31	NA	WDR33	CNKSR1	NA	CD72
32	NA	NA	ARPP21	NA	CD180
33	NA	NA	FRS3	NA	SPIB
34	NA	NA	LILRB1	NA	BLK
35	NA	NA	CLDN14	NA	CD19
36	NA	NA	PLA2G2D	NA	MS4A1
37	NA	NA	OR7A5	NA	CD22
38	NA	NA	AKAP8L	NA	CD37
39	NA	NA	STRN4	NA	CD72
40	NA	NA	GNL2	NA	CD79A
41	NA	NA	TNFRSF12A	NA	CSNK1G3

42	NA	NA	LARP7	NA	DSP
43	NA	NA	BTBD7	NA	FCER2
44	NA	NA	SPATA7	NA	GMFB
45	NA	NA	HAMP	NA	PNOC
46	NA	NA	C2orf49	NA	CD1A
47	NA	NA	CXorf36	NA	CD19
48	NA	NA	LRRTM4	NA	MS4A1
49	NA	NA	FIP1L1	NA	CD22
50	NA	NA	SLC25A31	NA	CD37
51	NA	NA	SCRT1	NA	CD72
52	NA	NA	IMP4	NA	CD79A
53	NA	NA	HSPB6	NA	CSNK1G3
54	NA	NA	ZNF81	NA	DSP
55	NA	NA	ZNF674	NA	FCER2
56	NA	NA	ADARB2	NA	GMFB
57	NA	NA	ADCY8	NA	MGAT5
58	NA	NA	AGXT	NA	PNOC
59	NA	NA	ALOX15B	NA	SNX2
60	NA	NA	ANXA3	NA	AP3B1
61	NA	NA	APOC3	NA	MBD4
62	NA	NA	ARG1	NA	STAG3
63	NA	NA	ART4	NA	PRDM4
64	NA	NA	BMX	NA	PWP1
65	NA	NA	CA1	NA	RRAS2
66	NA	NA	CCKAR	NA	GGA2
67	NA	NA	SIGLEC6	NA	SIPA1L3
68	NA	NA	CETP	NA	STAP1
69	NA	NA	CLCN1	NA	P2RY10
70	NA	NA	CNTFR	NA	VPREB3
71	NA	NA	CRH	NA	DEF8
72	NA	NA	CSHL1	NA	MFN1
73	NA	NA	CTSG	NA	FCRL2
74	NA	NA	CYP2A7	NA	BLK
75	NA	NA	DCC	NA	CAPN3
76	NA	NA	DLX4	NA	CD1A
77	NA	NA	DNTT	NA	CD19
78	NA	NA	DPYS	NA	MS4A1
79	NA	NA	DSP	NA	CD22
80	NA	NA	EFNA2	NA	CD37
81	NA	NA	FCAR	NA	CD72
82	NA	NA	FCN2	NA	CD79A
83	NA	NA	FGF8	NA	CD79B
84	NA	NA	MSTN	NA	CSNK1G3

85	NA	NA	GDF10	NA	DSP
86	NA	NA	GPR3	NA	FCER2
87	NA	NA	GPR4	NA	GMFB
88	NA	NA	GRIK3	NA	HSPA4
89	NA	NA	GYS2	NA	MGAT5
90	NA	NA	HCRTR2	NA	PNOC
91	NA	NA	ONECUT1	NA	SNX2
92	NA	NA	PRMT1	NA	GCM1
93	NA	NA	HTR1B	NA	AP3B1
94	NA	NA	HTR5A	NA	MBD4
95	NA	NA	IFNA1	NA	STAG3
96	NA	NA	IGLL1	NA	PRDM4
97	NA	NA	IL12B	NA	PWP1
98	NA	NA	KCNJ9	NA	SP140
99	NA	NA	KCNJ13	NA	RRAS2
100	NA	NA	KRT12	NA	GGA2
101	NA	NA	KRT19	NA	SIPA1L3
102	NA	NA	LLGL1	NA	STAP1
103	NA	NA	LTC4S	NA	P2RY10
104	NA	NA	MAG	NA	VPREB3
105	NA	NA	MKI67	NA	DEF8
106	NA	NA	TRPM1	NA	MFN1
107	NA	NA	MUC6	NA	FCRL2
108	NA	NA	MYH4	NA	C10orf76
109	NA	NA	MYH8	NA	SMC6
110	NA	NA	NEUROG1	NA	MCM9
111	NA	NA	NOTCH4	NA	EGOT
112	NA	NA	OMG	NA	CXCR5
113	NA	NA	PARK2	NA	BMP3
114	NA	NA	PMP2	NA	CACNA1F
115	NA	NA	POU1F1	NA	CAPN3
116	NA	NA	PPEF2	NA	CD19
117	NA	NA	PRB4	NA	MS4A1
118	NA	NA	PSG11	NA	CD22
119	NA	NA	RAD23A	NA	CD72
120	NA	NA	RAG2	NA	COL19A1
121	NA	NA	RAPSN	NA	CSNK1G3
122	NA	NA	RBP3	NA	DAZL
123	NA	NA	MRPL12	NA	DSP
124	NA	NA	RRM2	NA	FCER2
125	NA	NA	CCL17	NA	GNG3
126	NA	NA	TACR3	NA	GPR18
127	NA	NA	TCF3	NA	MATN1

128	NA	NA	TESK1	NA	MAP3K9
129	NA	NA	TGM3	NA	MMP17
130	NA	NA	THPO	NA	MYBPC2
131	NA	NA	TNNT2	NA	PAX5
132	NA	NA	UCP3	NA	PHKG1
133	NA	NA	VPREB1	NA	PYGM
134	NA	NA	ZNF155	NA	ZNF154
135	NA	NA	CSRP3	NA	PRDM2
136	NA	NA	HIST1H2BL	NA	USP7
137	NA	NA	HIST1H2BM	NA	TCL1A
138	NA	NA	SOX14	NA	SYN3
139	NA	NA	EDF1	NA	ADAM20
140	NA	NA	ADAM21	NA	USP6
141	NA	NA	KCNQ4	NA	AKAP6
142	NA	NA	OTOF	NA	TCL1B
143	NA	NA	KIF23	NA	BCL2L10
144	NA	NA	CNKSR1	NA	FRS2
145	NA	NA	NMUR1	NA	PRDM4
146	NA	NA	PLK4	NA	RRAS2
147	NA	NA	ARPP21	NA	GGA2
148	NA	NA	FRS3	NA	SIPA1L3
149	NA	NA	LILRB1	NA	TCL6
150	NA	NA	STIP1	NA	TSPAN13
151	NA	NA	LILRB4	NA	P2RY10
152	NA	NA	KERA	NA	MYO3A
153	NA	NA	ADAMTS8	NA	SDK2
154	NA	NA	CLCA4	NA	WDR74
155	NA	NA	FSTL4	NA	UBE2O
156	NA	NA	PMPCA	NA	RBM15
157	NA	NA	ATP1B4	NA	SMC6
158	NA	NA	CLDN14	NA	KHDRBS2
159	NA	NA	PADI4	NA	CXCR5
160	NA	NA	TSSK2	NA	BMP3
161	NA	NA	CA14	NA	CACNA1F
162	NA	NA	FBXO24	NA	CAPN3
163	NA	NA	SLC13A4	NA	CD19
164	NA	NA	OR7A5	NA	MS4A1
165	NA	NA	AKAP8L	NA	CD22
166	NA	NA	DKKL1	NA	CD72
167	NA	NA	AHDC1	NA	COL19A1
168	NA	NA	BMP10	NA	CSNK1G3
169	NA	NA	VPREB3	NA	DAZL
170	NA	NA	ANAPC2	NA	FCER2

171	NA	NA	VSX1	NA	GNG3
172	NA	NA	CALY	NA	MAP3K9
173	NA	NA	HP1BP3	NA	MMP17
174	NA	NA	PDE11A	NA	MYBPC2
175	NA	NA	CLEC1A	NA	PAX5
176	NA	NA	GMIP	NA	PHKG1
177	NA	NA	TNFRSF12A	NA	PRDM2
178	NA	NA	SPTBN5	NA	USP7
179	NA	NA	ZMYND10	NA	TCL1A
180	NA	NA	LARP7	NA	SYN3
181	NA	NA	COQ3	NA	ADAM20
182	NA	NA	CNGB3	NA	USP6
183	NA	NA	ZNF407	NA	AKAP6
184	NA	NA	IQCC	NA	TCL1B
185	NA	NA	BTBD7	NA	FRS2
186	NA	NA	SPATA7	NA	PRDM4
187	NA	NA	NXF3	NA	RRAS2
188	NA	NA	PAPOLB	NA	GGA2
189	NA	NA	RPGRIP1	NA	SIPA1L3
190	NA	NA	SLURP1	NA	TCL6
191	NA	NA	SPC25	NA	TSPAN13
192	NA	NA	HAMP	NA	P2RY10
193	NA	NA	MYL7	NA	WDR74
194	NA	NA	KLHL12	NA	UBE2O
195	NA	NA	FBRS	NA	SMC6
196	NA	NA	RNF25	NA	KHDRBS2
197	NA	NA	TUT1	NA	RERE
198	NA	NA	MRPS15	NA	CXCR5
199	NA	NA	KRI1	NA	BMP3
200	NA	NA	NOL12	NA	CACNA1F
201	NA	NA	CXorf36	NA	CAPN3
202	NA	NA	KRTAP1-3	NA	CD1A
203	NA	NA	PCDH11Y	NA	CD19
204	NA	NA	IMP4	NA	MS4A1
205	NA	NA	HSPB6	NA	CD22
206	NA	NA	PPP4R2	NA	CD72
207	NA	NA	KCNV2	NA	COL19A1
208	NA	NA	PSORS1C2	NA	CSNK1G3
209	NA	NA	R3HCC1	NA	DAZL
210	NA	NA	ASPM	NA	DSP
211	NA	NA	NACA2	NA	FCER2
212	NA	NA	ARG1	NA	GH1
213	NA	NA	CLCN1	NA	GNG3

214	NA	NA	CNTFR	NA	HLA-DOA
215	NA	NA	CSHL1	NA	LY9
216	NA	NA	DCC	NA	MATN1
217	NA	NA	DNTT	NA	CIITA
218	NA	NA	FCAR	NA	MAP3K9
219	NA	NA	FGF8	NA	MMP17
220	NA	NA	GPR3	NA	MYBPC2
221	NA	NA	HTR1B	NA	PAX5
222	NA	NA	IGLL1	NA	PGAM2
223	NA	NA	LTC4S	NA	PHKG1
224	NA	NA	MEP1B	NA	POU2F1
225	NA	NA	TRPM1	NA	PRKCB
226	NA	NA	MUC6	NA	PYGM
227	NA	NA	PRB4	NA	RB1
228	NA	NA	PSG11	NA	TRA2B
229	NA	NA	RAG2	NA	ZNF154
230	NA	NA	MRPL12	NA	SLC30A4
231	NA	NA	SGCA	NA	PRDM2
232	NA	NA	TACR3	NA	USP7
233	NA	NA	TCOF1	NA	CUBN
234	NA	NA	TESK1	NA	TCL1A
235	NA	NA	TGM3	NA	SYN3
236	NA	NA	VPREB1	NA	CDK13
237	NA	NA	ZNF155	NA	PTCH2
238	NA	NA	HIST1H2BL	NA	ADAM20
239	NA	NA	SOX14	NA	USP6
240	NA	NA	ADAM21	NA	AKAP6
241	NA	NA	KCNQ4	NA	TCL1B
242	NA	NA	ARPP21	NA	TBC1D5
243	NA	NA	FRS3	NA	BCL2L11
244	NA	NA	LILRB1	NA	STAG3
245	NA	NA	ADAMTS8	NA	FRS2
246	NA	NA	LAMB4	NA	PRDM4
247	NA	NA	CLDN14	NA	RRAS2
248	NA	NA	FBXO24	NA	GGA2
249	NA	NA	AKAP8L	NA	SIPA1L3
250	NA	NA	AHDC1	NA	N4BP3
251	NA	NA	BMP10	NA	TCL6
252	NA	NA	VSX1	NA	TSPAN13
253	NA	NA	PCDHA5	NA	P2RY10
254	NA	NA	OTUD7B	NA	SNTG2
255	NA	NA	SPC25	NA	SDK2
256	NA	NA	HAMP	NA	WDR74

257	NA	NA	MYL7	NA	UBE2O
258	NA	NA	DPEP3	NA	NOC3L
259	NA	NA	C2orf49	NA	RBM15
260	NA	NA	CXorf36	NA	FCRL2
261	NA	NA	IMP4	NA	SMC6
262	NA	NA	HSPB6	NA	TRAPPC9
263	NA	NA	AZU1	NA	PIKFYVE
264	NA	NA	BLK	NA	KHDRBS2
265	NA	NA	CD72	NA	42802
266	NA	NA	CD79B	NA	NA
267	NA	NA	CENPA	NA	NA
268	NA	NA	CETP	NA	NA
269	NA	NA	DNTT	NA	NA
270	NA	NA	FOXM1	NA	NA
271	NA	NA	FLT3	NA	NA
272	NA	NA	H2AFX	NA	NA
273	NA	NA	IGLL1	NA	NA
274	NA	NA	KIF11	NA	NA
275	NA	NA	LY6H	NA	NA
276	NA	NA	MKI67	NA	NA
277	NA	NA	MYBL2	NA	NA
278	NA	NA	PDE6D	NA	NA
279	NA	NA	POLA1	NA	NA
280	NA	NA	PRTN3	NA	NA
281	NA	NA	RAG2	NA	NA
282	NA	NA	RFC2	NA	NA
283	NA	NA	RFC5	NA	NA
284	NA	NA	RRM2	NA	NA
285	NA	NA	SMARCA4	NA	NA
286	NA	NA	SNRPD1	NA	NA
287	NA	NA	SPTA1	NA	NA
288	NA	NA	TCF3	NA	NA
289	NA	NA	TERT	NA	NA
290	NA	NA	TOP2B	NA	NA
291	NA	NA	TSSC1	NA	NA
292	NA	NA	VPREB1	NA	NA
293	NA	NA	XPNPEP2	NA	NA
294	NA	NA	PTTG1	NA	NA
295	NA	NA	TCL1B	NA	NA
296	NA	NA	ESPL1	NA	NA
297	NA	NA	KIF14	NA	NA
298	NA	NA	P2RY14	NA	NA
299	NA	NA	SMC4	NA	NA

300	NA	NA	TACC3	NA	NA
301	NA	NA	NOP56	NA	NA
302	NA	NA	SIVA1	NA	NA
303	NA	NA	ARPP21	NA	NA
304	NA	NA	HNRNPA0	NA	NA
305	NA	NA	UBE2C	NA	NA
306	NA	NA	KIF4A	NA	NA
307	NA	NA	OR7A5	NA	NA
308	NA	NA	VPREB3	NA	NA
309	NA	NA	TRA2A	NA	NA
310	NA	NA	SAC3D1	NA	NA
311	NA	NA	MRTO4	NA	NA
312	NA	NA	NUSAP1	NA	NA
313	NA	NA	AHSP	NA	NA
314	NA	NA	GTSE1	NA	NA
315	NA	NA	CEP55	NA	NA
316	NA	NA	QRSL1	NA	NA
317	NA	NA	SPC25	NA	NA
318	NA	NA	LSM2	NA	NA
319	NA	NA	CCDC81	NA	NA
320	NA	NA	SHCBP1	NA	NA
321	NA	NA	C16orf59	NA	NA
322	NA	NA	HPS4	NA	NA
323	NA	NA	BLK	NA	NA
324	NA	NA	CD72	NA	NA
325	NA	NA	CD79B	NA	NA
326	NA	NA	DNTT	NA	NA
327	NA	NA	FLT3	NA	NA
328	NA	NA	IGLL1	NA	NA
329	NA	NA	PRTN3	NA	NA
330	NA	NA	RAG2	NA	NA
331	NA	NA	VPREB1	NA	NA
332	NA	NA	ARPP21	NA	NA
333	NA	NA	VPREB3	NA	NA
334	NA	NA	QRSL1	NA	NA
335	NA	NA	CCDC81	NA	NA
336	NA	NA	BLK	NA	NA
337	NA	NA	CD72	NA	NA
338	NA	NA	CD79B	NA	NA
339	NA	NA	DNTT	NA	NA
340	NA	NA	FLT3	NA	NA
341	NA	NA	IGLL1	NA	NA
342	NA	NA	LY6H	NA	NA

343	NA	NA	MYBL2	NA	NA
344	NA	NA	PRTN3	NA	NA
345	NA	NA	RAG2	NA	NA
346	NA	NA	VPREB1	NA	NA
347	NA	NA	ARPP21	NA	NA
348	NA	NA	VPREB3	NA	NA
349	NA	NA	QRSL1	NA	NA
350	NA	NA	CCDC81	NA	NA

Table_S2_PovertyEx_vs_UnExp_upr

	Top	p.value	FDR	logFC
RAG1	1	2.25E-88	6.67E-84	3.554289072
PCDH9	10	2.41E-61	7.14E-58	3.158456629
TERF2	5	1.26E-71	7.44E-68	3.016238331
IGF2BP1	2	1.11E-77	1.64E-73	2.664836213
TCL1A	15	3.25E-52	6.42E-49	2.480287049
NRN1	11	7.41E-61	1.99E-57	2.394049148
TP53INP1	22	2.69E-44	3.61E-41	2.362609764
GNG11	12	2.28E-58	5.63E-55	2.309571438
STAG3	21	1.10E-44	1.55E-41	2.283671314
MME	29	3.51E-42	3.58E-39	2.248374891
FYB1	33	1.51E-40	1.35E-37	2.171166417
HPS4	58	8.71E-34	4.45E-31	2.081803009
PTPRK	14	1.72E-54	3.64E-51	2.053654891
MCTP2	17	5.70E-51	9.93E-48	1.938042477
SEMA6A	27	6.62E-43	7.25E-40	1.914447715
TNS1	18	1.58E-49	2.60E-46	1.911330794
SDC2	19	2.36E-47	3.67E-44	1.906945926
ABHD3	64	5.32E-33	2.46E-30	1.90236241
SCN3A	31	2.33E-41	2.22E-38	1.862227646
ERGIC1	74	5.42E-31	2.17E-28	1.807464459
PLEKHG4B	23	8.51E-44	1.09E-40	1.797918858
INSR	76	1.26E-30	4.91E-28	1.78219652
SOCS2	132	3.03E-23	6.80E-21	1.763923656
CD19	112	6.28E-25	1.66E-22	1.7449401
SSBP2	104	7.68E-26	2.19E-23	1.723628636
GAB1	110	2.96E-25	7.97E-23	1.713559795
ARHGAP24	35	1.23E-39	1.04E-36	1.712228876
CACNB2	50	8.36E-36	4.95E-33	1.681703199
POU2AF1	47	1.23E-36	7.73E-34	1.626945799
MYO10	30	1.41E-41	1.39E-38	1.611554137
PHYH	91	3.67E-28	1.19E-25	1.598110747
IGLL1	242	2.83E-17	3.47E-15	1.590059179
PCLO	43	3.72E-37	2.56E-34	1.588537521
FHIT	114	8.45E-25	2.19E-22	1.565663649
LINC01013	190	1.60E-19	2.50E-17	1.549685986
EDEM1	138	6.67E-23	1.43E-20	1.54393183
TMED6	44	7.41E-37	4.93E-34	1.538334838
CMTM7	187	8.15E-20	1.29E-17	1.532507156
IDI1	232	1.19E-17	1.52E-15	1.522251487
CRELD2	67	9.87E-33	4.36E-30	1.480353732
BEST3	49	4.59E-36	2.77E-33	1.477857809

MYADM	85	1.13E-29	3.93E-27	1.477003699
SMAD1	156	6.80E-22	1.29E-19	1.475411078
TNFRSF21	87	7.72E-29	2.63E-26	1.471144129
SPTBN1	169	5.33E-21	9.34E-19	1.453743143
DPEP1	274	4.27E-16	4.62E-14	1.435085685
SFXN1	149	4.28E-22	8.50E-20	1.422602757
WASF2	78	1.93E-30	7.31E-28	1.41583946
BLACE	181	2.80E-20	4.58E-18	1.40251741
MIB1	143	1.32E-22	2.73E-20	1.402427799
PAX5	142	1.26E-22	2.63E-20	1.402400876
NEIL1	317	1.08E-14	1.01E-12	1.393439873
STK32B	158	9.01E-22	1.69E-19	1.390087228
CALN1	41	1.98E-37	1.43E-34	1.382201395
CIITA	105	1.58E-25	4.45E-23	1.380669674
FBXW7	307	5.81E-15	5.60E-13	1.373621606
SLC35E3	285	1.20E-15	1.25E-13	1.373057929
ISG20	217	3.51E-18	4.79E-16	1.364679159
LAIR1	243	3.06E-17	3.73E-15	1.363965475
MDM2	183	3.04E-20	4.92E-18	1.341750835
H1-0	197	3.34E-19	5.02E-17	1.340331425
PEAK1	126	9.70E-24	2.28E-21	1.336445147
FARP1	62	3.30E-33	1.58E-30	1.330934334
BIRC7	69	5.33E-32	2.29E-29	1.282970311
VPREB3	289	1.60E-15	1.63E-13	1.280094565
SHROOM3	97	3.07E-27	9.38E-25	1.274728845
UXS1	293	2.26E-15	2.28E-13	1.27395114
SP4	260	1.16E-16	1.31E-14	1.265807639
CBFA2T3	144	1.43E-22	2.93E-20	1.259948293
TFPI	173	9.02E-21	1.54E-18	1.255151353
MDK	204	1.09E-18	1.59E-16	1.25441367
ITPR1	286	1.42E-15	1.47E-13	1.237783086
BACH2	218	4.27E-18	5.78E-16	1.237361629
KNTC1	265	1.89E-16	2.11E-14	1.232069484
FCHSD2	256	9.06E-17	1.05E-14	1.210484086
GNG7	226	6.61E-18	8.66E-16	1.199873364
STMN1	570	5.33E-10	2.77E-08	1.197319131
HLA-DOA	386	4.64E-13	3.55E-11	1.186907905
TSPO	309	6.66E-15	6.38E-13	1.167579085
HSPB1	180	1.73E-20	2.84E-18	1.163102802
SH2D4B	368	2.46E-13	1.97E-11	1.157828924
DRAM1	207	1.23E-18	1.76E-16	1.157692364
KCNN1	54	2.07E-34	1.14E-31	1.142608265
PDE4D	108	2.07E-25	5.66E-23	1.14151581

FADS3	224	6.28E-18	8.29E-16	1.12925717
HAP1	68	5.20E-32	2.26E-29	1.12595743
EGFL7	330	2.73E-14	2.45E-12	1.12157289
SYK	417	3.94E-12	2.79E-10	1.105162725
DOK3	393	7.02E-13	5.29E-11	1.103023695
ANKRD30B	93	8.45E-28	2.69E-25	1.099309604
MTCO1P12	266	2.01E-16	2.23E-14	1.095409006
OVCH2	436	9.82E-12	6.65E-10	1.088683532
TUSC3	82	3.40E-30	1.23E-27	1.087206132
LINC01416	77	1.49E-30	5.74E-28	1.080805865
FOXO1	452	1.78E-11	1.16E-09	1.076869121
FCMR	295	2.49E-15	2.50E-13	1.068192914
NKAIN4	84	5.31E-30	1.87E-27	1.060596122
AKAP12	163	1.99E-21	3.60E-19	1.056025629
HEMGN	396	1.06E-12	7.90E-11	1.051977499
CDK6	482	4.36E-11	2.67E-09	1.05032313
ATP1B3	668	5.97E-09	2.64E-07	1.048481604
COL24A1	117	1.54E-24	3.89E-22	1.042756073
FAM107B	360	1.34E-13	1.10E-11	1.036668119
FKBP1A	495	6.84E-11	4.09E-09	1.034327569
NASP	656	4.53E-09	2.04E-07	1.026700909
CD27	102	4.36E-26	1.26E-23	1.023768611
NR3C2	107	2.00E-25	5.53E-23	1.022664025
DSC3	103	4.57E-26	1.31E-23	1.010693464
TCL1B	46	1.04E-36	6.70E-34	1.00851187
HLA-DRA	202	7.64E-19	1.12E-16	1.003046135
PRDX1	494	6.75E-11	4.05E-09	1.000735078
INO80	522	1.70E-10	9.65E-09	0.999650257
ARHGEF4	120	3.74E-24	9.22E-22	0.996857078
NREP	414	2.89E-12	2.06E-10	0.986852803
RUBCNL	318	1.21E-14	1.13E-12	0.98286308
ADGRF1	195	3.23E-19	4.88E-17	0.982596508
LOC1025462	116	1.12E-24	2.86E-22	0.979523568
HLA-DPA1	468	2.77E-11	1.75E-09	0.972753662
TCF3	407	2.21E-12	1.61E-10	0.972704194
LINC00676	106	1.74E-25	4.86E-23	0.970058212
UNC79	185	3.89E-20	6.22E-18	0.969717928
MSR1	248	5.58E-17	6.66E-15	0.968717708
LTB	389	5.65E-13	4.29E-11	0.967287378
ATP6V1G1	599	1.35E-09	6.66E-08	0.967179594
LOC283299	496	7.17E-11	4.28E-09	0.962224433
LINC00487	131	2.67E-23	6.04E-21	0.961733834
KIF26B	115	1.11E-24	2.86E-22	0.958568248

PTPN7	247	4.81E-17	5.76E-15	0.958551453
FOXP1	563	4.70E-10	2.47E-08	0.956491892
PIK3C3	608	1.54E-09	7.48E-08	0.956312435
AK7	130	2.35E-23	5.36E-21	0.952244504
CDCA7	598	1.26E-09	6.23E-08	0.948877933
LINC00670	72	1.51E-31	6.22E-29	0.945928005
CRMP1	196	3.23E-19	4.88E-17	0.944952775
INO80C	399	1.28E-12	9.48E-11	0.944139632
MLXIP	577	7.40E-10	3.79E-08	0.931416775
UGP2	728	1.92E-08	7.80E-07	0.929960033
TSPAN7	714	1.44E-08	5.98E-07	0.929559036
ARPP21	849	1.15E-07	4.01E-06	0.9289535
NOTCH1	322	1.84E-14	1.69E-12	0.928687936
TCFL5	394	8.25E-13	6.20E-11	0.924842646
ARHGEF12	193	2.87E-19	4.40E-17	0.922968551
HLA-DQB1	475	3.23E-11	2.01E-09	0.920725084
CALD1	150	4.70E-22	9.26E-20	0.918575977
GNAS	535	2.44E-10	1.35E-08	0.916025075
SPTAN1	730	1.96E-08	7.96E-07	0.913942045
ANKRD10	442	1.18E-11	7.93E-10	0.912655417
NDUFAF6	444	1.31E-11	8.74E-10	0.909631048
IKZF1	678	7.00E-09	3.05E-07	0.90864318
HLA-DPB1	401	1.30E-12	9.57E-11	0.906179447
GIMAP2	538	2.70E-10	1.49E-08	0.899099433
ZNF608	361	1.45E-13	1.19E-11	0.897683871
BMP3	512	1.24E-10	7.16E-09	0.897190977
TXLNGY	665	5.37E-09	2.39E-07	0.897148308
TENM4	225	6.57E-18	8.63E-16	0.895873822
ZNF827	305	5.17E-15	5.02E-13	0.890719947
TRAF5	466	2.60E-11	1.65E-09	0.8844134
CMTM8	315	9.46E-15	8.89E-13	0.883418018
LINC02273	461	2.18E-11	1.40E-09	0.877502072
MZB1	534	2.42E-10	1.34E-08	0.876314333
CHD7	778	3.96E-08	1.51E-06	0.873995014
JUN	529	2.09E-10	1.17E-08	0.873617781
PRKCB	799	5.23E-08	1.94E-06	0.873292045
NETO1	188	1.03E-19	1.62E-17	0.873196703
TMEM243	707	1.31E-08	5.50E-07	0.867599081
CIAO3	701	1.18E-08	5.00E-07	0.864863943
SDHA	961	3.92E-07	1.21E-05	0.864354634
CEMIP2	595	1.06E-09	5.27E-08	0.862907605
PSME2	886	1.71E-07	5.70E-06	0.8588975
TPTEP1	241	2.62E-17	3.22E-15	0.853974448

CDH4	166	3.22E-21	5.74E-19	0.841536414
SOCS2-AS1	698	1.12E-08	4.76E-07	0.841404451
LIG4	583	8.14E-10	4.13E-08	0.838533562
EBF1	645	3.72E-09	1.71E-07	0.8378749
UCP2	1099	1.66E-06	4.46E-05	0.836733706
POLE	979	4.62E-07	1.40E-05	0.832101795
UBA7	1012	6.44E-07	1.88E-05	0.830457022
SORBS2	222	5.57E-18	7.43E-16	0.830036179
ENOSF1	381	3.94E-13	3.06E-11	0.829517148
NPY	1004	5.98E-07	1.76E-05	0.827271841
SLC12A2	568	5.24E-10	2.73E-08	0.827171039
RBMS3	170	6.92E-21	1.20E-18	0.826107324
CHCHD7	885	1.69E-07	5.65E-06	0.823940024
CBX5	1093	1.54E-06	4.17E-05	0.823434002
HLA-DQB2	346	6.17E-14	5.27E-12	0.822567789
MYO18B	451	1.77E-11	1.16E-09	0.819664105
SCMH1	673	6.48E-09	2.85E-07	0.817149346
CPXM1	460	2.11E-11	1.36E-09	0.812478869
BMPR1B	192	2.21E-19	3.41E-17	0.807796442
RCSD1	752	2.78E-08	1.10E-06	0.805925522
GOLGA8B	240	2.43E-17	2.99E-15	0.80068343
LPAR6	1176	3.81E-06	9.58E-05	0.80040069
MTCO1P40	167	4.32E-21	7.66E-19	0.795850243
COMMD4	510	1.09E-10	6.30E-09	0.793557722
CHD9	1074	1.29E-06	3.57E-05	0.791407426
UBE2I	711	1.40E-08	5.81E-07	0.788625
HBS1L	1185	4.08E-06	0.0001018	0.788455353
IGHV5-78	523	1.73E-10	9.81E-09	0.785219067
FUS	817	6.44E-08	2.33E-06	0.784058438
LILRA2	1017	6.69E-07	1.95E-05	0.78162401
ARID5B	1410	2.13E-05	0.00044676	0.780981484
CLIC5	134	5.28E-23	1.17E-20	0.780592179
CD52	735	2.32E-08	9.33E-07	0.779289592
PARP1	1285	9.86E-06	0.00022712	0.77620083
ARHGDIB	749	2.76E-08	1.09E-06	0.774712531
FLI1	734	2.31E-08	9.30E-07	0.774616901
TAPT1-AS1	717	1.60E-08	6.60E-07	0.762561955
SLAMF6	587	9.37E-10	4.72E-08	0.761989573
PSD3	1198	4.56E-06	0.00011256	0.761385464
CUX1	989	5.16E-07	1.54E-05	0.755279172
NUCB2	1196	4.51E-06	0.00011157	0.748960817
CYB5R2	623	2.29E-09	1.09E-07	0.742780145
PLEKHA5	474	3.03E-11	1.89E-09	0.741610187

PTGDR	278	6.20E-16	6.60E-14	0.741180255
GNPTAB	1008	6.29E-07	1.85E-05	0.740872877
TOP2B	1223	5.76E-06	0.00013948	0.738919938
HMGN3	1133	2.41E-06	6.29E-05	0.732576667
INKA1	909	2.03E-07	6.61E-06	0.730602876
RERGL	209	1.63E-18	2.31E-16	0.729370963
LITAF	560	4.29E-10	2.27E-08	0.725449884
FAM214A	889	1.74E-07	5.79E-06	0.719758676
MIR5195	434	9.56E-12	6.52E-10	0.716880282
GBP4	1274	9.32E-06	0.00021656	0.715966443
SCARB1	819	6.78E-08	2.45E-06	0.7157405
TAFA1	194	3.23E-19	4.88E-17	0.715739727
WBP1L	948	3.29E-07	1.03E-05	0.713164545
BID	852	1.19E-07	4.12E-06	0.712454096
BCL7A	878	1.58E-07	5.32E-06	0.709253983
OAZ1	860	1.25E-07	4.31E-06	0.705646211
MYOCD	182	2.83E-20	4.60E-18	0.701457966
CALM3	721	1.80E-08	7.40E-07	0.69684031
LINC01237	415	3.47E-12	2.47E-10	0.695429472
PRX	349	7.78E-14	6.60E-12	0.695334425
H2AC6	1512	3.82E-05	0.00074701	0.692193148
RAG2	501	7.95E-11	4.69E-09	0.691760768
HLA-DOB	258	9.55E-17	1.10E-14	0.690644798
ARGLU1	787	4.43E-08	1.67E-06	0.69039446
SNRNP27	676	6.90E-09	3.02E-07	0.689852586
TRIM24	655	4.53E-09	2.04E-07	0.685740548
TRIM27	1471	3.13E-05	0.00062902	0.682692173
HLA-DMB	1548	4.52E-05	0.00086348	0.682598865
RSRC2	1257	7.73E-06	0.00018204	0.682025119
PLCG1	339	3.91E-14	3.41E-12	0.682003663
HHIP	287	1.53E-15	1.58E-13	0.68057874
GIMAP4	1360	1.64E-05	0.00035675	0.680484435
ZNF107	1091	1.54E-06	4.17E-05	0.676022435
TRIO	755	2.87E-08	1.12E-06	0.672513232
B2M	382	4.11E-13	3.19E-11	0.671652045
CBX2	362	1.49E-13	1.22E-11	0.671028933
CCDC93	811	6.13E-08	2.23E-06	0.670796349
MCM2	1363	1.67E-05	0.0003616	0.670258824
PIK3IP1	1297	1.11E-05	0.00025217	0.669902386
DLGAP2	343	5.31E-14	4.58E-12	0.660540054
TSPYL5	297	3.41E-15	3.39E-13	0.660114342
NUMA1	1218	5.41E-06	0.00013134	0.657840066
LAPTM5	739	2.47E-08	9.88E-07	0.657777272

RASAL2	491	5.85E-11	3.52E-09	0.657231791
VGLL4	702	1.21E-08	5.09E-07	0.655837756
CPNE2	971	4.48E-07	1.37E-05	0.655483732
PEG3	377	3.65E-13	2.87E-11	0.655105343
TRIM38	1624	6.64E-05	0.0012098	0.65488439
PCCA	614	1.69E-09	8.17E-08	0.654710311
TMSB4X	569	5.28E-10	2.74E-08	0.652976335
NCF4	1319	1.29E-05	0.00028951	0.651479118
TMPO	1649	7.40E-05	0.00132713	0.648488007
ZCCHC7	1392	1.98E-05	0.00042101	0.647921996
HNRNPA2B1	986	5.04E-07	1.51E-05	0.645944552
THRAP3	1343	1.52E-05	0.00033523	0.644601717
MYLK	754	2.82E-08	1.11E-06	0.644353732
STK39	519	1.61E-10	9.17E-09	0.64385282
TIA1	1634	6.99E-05	0.00126673	0.643591864
CD74	301	3.96E-15	3.89E-13	0.642742826
SLFN13	427	7.21E-12	5.00E-10	0.639500626
ACTB	790	4.55E-08	1.71E-06	0.639077278
ZMYND8	1421	2.31E-05	0.00048151	0.638264229
NEK6	896	1.83E-07	6.05E-06	0.637374293
GLG1	1504	3.67E-05	0.00072213	0.634032139
H2BC12	1752	0.00011779	0.00198947	0.632795241
VPS13C	1516	3.86E-05	0.00075313	0.63262097
NBPF1	914	2.15E-07	6.95E-06	0.628428599
H3C4	606	1.53E-09	7.47E-08	0.626223262
NIP7	1304	1.15E-05	0.0002614	0.625832416
DPF3	263	1.65E-16	1.86E-14	0.625679093
UBE2E3	499	7.58E-11	4.50E-09	0.624820709
KHDRBS3	574	5.93E-10	3.05E-08	0.624737368
RIMKLB	1662	7.92E-05	0.00141065	0.623462318
TMEM263	1932	0.00025254	0.00386794	0.622010159
YEATS2	1333	1.40E-05	0.00031046	0.621356556
TKT	2097	0.00048623	0.00686124	0.620548023
ALDH5A1	1317	1.28E-05	0.00028679	0.620479719
HLA-DMA	1373	1.74E-05	0.00037548	0.620447749
UTY	1086	1.44E-06	3.94E-05	0.619991067
KLHL6	1528	4.08E-05	0.00078921	0.619509831
PSMA5	1648	7.39E-05	0.00132713	0.61947284
HSPA4	1608	6.11E-05	0.00112359	0.619289844
SRP9	1738	0.00010851	0.00184745	0.619063921
PID1	259	1.13E-16	1.29E-14	0.618975484
MPP6	357	9.92E-14	8.22E-12	0.618704344
ADGRA3	913	2.15E-07	6.95E-06	0.61818174

PRDM2	1489	3.35E-05	0.00066598	0.61799659
RFTN1	1329	1.37E-05	0.00030444	0.617043903
HGSNAT	487	5.05E-11	3.07E-09	0.611446679
DAGLB	1522	3.93E-05	0.00076487	0.610518725
MTF2	2060	0.00041664	0.00598489	0.609250989
H2BC5	1208	4.99E-06	0.00012214	0.606776416
ODF2L	704	1.24E-08	5.23E-07	0.60584183
MYB	1913	0.00022533	0.00348543	0.603396486
LDLRAD4	1477	3.19E-05	0.00063962	0.602688899
ADARB2-AS1	335	3.61E-14	3.19E-12	0.602013947
KIF16B	939	2.79E-07	8.79E-06	0.597136477
TLE1	1181	3.88E-06	9.72E-05	0.595657366
PCNA	2200	0.00067673	0.00910234	0.595234961
SMARCA4	1701	9.43E-05	0.00164103	0.594632028
VAV3	1222	5.70E-06	0.00013812	0.592147374
MAML2	789	4.55E-08	1.70E-06	0.590139502
ABCG2	363	1.57E-13	1.28E-11	0.588818605
SYVN1	1059	1.14E-06	3.19E-05	0.588562767
SOX11	298	3.42E-15	3.39E-13	0.588527775
MBNL3	1398	2.01E-05	0.00042604	0.588397444
GOLGA8A	511	1.24E-10	7.16E-09	0.588318438
VAV1	1647	7.38E-05	0.00132664	0.587587698
TOX	1154	3.03E-06	7.78E-05	0.586392961
PARP14	2087	0.00047457	0.00672776	0.586148774
GCSAM	697	1.12E-08	4.75E-07	0.58611601
OAS3	1656	7.65E-05	0.00136653	0.585510267
HAUS5	1122	2.14E-06	5.65E-05	0.584207782
NDFIP1	300	3.73E-15	3.68E-13	0.583832467
SERF2	1109	1.86E-06	4.96E-05	0.583455356
IGF1R	1159	3.22E-06	8.23E-05	0.581448703
ETV5	596	1.12E-09	5.57E-08	0.581241293
RAB3IP	449	1.68E-11	1.11E-09	0.580421004
AGPAT2	967	4.21E-07	1.29E-05	0.580338918
GSDME	643	3.55E-09	1.64E-07	0.580285313

Table_S2_PovertyEx_vs_UnExp_dow

	Top	p.value	FDR	logFC
LSP1	4	8.94E-74	6.61E-70	-3.037010854
FLT3	13	5.24E-55	1.19E-51	-2.785873788
S100A16	16	1.47E-51	2.73E-48	-2.70382188
ANXA2	6	2.56E-65	1.26E-61	-2.499674632
CD9	66	9.74E-33	4.36E-30	-2.4403548
DDIT4	7	2.92E-63	1.24E-59	-2.406694883
PLP2	3	1.08E-74	1.07E-70	-2.388321336
CD164	48	2.33E-36	1.44E-33	-2.370690011
FLNA	8	4.46E-63	1.65E-59	-2.368678289
IRF8	25	3.09E-43	3.66E-40	-2.306257139
PDLIM1	61	2.04E-33	9.92E-31	-2.290478335
SRGN	9	6.12E-62	2.01E-58	-2.126843382
IL3RA	45	7.49E-37	4.93E-34	-2.020848937
DENND3	80	2.42E-30	8.95E-28	-2.001652962
PLEK	24	2.81E-43	3.46E-40	-1.980562594
CD44	36	3.88E-39	3.19E-36	-1.957697578
MOB3A	26	6.30E-43	7.17E-40	-1.935162891
KLF6	147	3.05E-22	6.13E-20	-1.902254304
MICAL1	79	2.18E-30	8.15E-28	-1.856455652
MS4A6A	20	4.79E-46	7.09E-43	-1.845336572
CYTH1	63	3.44E-33	1.62E-30	-1.836564477
LYST	55	2.98E-34	1.60E-31	-1.834312628
CDKN1A	40	7.55E-38	5.58E-35	-1.827575774
VIM	98	5.35E-27	1.62E-24	-1.807283593
FOS	219	4.28E-18	5.78E-16	-1.787216272
CD82	70	9.75E-32	4.09E-29	-1.763293747
LCP1	171	7.41E-21	1.28E-18	-1.719521263
ACTN1	37	9.32E-39	7.46E-36	-1.71837951
FLNB	59	1.50E-33	7.53E-31	-1.676566984
GAS7	39	1.39E-38	1.06E-35	-1.667218342
STK17B	118	1.77E-24	4.43E-22	-1.602343109
SH3BP2	94	9.59E-28	3.02E-25	-1.597100745
CHST12	34	3.48E-40	3.03E-37	-1.596265771
CYBB	88	1.48E-28	4.97E-26	-1.577298014
NKG7	28	7.56E-43	7.99E-40	-1.560447585
IL2RG	191	1.74E-19	2.70E-17	-1.557554561
IL17RA	56	7.01E-34	3.70E-31	-1.555333274
USP36	101	4.20E-26	1.23E-23	-1.540252452
KCNAB2	42	2.98E-37	2.10E-34	-1.528223243
BLK	81	3.22E-30	1.18E-27	-1.52367489
ST3GAL1	162	1.50E-21	2.73E-19	-1.515740927

NIBAN3	157	8.56E-22	1.61E-19	-1.509113491
RAP1GAP2	71	9.82E-32	4.09E-29	-1.508486634
NFE2	32	5.78E-41	5.34E-38	-1.496496826
FUT7	38	1.04E-38	8.09E-36	-1.496394939
LAT2	272	3.07E-16	3.34E-14	-1.492214044
KLF10	160	1.46E-21	2.70E-19	-1.491762939
TSC22D3	327	2.14E-14	1.94E-12	-1.490801334
CYTIP	52	6.87E-35	3.91E-32	-1.489268962
EVI2B	127	1.69E-23	3.95E-21	-1.488360528
DDIT4L	57	7.53E-34	3.91E-31	-1.474026768
SERPINB1	231	1.16E-17	1.49E-15	-1.473194233
NFKBIZ	95	1.19E-27	3.72E-25	-1.462027386
MYT1L	60	1.87E-33	9.20E-31	-1.443982286
BLNK	233	1.53E-17	1.94E-15	-1.442843817
MGAT4A	154	6.54E-22	1.26E-19	-1.428915635
P2RX5	53	8.47E-35	4.73E-32	-1.411313362
HSH2D	213	2.59E-18	3.60E-16	-1.406955251
ITGB2	137	6.52E-23	1.41E-20	-1.390869545
PDE4B	239	2.39E-17	2.96E-15	-1.386062961
OGT	223	5.70E-18	7.56E-16	-1.378129255
UBE2G2	211	2.32E-18	3.25E-16	-1.375524286
FKBP5	215	2.68E-18	3.69E-16	-1.373843817
NBEAL2	73	4.75E-31	1.93E-28	-1.358727923
MYO1F	119	3.21E-24	7.99E-22	-1.355089286
PPM1F	136	6.35E-23	1.38E-20	-1.349421864
PTTG1IP	255	8.68E-17	1.01E-14	-1.343621907
NAV1	269	2.21E-16	2.43E-14	-1.340937647
S100A4	51	9.59E-36	5.57E-33	-1.339679484
CORO1A	288	1.57E-15	1.62E-13	-1.326651137
SAT1	379	3.78E-13	2.95E-11	-1.32616442
LGALS3BP	296	3.33E-15	3.32E-13	-1.310829748
STX7	268	2.15E-16	2.37E-14	-1.305605801
STING1	139	6.81E-23	1.45E-20	-1.303040016
GLUL	210	2.01E-18	2.83E-16	-1.298055639
CNN2	184	3.30E-20	5.31E-18	-1.297134974
IQGAP2	141	9.58E-23	2.01E-20	-1.284231346
BCLAF1	333	2.99E-14	2.66E-12	-1.282725261
PPA1	135	5.44E-23	1.19E-20	-1.279695157
C12orf75	128	2.12E-23	4.90E-21	-1.277293482
MAP2K3	237	1.87E-17	2.34E-15	-1.268549285
RFLNB	251	6.95E-17	8.20E-15	-1.265803905
TASL	212	2.39E-18	3.34E-16	-1.258072974
IFITM3	254	8.35E-17	9.73E-15	-1.255464932

AMD1	238	1.97E-17	2.45E-15	-1.247352994
VSIR	178	1.14E-20	1.89E-18	-1.226755151
RAB37	246	4.80E-17	5.76E-15	-1.207322107
ANTXR2	83	4.30E-30	1.53E-27	-1.20654684
POU2F2	96	1.95E-27	6.01E-25	-1.196023024
FERMT3	319	1.22E-14	1.13E-12	-1.194494399
PTPN6	371	2.50E-13	1.99E-11	-1.194235974
ADGRG1	228	7.39E-18	9.59E-16	-1.190413936
C20orf27	65	9.53E-33	4.34E-30	-1.179693533
MSN	408	2.30E-12	1.67E-10	-1.178927142
CAPG	323	1.89E-14	1.73E-12	-1.176902003
PSAP	520	1.70E-10	9.65E-09	-1.173922497
EVL	284	1.04E-15	1.08E-13	-1.165771317
KLF2	129	2.26E-23	5.19E-21	-1.159842763
PLXNB2	270	2.74E-16	3.00E-14	-1.159104308
FOSL2	86	2.39E-29	8.22E-27	-1.155027747
SAMHD1	172	7.98E-21	1.37E-18	-1.153136398
ADGRE2	109	2.54E-25	6.89E-23	-1.147734607
SIK1	111	4.61E-25	1.23E-22	-1.147176041
B4GALT1	262	1.40E-16	1.58E-14	-1.145211758
PRNP	277	5.84E-16	6.24E-14	-1.137826795
IGBP1	409	2.33E-12	1.69E-10	-1.137447284
RHBDF2	165	2.66E-21	4.76E-19	-1.135776269
PLVAP	75	1.21E-30	4.77E-28	-1.134963208
CSF3R	306	5.51E-15	5.33E-13	-1.12756384
SLC2A3	264	1.72E-16	1.93E-14	-1.124508576
CTNND1	152	5.45E-22	1.06E-19	-1.121483856
SH3BP5	100	3.51E-26	1.04E-23	-1.112449542
ANXA7	462	2.21E-11	1.41E-09	-1.09460745
SLC2A5	123	6.65E-24	1.60E-21	-1.094405012
ITGAE	294	2.27E-15	2.28E-13	-1.090463919
SOD2	456	1.86E-11	1.21E-09	-1.081207661
CAST	276	5.41E-16	5.80E-14	-1.076812995
RASD1	331	2.85E-14	2.55E-12	-1.075718004
LINC00707	92	7.98E-28	2.57E-25	-1.071836793
ADGRE5	480	4.00E-11	2.47E-09	-1.071702616
CSGALNACT1	359	1.26E-13	1.04E-11	-1.069816003
PFKFB3	121	3.91E-24	9.56E-22	-1.065009189
CD69	828	7.98E-08	2.85E-06	-1.063660268
LILRB2	344	5.48E-14	4.71E-12	-1.056987334
MX1	775	3.93E-08	1.50E-06	-1.05457155
C9orf72	261	1.22E-16	1.39E-14	-1.050352556
SFMBT2	273	3.19E-16	3.46E-14	-1.045108806

MAP3K8	267	2.08E-16	2.31E-14	-1.044003812
STAB1	89	1.76E-28	5.84E-26	-1.03830206
ZFP36	410	2.36E-12	1.70E-10	-1.033899005
PROM1	279	6.27E-16	6.65E-14	-1.026965497
XIST	504	9.08E-11	5.33E-09	-1.024960023
SPOCK2	133	3.32E-23	7.40E-21	-1.023071715
LIMD2	252	7.71E-17	9.05E-15	-1.01080629
DYNLT1	351	7.91E-14	6.67E-12	-1.010245675
C15orf39	90	2.69E-28	8.83E-26	-1.008481905
DDX21	455	1.85E-11	1.20E-09	-1.005840816
TCP1	722	1.83E-08	7.50E-07	-0.991620661
GPM6B	376	3.50E-13	2.75E-11	-0.988771329
RBM3	732	2.16E-08	8.73E-07	-0.983614173
IGHD	375	3.34E-13	2.64E-11	-0.983208009
FAM53B	310	6.84E-15	6.53E-13	-0.977843393
SNHG5	435	9.69E-12	6.59E-10	-0.974850846
VNN1	99	1.64E-26	4.91E-24	-0.973750273
SYNGR1	507	9.78E-11	5.71E-09	-0.970946453
RNF24	332	2.90E-14	2.58E-12	-0.97083995
PREX1	465	2.58E-11	1.64E-09	-0.970039153
SLITRK4	174	9.21E-21	1.57E-18	-0.967849468
TACC3	325	2.03E-14	1.85E-12	-0.967465017
LAP3	649	3.81E-09	1.74E-07	-0.963729449
GOLIM4	148	4.07E-22	8.14E-20	-0.961756217
IL6R	113	8.32E-25	2.18E-22	-0.954943421
EZR	908	2.02E-07	6.58E-06	-0.95475307
TALDO1	744	2.57E-08	1.02E-06	-0.952832802
OGFRL1	313	7.99E-15	7.56E-13	-0.948563565
JPT1	549	3.38E-10	1.82E-08	-0.946908111
RIPOR2	675	6.76E-09	2.96E-07	-0.94639335
PFKP	299	3.58E-15	3.54E-13	-0.943507837
PDCD4	514	1.44E-10	8.28E-09	-0.941554729
ARMH1	493	6.04E-11	3.63E-09	-0.941038424
CSGALNACT2	140	9.12E-23	1.93E-20	-0.940520853
NDE1	422	4.88E-12	3.42E-10	-0.939515386
AP1S2	575	6.94E-10	3.57E-08	-0.935586397
GLIPR1	348	6.96E-14	5.92E-12	-0.933130793
VPS26A	486	5.00E-11	3.04E-09	-0.931124985
SERPINF1	199	4.52E-19	6.71E-17	-0.931081527
C18orf63	201	6.27E-19	9.23E-17	-0.930738923
ASCC1	342	4.44E-14	3.84E-12	-0.928694166
FAM30A	186	4.55E-20	7.24E-18	-0.925306988
RASGRP2	321	1.71E-14	1.57E-12	-0.925117859

NIN	620	2.08E-09	9.95E-08	-0.92310915
RNF125	290	1.85E-15	1.89E-13	-0.922426395
ECHDC1	454	1.84E-11	1.20E-09	-0.922366595
ADA	774	3.87E-08	1.48E-06	-0.919964091
RNF130	378	3.71E-13	2.91E-11	-0.919956033
EVI2A	347	6.75E-14	5.76E-12	-0.919248648
LRRFIP1	509	1.05E-10	6.08E-09	-0.91835941
ARFGAP3	458	1.88E-11	1.21E-09	-0.915413077
AHNAK	214	2.61E-18	3.60E-16	-0.914437247
EMP3	151	5.41E-22	1.06E-19	-0.907154545
RAB34	476	3.53E-11	2.20E-09	-0.904803731
GNA15	413	2.83E-12	2.03E-10	-0.900281002
TMED10	843	1.00E-07	3.52E-06	-0.900177562
SRP72	812	6.21E-08	2.26E-06	-0.900084819
XAF1	1079	1.33E-06	3.65E-05	-0.899881343
GRB2	600	1.35E-09	6.68E-08	-0.89945424
TNFAIP3	781	4.07E-08	1.54E-06	-0.89790331
FRMD4B	751	2.78E-08	1.09E-06	-0.89394358
GAB3	518	1.55E-10	8.87E-09	-0.893478893
ANKRD44	432	9.32E-12	6.38E-10	-0.8929276
PLEC	384	4.46E-13	3.44E-11	-0.892442443
APAF1	250	5.91E-17	7.00E-15	-0.890961739
WDFY4	505	9.17E-11	5.37E-09	-0.889366757
ENTPD1	235	1.78E-17	2.24E-15	-0.880364395
BRF1	403	1.74E-12	1.28E-10	-0.878364422
SH2D3C	719	1.68E-08	6.91E-07	-0.877038444
NUFIP2	636	3.13E-09	1.46E-07	-0.873633495
PTP4A1	911	2.12E-07	6.89E-06	-0.872592207
SLC25A37	713	1.43E-08	5.94E-07	-0.870355331
CANX	992	5.34E-07	1.59E-05	-0.869467443
GSTO1	463	2.30E-11	1.47E-09	-0.86900805
PLIN2	829	8.11E-08	2.89E-06	-0.865321557
PPP1R15A	921	2.40E-07	7.70E-06	-0.864456777
SERINC1	760	3.11E-08	1.21E-06	-0.86442597
BTAF1	638	3.18E-09	1.47E-07	-0.859579766
SARAF	1087	1.47E-06	3.99E-05	-0.85917493
NDRG1	153	6.49E-22	1.26E-19	-0.858050158
PMAIP1	1064	1.18E-06	3.29E-05	-0.85776327
METTL7A	383	4.14E-13	3.20E-11	-0.856742742
ATP8A1	326	2.10E-14	1.91E-12	-0.855273817
NFATC3	537	2.56E-10	1.41E-08	-0.85351008
CARD19	200	4.82E-19	7.13E-17	-0.852909206
SNX27	709	1.36E-08	5.70E-07	-0.852451623

ITGA4	919	2.35E-07	7.56E-06	-0.851602706
SNX6	808	5.92E-08	2.17E-06	-0.850514923
TMX1	580	7.79E-10	3.97E-08	-0.850229378
CTSS	863	1.31E-07	4.49E-06	-0.849659772
ALOX5	963	3.95E-07	1.21E-05	-0.848953113
SMAD3	350	7.89E-14	6.67E-12	-0.848734111
SLC7A5	358	1.14E-13	9.44E-12	-0.848226374
RRP1B	489	5.57E-11	3.37E-09	-0.84479768
S100A6	146	2.24E-22	4.53E-20	-0.843946178
ABCA2	236	1.81E-17	2.27E-15	-0.843453873
CCNC	725	1.85E-08	7.56E-07	-0.841362578
MYC	337	3.81E-14	3.34E-12	-0.838674132
ALDH3B1	159	1.22E-21	2.28E-19	-0.837954368
SMAGP	354	8.79E-14	7.35E-12	-0.833733975
MGAT1	802	5.28E-08	1.95E-06	-0.833587487
SPPL2B	586	9.20E-10	4.65E-08	-0.833502448
ANKRD28	651	4.22E-09	1.92E-07	-0.833466438
ADAM8	282	7.88E-16	8.26E-14	-0.831600426
NEAT1	658	4.74E-09	2.13E-07	-0.831311845
LINC-PINT	308	6.14E-15	5.90E-13	-0.831166856
BTNL9	234	1.76E-17	2.23E-15	-0.830901506
NR4A2	291	1.88E-15	1.91E-13	-0.830577143
HBEGF	385	4.57E-13	3.51E-11	-0.829346574
ARHGEF10	561	4.52E-10	2.38E-08	-0.827006829
PAN3	842	9.78E-08	3.44E-06	-0.826229674
NCF2	582	7.98E-10	4.06E-08	-0.82460508
CPNE3	805	5.68E-08	2.09E-06	-0.81691377
ASAP1	792	4.66E-08	1.74E-06	-0.816491208
SMIM24	374	3.12E-13	2.47E-11	-0.814468255
FHL1	1150	2.89E-06	7.42E-05	-0.812067671
DYNC1H1	920	2.35E-07	7.56E-06	-0.811208805
JAK3	602	1.39E-09	6.83E-08	-0.811087546
NAPSB	198	3.91E-19	5.84E-17	-0.808921224
HSP90AB1	1423	2.36E-05	0.00049146	-0.807642663
SMAD2	855	1.22E-07	4.23E-06	-0.807155299
CYTH4	862	1.28E-07	4.40E-06	-0.80617889
TRPM2	687	8.42E-09	3.63E-07	-0.805759854
TIMP1	464	2.50E-11	1.59E-09	-0.805197591
CFP	189	1.23E-19	1.93E-17	-0.804611733
UBQLN2	830	8.32E-08	2.97E-06	-0.804196124
ATP2B4	960	3.91E-07	1.21E-05	-0.802584612
MAPKBP1	388	5.10E-13	3.89E-11	-0.801954554
CASP1	302	4.15E-15	4.07E-13	-0.801530904

ATP6V0D1	836	8.99E-08	3.18E-06	-0.797169977
CCND2	1060	1.14E-06	3.19E-05	-0.79610333
SCPEP1	831	8.45E-08	3.01E-06	-0.795656334
MYH11	345	5.52E-14	4.74E-12	-0.795080847
CD34	1085	1.44E-06	3.93E-05	-0.795046165
VMP1	901	1.89E-07	6.22E-06	-0.794378175
TNFSF13B	161	1.48E-21	2.72E-19	-0.793011166
GAS5	981	4.78E-07	1.44E-05	-0.792045339
ETS2	1131	2.37E-06	6.19E-05	-0.791224381
PGD	1028	8.41E-07	2.42E-05	-0.789410125
SEC14L1	395	8.66E-13	6.49E-11	-0.788897954
CD55	809	5.93E-08	2.17E-06	-0.788154227
UGT3A2	418	4.23E-12	2.99E-10	-0.786143261
EIF4A1	542	2.91E-10	1.59E-08	-0.785350737
SNHG29	710	1.39E-08	5.78E-07	-0.78515897
SLC9A3R1	392	6.50E-13	4.91E-11	-0.78373007
RIOK1	527	1.90E-10	1.07E-08	-0.781648166
SF3B5	508	1.00E-10	5.84E-09	-0.780763063
TRBC2	155	6.70E-22	1.28E-19	-0.780538342
TAGLN2	894	1.80E-07	5.96E-06	-0.779056226
PML	584	8.46E-10	4.29E-08	-0.778144236
TSC22D1	791	4.56E-08	1.71E-06	-0.774506229
SYNCRIP	1096	1.58E-06	4.28E-05	-0.773023018
KIF1B	275	4.90E-16	5.27E-14	-0.771360326
USO1	748	2.76E-08	1.09E-06	-0.771066231
NPC2	619	2.08E-09	9.95E-08	-0.768712198
UBE2J1	1023	7.55E-07	2.18E-05	-0.76645075
PTPRC	541	2.89E-10	1.58E-08	-0.766326858
FXYD5	970	4.42E-07	1.35E-05	-0.765758264
SETBP1	646	3.72E-09	1.71E-07	-0.763894429
GRN	1160	3.24E-06	8.27E-05	-0.763498108
DYM	940	2.88E-07	9.06E-06	-0.762621388
DDX3X	1294	1.07E-05	0.00024472	-0.761826104
ATP2C1	367	2.19E-13	1.77E-11	-0.759543525
BIN2	221	5.04E-18	6.74E-16	-0.759401752
EIF4A3	955	3.68E-07	1.14E-05	-0.756298256
CLIP2	632	2.79E-09	1.31E-07	-0.754342672
KRI1	1062	1.16E-06	3.22E-05	-0.754180303
C1QBP	1092	1.54E-06	4.17E-05	-0.752974781
SH3RF1	703	1.24E-08	5.23E-07	-0.752932634
LASP1	897	1.86E-07	6.12E-06	-0.751919608
ATP6AP2	1262	8.34E-06	0.00019539	-0.751740858
FES	888	1.73E-07	5.77E-06	-0.75121898

UTP6	984	4.91E-07	1.48E-05	-0.750992514
TINF2	1105	1.78E-06	4.77E-05	-0.750601998
EEF1B2	995	5.42E-07	1.61E-05	-0.74875971
MFSD1	803	5.42E-08	2.00E-06	-0.74834106
RAB9A	603	1.44E-09	7.05E-08	-0.747409239
FLII	1117	2.09E-06	5.55E-05	-0.746464256
CNN3	515	1.44E-10	8.28E-09	-0.745559717
OFD1	1339	1.49E-05	0.00032899	-0.745322713
HSDL2	411	2.36E-12	1.70E-10	-0.742233738
HOOK3	785	4.39E-08	1.65E-06	-0.740451243
ADPGK	1047	9.69E-07	2.74E-05	-0.738423705
NUP210	572	5.49E-10	2.84E-08	-0.738043388
SNHG3	917	2.30E-07	7.41E-06	-0.735715427
SNHG8	705	1.27E-08	5.34E-07	-0.733716372
PQBP1	761	3.14E-08	1.22E-06	-0.733139375
GATB	416	3.81E-12	2.71E-10	-0.732794608
GNG2	918	2.32E-07	7.49E-06	-0.732292657
NLRP1	1111	1.93E-06	5.13E-05	-0.731326972
PKIG	280	6.88E-16	7.27E-14	-0.730685206
ACAT1	769	3.51E-08	1.35E-06	-0.730478509
HDAC9	437	9.83E-12	6.65E-10	-0.73022244
MS4A4E	125	8.63E-24	2.04E-21	-0.729548025
MED23	814	6.24E-08	2.27E-06	-0.729360871
PSMC6	1174	3.80E-06	9.57E-05	-0.728989749
STAT3	1090	1.52E-06	4.14E-05	-0.728751281
SUN1	890	1.76E-07	5.84E-06	-0.726116773
PRSS57	124	7.80E-24	1.86E-21	-0.725594609
ABCE1	633	2.81E-09	1.31E-07	-0.724741497
B3GNTL1	445	1.31E-11	8.74E-10	-0.724476513
TCOF1	1226	5.90E-06	0.00014248	-0.723779007
HVCN1	544	3.05E-10	1.66E-08	-0.722516666
RABGAP1L	910	2.11E-07	6.86E-06	-0.721886662
PIK3R5	762	3.15E-08	1.22E-06	-0.7214575
USP9X	1255	7.62E-06	0.00017972	-0.719184943
DUSP3	304	4.59E-15	4.47E-13	-0.718479548
TRAF3IP3	825	7.54E-08	2.71E-06	-0.717601337
PDE3B	324	2.00E-14	1.83E-12	-0.716642101
SEMA4A	257	9.21E-17	1.06E-14	-0.715425368
KCNK17	316	1.08E-14	1.01E-12	-0.714788856
CALHM2	421	4.88E-12	3.42E-10	-0.714615478
GHITM	1764	0.00012495	0.00209604	-0.712424748
NUMB	1355	1.61E-05	0.00035087	-0.711804367
SH3KBP1	1167	3.39E-06	8.60E-05	-0.710577432

PNISR	1158	3.22E-06	8.22E-05	-0.709337912
PSMB1	1537	4.32E-05	0.00083079	-0.709321304
TSPAN13	1197	4.54E-06	0.00011231	-0.707271715
ITSN1	488	5.20E-11	3.16E-09	-0.706831068
LATS2	402	1.33E-12	9.82E-11	-0.706652106
TMEM123	1631	6.90E-05	0.00125231	-0.704190277
PDXK	373	2.96E-13	2.35E-11	-0.702132113
GSTP1	1194	4.47E-06	0.00011068	-0.700178653
GPR132	571	5.49E-10	2.84E-08	-0.699665197
CCDC200	937	2.71E-07	8.56E-06	-0.699484809
AFF3	1228	6.01E-06	0.00014488	-0.699262662
CNIH1	965	4.07E-07	1.25E-05	-0.698653319
AKNA	1024	7.69E-07	2.22E-05	-0.698198977
ELAC2	998	5.65E-07	1.67E-05	-0.69656593
PNP	640	3.38E-09	1.56E-07	-0.6952331
ABR	540	2.82E-10	1.54E-08	-0.695195415
ZYX	227	7.16E-18	9.33E-16	-0.694819825
PSEN1	1089	1.49E-06	4.06E-05	-0.694459975
RGL2	816	6.43E-08	2.33E-06	-0.694259305
IL1B	1666	8.10E-05	0.00143817	-0.694165606
C9orf139	206	1.20E-18	1.73E-16	-0.694098726
WAPL	585	9.19E-10	4.65E-08	-0.693623392
MED13L	1137	2.49E-06	6.49E-05	-0.69287417
LSM2	936	2.70E-07	8.55E-06	-0.690406249
ABCB7	1094	1.56E-06	4.21E-05	-0.690307146
SH3BGRL	1867	0.00018397	0.00291538	-0.6892195
ADK	663	5.26E-09	2.35E-07	-0.687736503
BTLA	175	9.52E-21	1.61E-18	-0.687484318
LAMP2	1441	2.64E-05	0.0005411	-0.687264893
JMJD6	835	8.89E-08	3.15E-06	-0.687074477
HDAC6	899	1.89E-07	6.22E-06	-0.686794667
SERPINB6	1063	1.16E-06	3.24E-05	-0.684662072
C11orf21	177	1.12E-20	1.87E-18	-0.684521543
SLBP	1166	3.36E-06	8.53E-05	-0.683743316
GCNT2	164	2.27E-21	4.09E-19	-0.681496681
ESYT1	756	2.92E-08	1.14E-06	-0.681386747
SETD3	1066	1.21E-06	3.36E-05	-0.681383642
CLEC2D	959	3.88E-07	1.20E-05	-0.680275313
MYL12B	1499	3.48E-05	0.00068754	-0.67997955
NUTM2A-AS	576	7.22E-10	3.71E-08	-0.678240556
RPF2	439	1.04E-11	7.00E-10	-0.676784047
SPTLC2	1529	4.09E-05	0.00079235	-0.675990072
ADGRG5	176	1.06E-20	1.79E-18	-0.675707565

ID2	1556	4.69E-05	0.00089179	-0.6752458
RBPJ	1483	3.29E-05	0.00065741	-0.674312412
ARPC5	1840	0.00016802	0.00270208	-0.673654368
TMEM30A	1053	1.02E-06	2.86E-05	-0.672404876
SNHG16	539	2.75E-10	1.51E-08	-0.672169697
FMNL1	727	1.88E-08	7.63E-07	-0.67181691
VAT1	750	2.77E-08	1.09E-06	-0.671607966
MOB3B	581	7.88E-10	4.01E-08	-0.670633272
SYAP1	952	3.60E-07	1.12E-05	-0.66961897
GALNT3	372	2.91E-13	2.32E-11	-0.669255147
CCDC69	696	1.11E-08	4.71E-07	-0.667466976
EIF2A	1276	9.37E-06	0.00021734	-0.667325845
ADD1	1435	2.54E-05	0.00052352	-0.66732228
COTL1	205	1.11E-18	1.60E-16	-0.666972029
MAML3	1051	1.00E-06	2.82E-05	-0.666673121
CTSB	1519	3.90E-05	0.00075899	-0.666441735
RHOH	1518	3.87E-05	0.00075497	-0.666247535
IVD	1056	1.05E-06	2.95E-05	-0.666155464
LDHA	2157	0.00059348	0.00814009	-0.666089522
MSL3	927	2.51E-07	8.01E-06	-0.665311226
LMO2	397	1.16E-12	8.62E-11	-0.665246751
CCDC26	168	4.62E-21	8.14E-19	-0.663511449
HDHD5	609	1.56E-09	7.59E-08	-0.662748874
ASPH	369	2.46E-13	1.98E-11	-0.662326604
CTC1	1186	4.21E-06	0.0001051	-0.66200198
CRYZL1	1532	4.16E-05	0.00080313	-0.660189288
RSL1D1	1416	2.27E-05	0.00047414	-0.659866828
FTSJ3	1127	2.24E-06	5.89E-05	-0.65867626
MEF2D	715	1.50E-08	6.21E-07	-0.656221328
KIN	846	1.06E-07	3.72E-06	-0.656212299
STK10	1206	4.90E-06	0.00012017	-0.655862215
RASSF4	551	3.59E-10	1.93E-08	-0.655394658
USP38	536	2.55E-10	1.41E-08	-0.654739641
SH3BP5-AS1	564	4.71E-10	2.47E-08	-0.654181255
ARAF	833	8.69E-08	3.09E-06	-0.654176979
GM2A	525	1.77E-10	9.96E-09	-0.65321021
IDH3A	453	1.81E-11	1.18E-09	-0.652777123
GDI2	1879	0.00019254	0.00303101	-0.652343527
TBC1D10C	1180	3.83E-06	9.62E-05	-0.651957544
PRKD2	974	4.54E-07	1.38E-05	-0.650675736
QKI	903	1.94E-07	6.34E-06	-0.649928269
STN1	674	6.73E-09	2.96E-07	-0.648697323
RGS18	412	2.68E-12	1.92E-10	-0.647796295

SPECC1	550	3.53E-10	1.90E-08	-0.646705765
VCL	1376	1.76E-05	0.00037888	-0.646223431
CD86	253	8.13E-17	9.51E-15	-0.645093543
CLEC2B	777	3.95E-08	1.50E-06	-0.643627912
SBF1	823	7.26E-08	2.61E-06	-0.643378273
MACROH2A1	1249	7.28E-06	0.00017252	-0.64325173
HADHA	1857	0.00017538	0.00279457	-0.64232458
CDH11	220	4.60E-18	6.18E-16	-0.641404739
CCDC12	1310	1.18E-05	0.000267	-0.641371027
TACC1	1371	1.73E-05	0.00037416	-0.640770197
UXT	771	3.73E-08	1.43E-06	-0.640583764
TRPV2	691	8.99E-09	3.85E-07	-0.640373657
SFT2D1	997	5.59E-07	1.66E-05	-0.640370452
SSR1	1260	8.06E-06	0.00018924	-0.640270793
FOXO3	788	4.49E-08	1.69E-06	-0.640228112
ITGAL	440	1.08E-11	7.28E-10	-0.640120616
MED14	1098	1.62E-06	4.36E-05	-0.638945396
CSTB	938	2.78E-07	8.76E-06	-0.638941041
CYRIB	1663	8.01E-05	0.00142462	-0.638158205
BNIP2	1665	8.09E-05	0.00143796	-0.63669339
MTHFD1	1072	1.28E-06	3.54E-05	-0.635548762
MAGT1	1401	2.06E-05	0.00043539	-0.635503696
RGS1	419	4.28E-12	3.02E-10	-0.63540926
HSP90B1	2047	0.00040261	0.00581998	-0.635209568
RLIM	1169	3.59E-06	9.09E-05	-0.634287955
OLFML2A	356	9.80E-14	8.14E-12	-0.633968653
PPP2R5C	1628	6.79E-05	0.00123356	-0.633926517
CHD3	1083	1.40E-06	3.83E-05	-0.633506322
MYL12A	1330	1.37E-05	0.00030502	-0.633442882
BCAT1	630	2.63E-09	1.24E-07	-0.633065105
TMCC3	216	3.09E-18	4.23E-16	-0.631702081
ANXA4	718	1.64E-08	6.77E-07	-0.631390356
RNASE6	244	3.20E-17	3.88E-15	-0.630928928
NDUFB11	1231	6.32E-06	0.00015199	-0.630770222
AHCTF1	887	1.72E-07	5.75E-06	-0.628880871
RBM25	1588	5.41E-05	0.00100739	-0.628115573
LPXN	650	3.89E-09	1.77E-07	-0.627921557
RIN3	179	1.24E-20	2.04E-18	-0.626002442
HSPA5	2281	0.00084586	0.0109732	-0.625586777
IKZF3	352	8.42E-14	7.07E-12	-0.625127005
MYO15B	1595	5.68E-05	0.00105285	-0.624050025
ANAPC16	1585	5.32E-05	0.00099276	-0.623005049
MED13	1544	4.42E-05	0.00084699	-0.622889866

SYTL1	716	1.53E-08	6.32E-07	-0.62180037
DNAJC1	430	7.94E-12	5.46E-10	-0.62161875
DERL1	1241	6.93E-06	0.00016519	-0.62103878
DIPK1C	768	3.47E-08	1.34E-06	-0.620603374
MS4A1	1375	1.76E-05	0.00037887	-0.620319058
WDR13	1130	2.34E-06	6.13E-05	-0.620311371
CCAR1	1756	0.00012091	0.00203752	-0.61877468
PPP2R5A	844	1.03E-07	3.62E-06	-0.617952331
RAB11FIP1	543	3.01E-10	1.64E-08	-0.617699667
MTMR14	1271	9.15E-06	0.00021307	-0.617221235
RSU1	1009	6.37E-07	1.87E-05	-0.617194183
GNPTG	941	2.89E-07	9.09E-06	-0.616206109
POLR2B	1568	4.91E-05	0.00092699	-0.614522974
UVRAG	625	2.39E-09	1.13E-07	-0.614418831
MAST3	647	3.74E-09	1.71E-07	-0.614023636
SH3TC1	1896	0.00021282	0.00332147	-0.61385196
TMBIM1	870	1.43E-07	4.87E-06	-0.613542948
ADCY7	292	2.19E-15	2.21E-13	-0.613501332
TLR1	796	4.82E-08	1.79E-06	-0.613316631
ASF1A	1050	9.91E-07	2.79E-05	-0.613082748
NSMAF	1193	4.47E-06	0.00011068	-0.612944057
PUDP	654	4.31E-09	1.95E-07	-0.612398693
GINM1	731	1.98E-08	8.01E-07	-0.61183909
TNFAIP8L2	483	4.55E-11	2.79E-09	-0.611474967
LIPA	1253	7.43E-06	0.0001755	-0.611340303
MTHFD2	641	3.38E-09	1.56E-07	-0.609496249
NPC1	1054	1.04E-06	2.92E-05	-0.609196543
NDRG3	1041	9.37E-07	2.66E-05	-0.607819589
EIF5A	1120	2.12E-06	5.59E-05	-0.607460313
RSL24D1	1853	0.00017411	0.00278041	-0.606135467
ETF1	1433	2.51E-05	0.00051791	-0.606102033
IPCEF1	880	1.61E-07	5.42E-06	-0.606049084
WDR45B	1514	3.85E-05	0.0007516	-0.605695008
HOPX	271	2.96E-16	3.23E-14	-0.605651737
HDAC2	2177	0.00063963	0.00869421	-0.60541108
LINC01410	336	3.77E-14	3.32E-12	-0.60474786
PAICS	1458	2.96E-05	0.00060116	-0.604276804
TP53	1290	1.04E-05	0.00023879	-0.603329955
DOCK11	1527	4.07E-05	0.00078816	-0.603062626
SLC43A2	450	1.68E-11	1.11E-09	-0.602641662
RUNX2	341	4.34E-14	3.77E-12	-0.601847459
SUSD3	431	8.34E-12	5.72E-10	-0.601828054
MARCHF5	1340	1.49E-05	0.00032984	-0.601693112

MYD88	2083	0.00046493	0.00660476	-0.600234941
NLRC5	1757	0.00012125	0.00204213	-0.599727404
SHOC2	1767	0.00012603	0.00211048	-0.599647955
RNF149	1412	2.16E-05	0.00045166	-0.598953081
ASCC3	1110	1.90E-06	5.07E-05	-0.597933871
CD83	666	5.64E-09	2.51E-07	-0.59785927
CA5B	706	1.30E-08	5.44E-07	-0.597630317
DAXX	1562	4.78E-05	0.00090633	-0.597450802
NMD3	1002	5.92E-07	1.75E-05	-0.597364842
MTDH	1486	3.31E-05	0.00066009	-0.596597282
ATG4C	804	5.50E-08	2.02E-06	-0.596423086
MCL1	1082	1.39E-06	3.80E-05	-0.594933947
CCT8	2575	0.00166065	0.0190836	-0.593556239
LOC1009963	328	2.37E-14	2.14E-12	-0.590948328
EEF1B2P3	800	5.23E-08	1.94E-06	-0.590143735
ECM1	1778	0.00013029	0.00216835	-0.588515432
FPGS	1915	0.0002259	0.00349063	-0.588403385
ADAM10	1800	0.00014235	0.00234023	-0.587818332
NEK9	1484	3.30E-05	0.00065749	-0.587317753
EIF3B	1224	5.77E-06	0.00013954	-0.586723881
KPNB1	1704	9.57E-05	0.00166211	-0.586127389
MPZL1	1006	6.06E-07	1.78E-05	-0.585895875
LCN8	1246	7.18E-06	0.00017041	-0.58552408
ZBTB21	670	6.26E-09	2.77E-07	-0.585269337
PAPSS1	779	4.04E-08	1.53E-06	-0.584799057
PTPRD	624	2.31E-09	1.09E-07	-0.584614681
IRAK1	1337	1.46E-05	0.0003229	-0.584354774
TMEM104	528	2.08E-10	1.17E-08	-0.58320189
CDKN1B	925	2.47E-07	7.90E-06	-0.58246425
AP2B1	1758	0.00012175	0.00204925	-0.58158094
FTSJ1	1184	4.08E-06	0.0001018	-0.581537653
EIF3A	2184	0.00066206	0.00897031	-0.581226955

TableS3

Genes in poverty-exposed signature	Genes in unexposed signature
ACTB	SMAD2
PIK3C3	BNIP2
NCF4	PSMB1
PSME2	ADA
GSDME	SLBP
PLCG1	ABCE1
VAV3	RRP1B
ATP6V1G1	UVRAG
VAV1	MS4A1
PSMA5	EIF3B
MYO10	TCP1
DOK3	PSMC6
ITPR1	TMEM123
WASF2	BLK
SYK	BTAF1
HGSNAT	B3GNTL1
B2M	POLR2B
LAIR1	LDHA
AGPAT2	ADAM10
CD19	PPP2R5C
JUN	CAST
UBA7	EEF1B2
MME	KPNB1
SPTAN1	MTHFD2
LAPTM5	GDI2
PIK3IP1	CORO1A
ARHGDIB	ETF1
CPXM1	RHOH
SDC2	MACROH2A1
BIRC7	SSR1
KLHL6	IGBP1
FADS3	DAXX
CALM3	TMX1
CD74	HDAC2
SLAMF6	NSMAF
PCNA	PFKFB3
MSR1	MYC
HLA-DMB	PUDP
RBMS3	IRF8
DRAM1	PAICS
TMSB4X	EIF4A3

HBS1L
FKBP1A
FOXP1
CHCHD7
RUBCNL
MYADM
TRAF5
PHYH
LITAF
NDFIP1
CD52
TSPO
ZNF608
OAS3
TRIM38
SOCS2
HNRNPA2B1
SMARCA4
CD27
PTPN7
FOXO1
GBP4
RAG1
HLA-DPA1
ISG20
RAG2
HLA-DQB1
CIITA
HLA-DQB2
H3C4
HLA-DRA
LTB
HLA-DPB1

WAPL
CNIH1
LSM2
ASF1A
UBE2J1
SYNCRIP
ABCB7
STK17B
GRB2
ITGA4
NFATC3
SRP72
BLNK
GLIPR1
FTSJ1
MSL3
EIF4A1
DDX21
IL2RG
RBM3
C1QBP
BCAT1
PLEK
NUP210
IRAK1
CCNC
SLC7A5
TP53
ELAC2
RSL1D1
LPXN
MTDH
ADK
CCT8
TCOF1
RABGAP1L
PMAIP1
LCP1
SH3TC1
CSGALNACT1
LILRB2
GPM6B
ALOX5

PNISR
P2RX5
CD9
CD69
EZR
SPPL2B
CDKN1B
SOD2
PGD
FRMD4B
MTHFD1
FHL1
PDLIM1
ACAT1
FOS
SH3BGRL
HSP90AB1
TALDO1
CANX
LAT2
RSU1
CPNE3
CD34
PPA1

TableS4_Flow Percentage

Sample Number	%CD45low	# of sequenced cells	% CD45high	# of sequenced cells	% CD45highCD3+	% CD45highCD19+	% CD45highCD14+
Unexposed 1	88.10%	185	11.80%	176	37.30%	27.70%	32.70%
Unexposed 2	30.80%	188	56.40%	88	10.30%	76.60%	3.20%
Unexposed 3	98.80%	185	0.98%	0	64.60%	8.04%	27.30%
Unexposed 4	95.80%	282	4.03%	88	32.20%	30.60%	33.70%
Unexposed 5	93.30%	187	6.08%	88	23.20%	56.80%	19.50%
Unexposed 6	87.50%	122	11.60%	87	39.30%	38.50%	10.70%
Unexposed 7	79.80%	137	18.80%	88	16.00%	70.90%	6.19%
Poverty-exposed 1	65.50%	188	31.90%	NA	49.80%	41.10%	5.63%
Poverty-exposed 2	89.90%	188	8.51%	88	31.20%	18.80%	43.80%
Poverty-exposed 3	3.21%	94	95.50%	88	16.85%	75.70%	1.01%
Poverty-exposed 4	85.50%	188	14.10%	87	54.40%	28.40%	7.55%
Poverty-exposed 5	86.90%	140	12.30%	88	24.10%	63.60%	1.80%
Poverty-exposed 6	95.50%	186	4.02%	88	52.70%	36.60%	4.30%
Poverty-exposed 7	79.40%	186	20.00%	88	28.00%	50.10%	13.60%

TableS5

GSE181157_ETV6-RUNX1	**GSE181157_Hyperdiploid**
Poverty-exposed_16-003	Poverty-exposed_16-049
Poverty-exposed_16-106	Poverty-exposed_16-257
Poverty-exposed_16-115	Poverty-exposed_16-291
Poverty-exposed_16-304	Poverty-exposed_16-335
Poverty-exposed_16-312	Poverty-exposed_16-342
Unexposed_16-001	Unexposed_16-048
Unexposed_16-002	Unexposed_16-090
Unexposed_16-006	Unexposed_16-131
Unexposed_16-012	Unexposed_16-141
Unexposed_16-050	Unexposed_16-158
Unexposed_16-065	Unexposed_16-161
Unexposed_16-070	Unexposed_16-176
Unexposed_16-074	Unexposed_16-182
Unexposed_16-076	Unexposed_16-186
Unexposed_16-094	Unexposed_16-194
Unexposed_16-100	Unexposed_16-199
Unexposed_16-108	Unexposed_16-215
Unexposed_16-140	Unexposed_16-239
Unexposed_16-152	Unexposed_16-249
Unexposed_16-221	Unexposed_16-272
Unexposed_16-238	Unexposed_16-273
Unexposed_16-267	Unexposed_16-279
Unexposed_16-293	Unexposed_16-287
Unexposed_16-322	Unexposed_16-302
Unexposed_16-350	Unexposed_16-306
Unexposed_16-352	Unexposed_16-315
Unexposed_16-354	Unexposed_16-338
Unexposed_16-363	Unexposed_16-339
	Unexposed_16-374